

Electronic Supporting Information

Mixed-Ligand based water-stable Mn(II)-MOF for quick, sensitive, and reusable IFE-PET-RET facilitated detection of Formaldehyde and Cr(VI)-Oxoanions in Food and Industrial Water like real-field samples: Experimental and Theoretical insights

Udayan Mondal,^{a,b} Somrita Nag,^{†,a,b} Rajeshwari Pal,^{†a,b} Priyabrata Banerjee^{*,a,b}

^a *Electric Mobility and Tribology Research Group, CSIR-Central Mechanical Engineering Research Institute, M. G. Avenue, Durgapur 713209, West Bengal, India.*

^b *Academy of Scientific and Innovative Research (AcSIR), Ghaziabad 201002, Uttar Pradesh, India.*

[†] S.N. and R.P. contributed equally to this work.

*Corresponding author, E-mail: pr_banerjee@cmeri.res.in, Homepage: www.cmeri.res.in, www.priyabratabanerjee.in

Contents

Entry	Description	Page No.
--	Experimental Section.	S3-S4
Fig. S1-S8, Table S1-S3	SCXRD, Hirshfeld surface and NCI-RDG plot of 1	S4-S11
Fig. S9-S16, Table S4	Structural Characterizations of 1	S11-S15
Fig. S17-S23	Photophysical Characterizations	S16-S19
Fig. S24-S34, Table S5-S6	Formaldehyde (FA) sensing application	S19-S32
Fig. S35-S45	Chromate and Dichromate sensing	S32-S42
Fig. S46-S50, Table S7	Mechanism for FA sensing	S43-S48
Fig. S51-S59, Table S8-S10	Mechanism towards Cr(VI) detection	S48-S56
Fig. S60-S62	FA quantification from food and water samples	S56-S58
Table S11, Fig. S63-S64	Cr(VI) sensing from real field matrices	S58-S61
Table S12-S13	Comparison of present work with recently reported FA and Cr(VI) sensors	S61-S65
--	References	S66-S68

Experimental Section.

Materials & Reagents.

The requisite precursor chemicals *viz.*, Manganese(II) acetate tetrahydrate $[(\text{CH}_3\text{COO})_2\text{Mn} \cdot 4\text{H}_2\text{O}]$, 5-hydroxyisophthalic acid (*hia*), 1,10-phenanthroline (*phen*) were procured from Sigma Aldrich (Merck), India and the MOF-reactions were carried out in oven-dried 15 mL glass vials. The targeted aldehydes (formaldehyde, benzaldehyde, furfural, glutaraldehyde, oxaldehyde/ glyoxal, propionaldehyde, valeraldehyde, syringaldehyde) and ancillary solvents (acetone, chloroform, dioxane, methanol, ethanol, tetrahydrofuran) were purchased from Merck, India. The sodium salts of acetate (OAc^-), arsenate (AsO_4^{3-}), meta-arsenite (AsO_2^-), carbonate (CO_3^{2-}), phosphate (PO_4^{3-}), sulphate (SO_4^{2-}), perchlorate (OClO_4^-), nitrate (NO_3^-) and potassium salts of chromate (CrO_4^{2-}), dichromate ($\text{Cr}_2\text{O}_7^{2-}$) and manganate (MnO_4^-) were acquired from Marck, India and HiMedia. The required solvents such as acetonitrile (ACN), dimethylformamide (DMF) and milli-Q water (MW) was purchased from Merck and Thermo Fisher Scientific.

X-ray Crystallographic Data Collection and Refinement

First, the single crystals of $\text{C}_{20}\text{H}_{12}\text{MnN}_2\text{O}_5 \cdot \text{H}_2\text{O}$ (**1**) were screened out with the help of a needle under an optical microscope. A suitable crystal (size: $0.09 \times 0.11 \times 0.12 \text{ mm}^3$) was selected and placed on the tip of a goniometer on a XtaLAB Synergy, Dualflex, HyPix3000 diffractometer (make: Rigaku). The crystal was kept at a temperature of 100.00 K during data collection. Using Olex2,¹ the structure was solved with the SHELXT structure solution program² using Intrinsic Phasing and refined with the SHELXL refinement package³ using Least Squares minimization. The crystal data (CCDC entry 2337818) and the refinement details have been provided in Table S1. In addition, selected bond lengths and bond angles are provided in Table S2 and Table S3, respectively.

Instrumental Techniques

The single-crystal and powder X-ray diffraction (XRD) of **1** was recorded from XtaLAB Synergy, Dualflex, HyPix3000 diffractometer and Bruker D8 Advance X-ray diffractometer, respectively using Cu K α radiation (λ : 1.54 Å). The N₂ sorption study at 77 K was performed after degassing the samples at 120°C (overnight) in a Quantachrome iQ2 Automated Gas analyzer (Serial No.

14715022003) for evaluation of the surface area measurement, pore size distribution *etc.* Thermogravimetric Analysis (TGA) analysis was performed using a NETZSCH STA 449F1 Jupiter system with a heating rate of $10^{\circ}\text{C min}^{-1}$ from 40°C to 600°C under a continuous N_2 atmosphere. The C,H,N elemental analysis was executed using a PerkinElmer 2400C elemental analyzer. The XPS study was carried out using a ULVAC PHI Versa Probe 4 with a monochromator Al K α X-ray source ($h\nu = 1486.6 \text{ eV}$). Fourier Transform - Infra Red (FT-IR) study was performed using a double beam Spectrum 100 model spectrophotometer (PerkinElmer) using KBr pellets. The surface morphology images (FE SEM) and energy-dispersive X-ray spectroscopy (EDX) analysis were executed using a Carl Zeiss MERLIN field emission scanning electron microscopy instrument. The atomic force microscopy (AFM) image was captured in an alpha300 instrument (make: Nanosurf C3000). An Agilent CARY-60 UV-Vis spectrophotometer with 1-cm path length quartz cuvette was used to record the UV-Vis spectroscopic data. The solution and solid state fluorescence studies were executed using Perkin Elmer LS-45 and Varian Cary Eclipse fluorescence (Serial No. EL08083865) spectrophotometers. The time-correlated single photon counting (TCSPC) analysis was performed in a HORIBA Jobin-Yvon instrument.

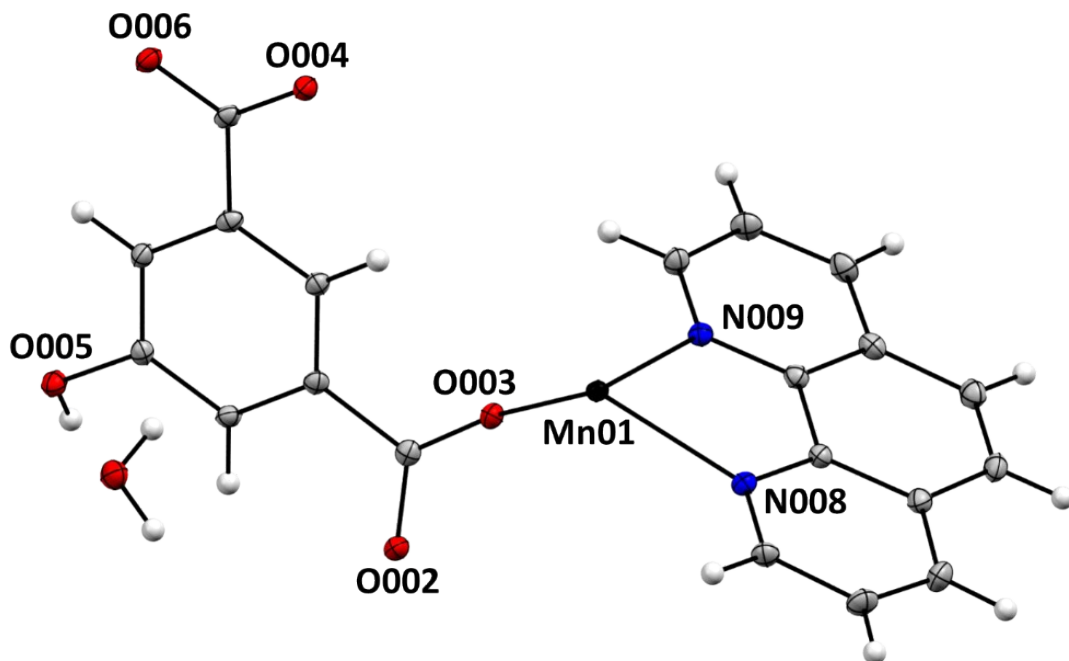


Fig. S1. Asymmetric unit of **1** (ORTEP with 30% ellipsoid plot)

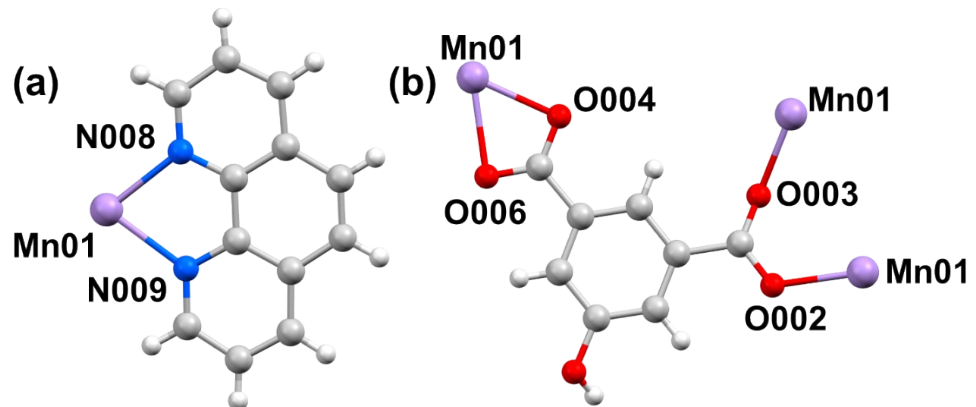


Fig. S2. Binding mode of constituting linkers in **1**

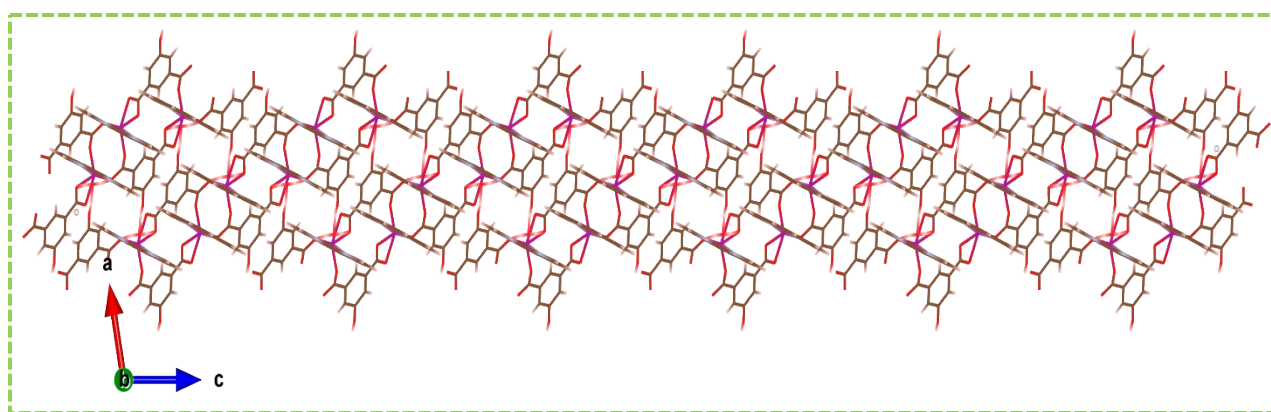


Fig. S3. Polymeric extension of **1** (viewed along crystallographic *b* axis)

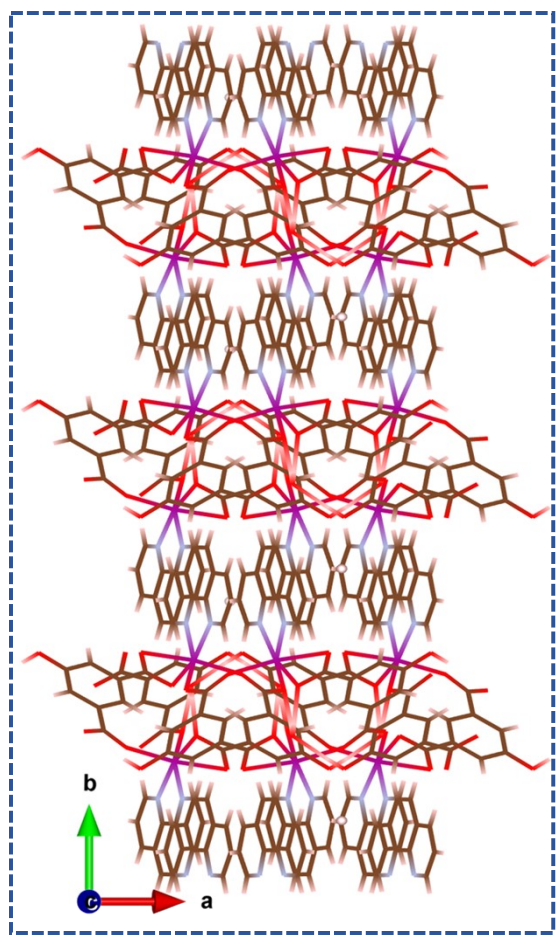


Fig. S4. Polymeric growth of **1** (viewed along *c* axis)

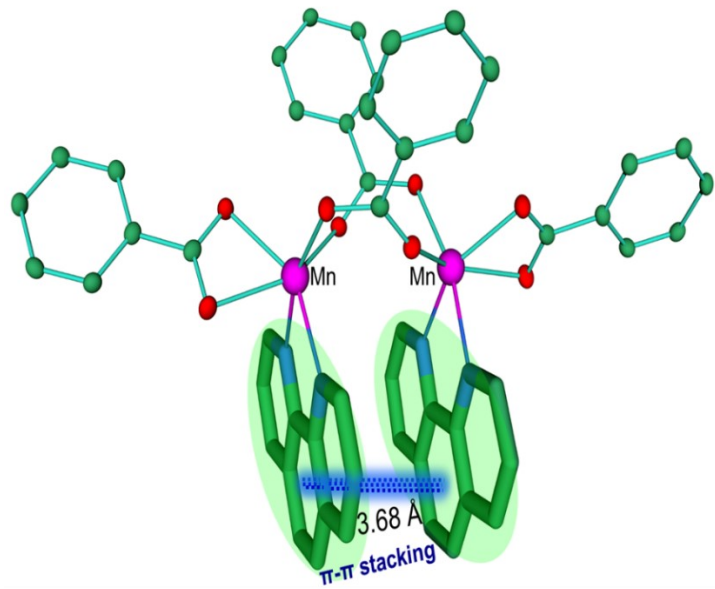


Fig. S5. π - π supramolecular interactions between *phen* rings of adjacent ladder

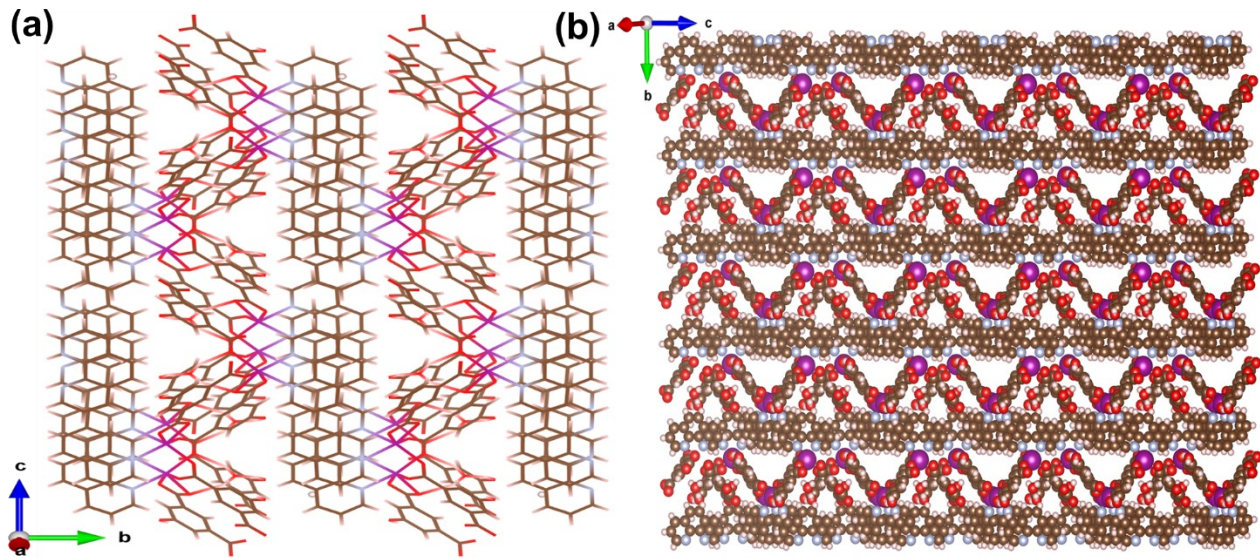


Fig. S6. (a) Polymeric extension of **1** along *a* axis; (b) ordered repetition of adjacent layers in the polymeric architecture

Table S1. Crystal and Structure Refinement Data for **1**.

CCDC No.	2337818
Empirical formula	C ₂₀ H ₁₂ MnN ₂ O ₅ , H ₂ O
Formula weight	433.24
Temperature (K)	100 K
Crystal system	Monoclinic
Space group	P 2/n (No. 13)
Hall group	-P 2yac
<i>a</i> /(Å)	8.4340(3)
<i>b</i> /(Å)	12.1634(4)
<i>c</i> /(Å)	17.4367(5)
α /(°)	90.000
β /(°)	100.576(2)
γ /(°)	90.000
Unit cell volume/(Å ³)	1758.38(10)
Z	4
Z'	1

Density (g/cm ³)	1.6367
μ /(mm ⁻¹)	6.501
F (000)	884.0
S	0.964
h, k, l _{max}	10,14,21
Index ranges	- 10 ≤ h ≤ 10, -14 ≤ k ≤ 14, -21 ≤ l ≤ 20
Theta Min-Max [Deg]	3.6, 68.3
N _{ref} , N _{par}	3209, 267
Radiation type	Cu K α
Wavelength/Å	1.54178
Crystal size/(mm ³)	0.09 × 0.11 × 0.12
Tmin, Tmax	0.481, 0.557
w	$^{^2}(FO^{^2}) + (0.0866P)^{^2}]$ where P = $(FO^{^2}+2FC^{^2})/3'$
wR2(reflections)	0.1166 (3209)
R _{int}	0.155
R, wR2, S	0.0400, 0.1166, 0.96
Observed Data [I > 0.0 sigma(I)]	2985

Table S2. Selected Bond lengths (Å) for 1

Atom1	Atom2	Length (Å)	Atom1	Atom2	Length (Å)
Mn01	O003	2.112(2)	C00C	C00L	1.396(3)
Mn01	N008	2.242(2)	C00C	C00M	1.402(3)
Mn01	N009	2.258(2)	C00D	C00F	1.441(4)
Mn01	O002	2.141(2)	C00D	C00G	1.415(3)
Mn01	O004	2.217(2)	C00E	C00G	1.432(3)
Mn01	O006	2.333(2)	C00F	C00P	1.408(3)
O002	C00B	1.279(3)	C00G	C00Q	1.412(4)
O002	Mn01	2.141(2)	C00H	C00S	1.398(4)

O003	C00B	1.253(3)		C00I	C00K	1.392(3)
O004	C00N	1.273(3)		C00I	C00M	1.395(3)
O004	Mn01	2.217(2)		C00J	C00R	1.402(3)
O005	C00K	1.371(3)		C00K	C00O	1.390(3)
O006	C00N	1.254(3)		C00L	C00N	1.502(3)
O006	Mn01	2.333(2)		C00L	C00O	1.395(3)
N008	C00F	1.362(3)		C00P	C00T	1.410(4)
N008	C00H	1.324(3)		C00Q	C00R	1.368(3)
N009	C00D	1.352(3)		C00S	C00T	1.374(4)
N009	C00J	1.323(3)				
C00A	C00E	1.355(4)				
C00A	C00P	1.438(3)				
C00B	C00M	1.499(3)				

Table S3. Selected Bond Angles($^{\circ}$) for **1**

Atom1	Atom2	Atom3	Angle/ $^{\circ}$
O003	Mn01	N008	120.38(6)
O003	Mn01	N009	82.74(6)
O003	Mn01	O002	93.68(6)
O003	Mn01	O004	92.95(6)
O003	Mn01	O006	147.15(6)
N008	Mn01	N009	73.49(7)
N008	Mn01	O002	95.95(6)
N008	Mn01	O004	144.03(6)
N008	Mn01	O006	86.30(6)
N009	Mn01	O002	164.74(7)
N009	Mn01	O004	100.12(6)
N009	Mn01	O006	87.77(6)
O002	Mn01	O004	94.87(6)
O002	Mn01	O006	102.78(6)

O004	Mn01	O006	57.84(6)
C00B	O002	Mn01	119.8(1)
Mn01	O003	C00B	149.7(2)
C00N	O004	Mn01	92.8(1)
C00N	O006	Mn01	88.0(1)
Mn01	N008	C00F	115.7(1)
Mn01	N008	C00H	125.4(2)
Mn01	N009	C00D	115.6(1)
Mn01	N009	C00J	125.6(2)

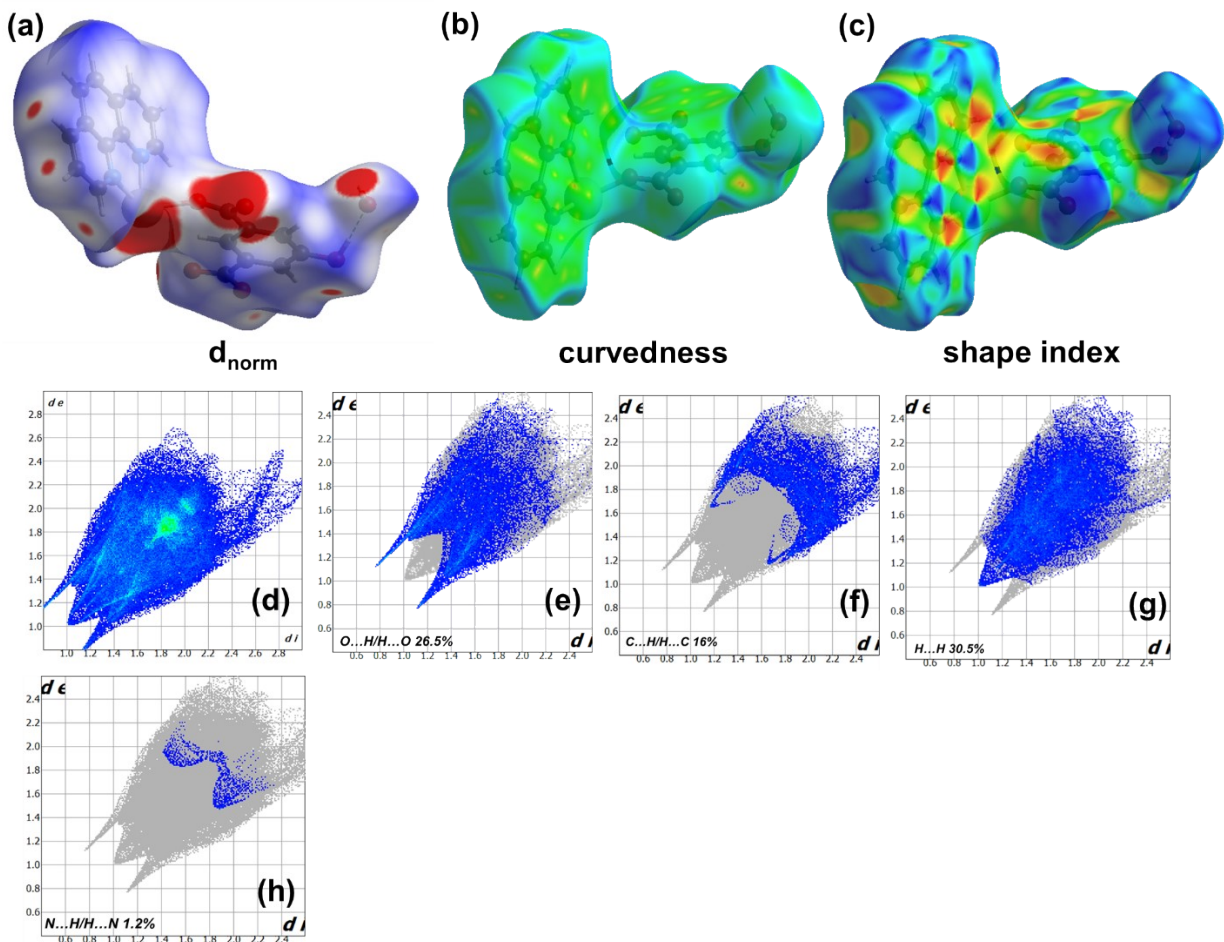


Fig. S7. Hirshfeld surface (a-c) of **1**, (d) full 2D fingerprint plot and (e-h) fingerprint plots delineated into O...H/H...O, C...H/H...C, H...H and N...H/H...N contacts.

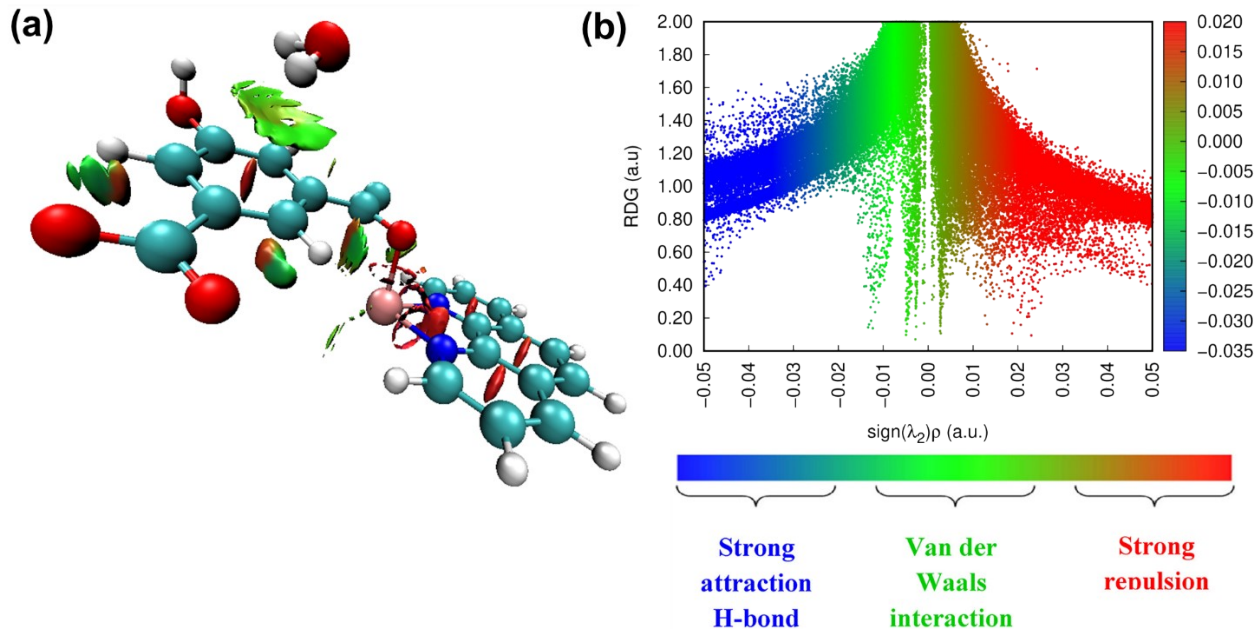


Fig. S8. Reduced density gradient based non-covalent interaction analysis plot of **1**: 3D iso-surface and 2D RDG scatter map.

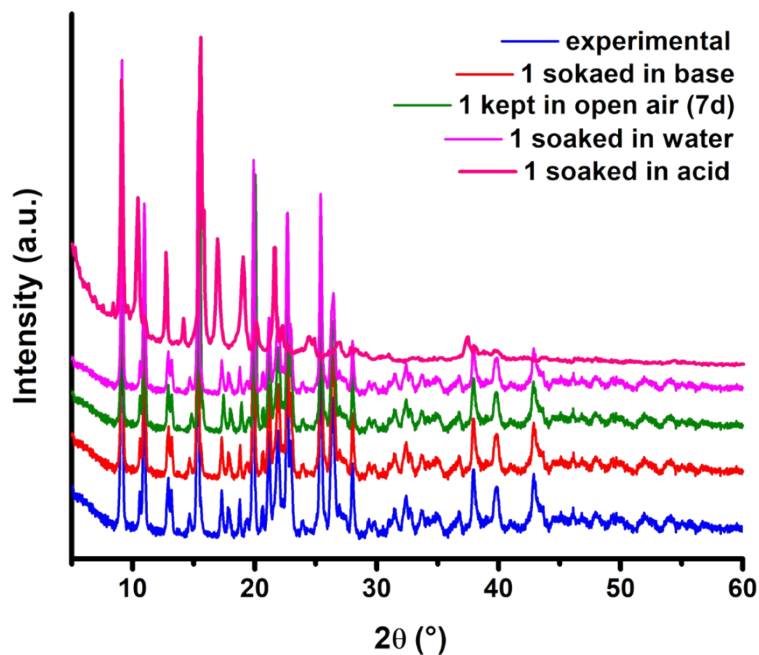


Fig. S9. PXRD pattern of **1** in several harsh chemical conditions

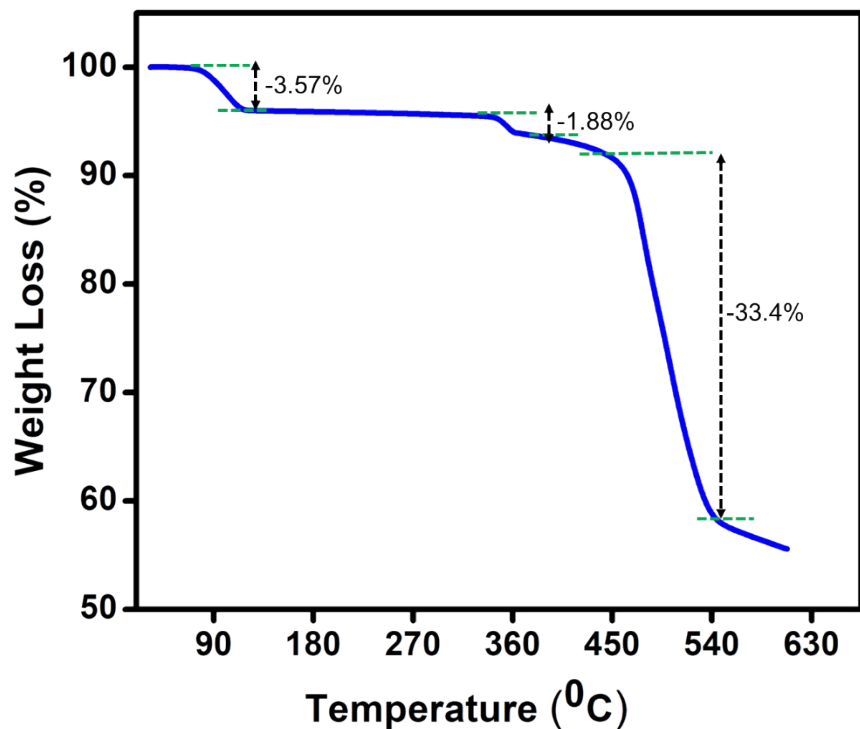


Fig. S10. Thermogravimetric analysis (TGA) of **1**

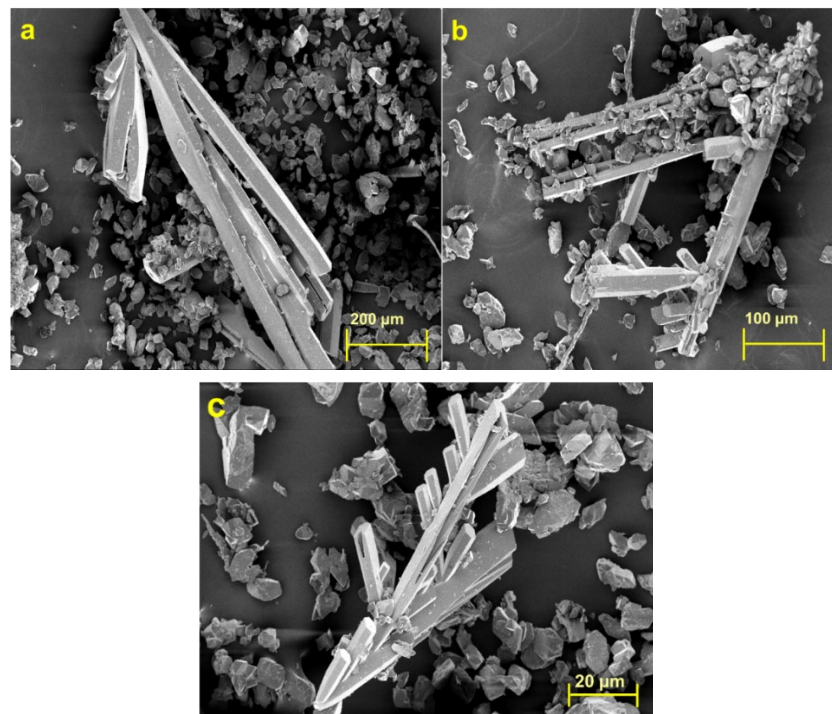


Fig. S11. Microstructure of the surface of **1**, from FE-SEM images at different magnifications

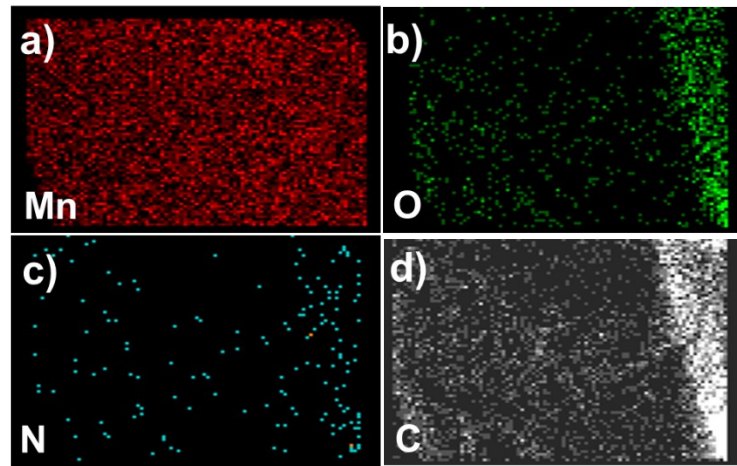


Fig. S12. (a-d) elemental X-Ray Mapping images of Mn, O, N, C in **1**.

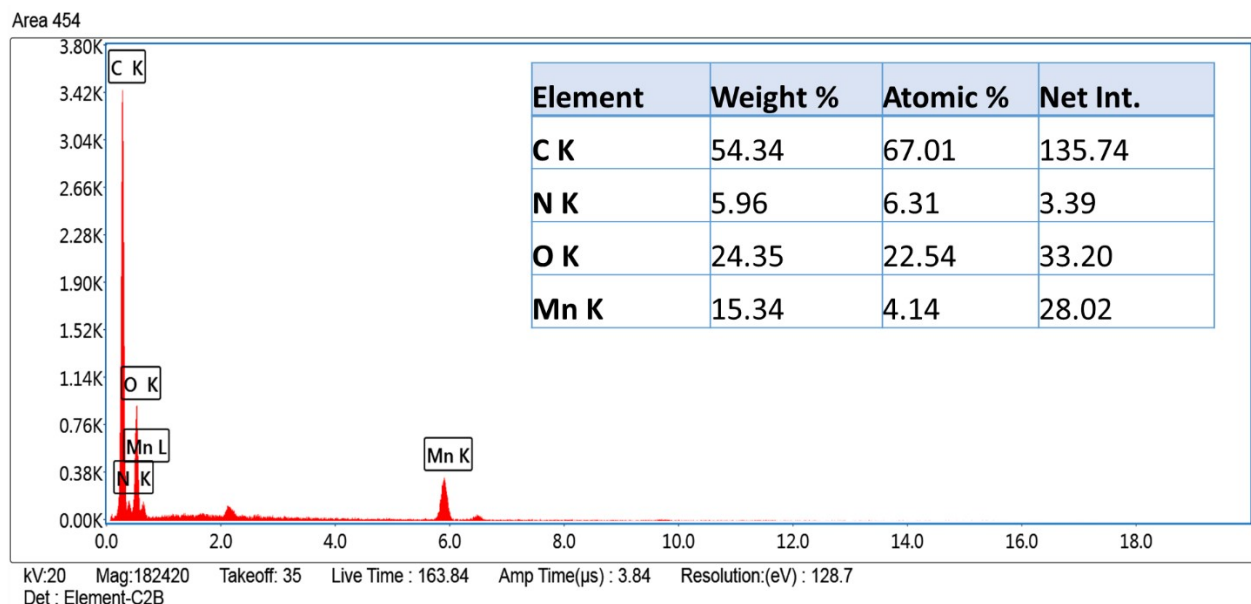


Fig. S13. EDAX analysis for identifying elemental composition of **1** along with probable weight %

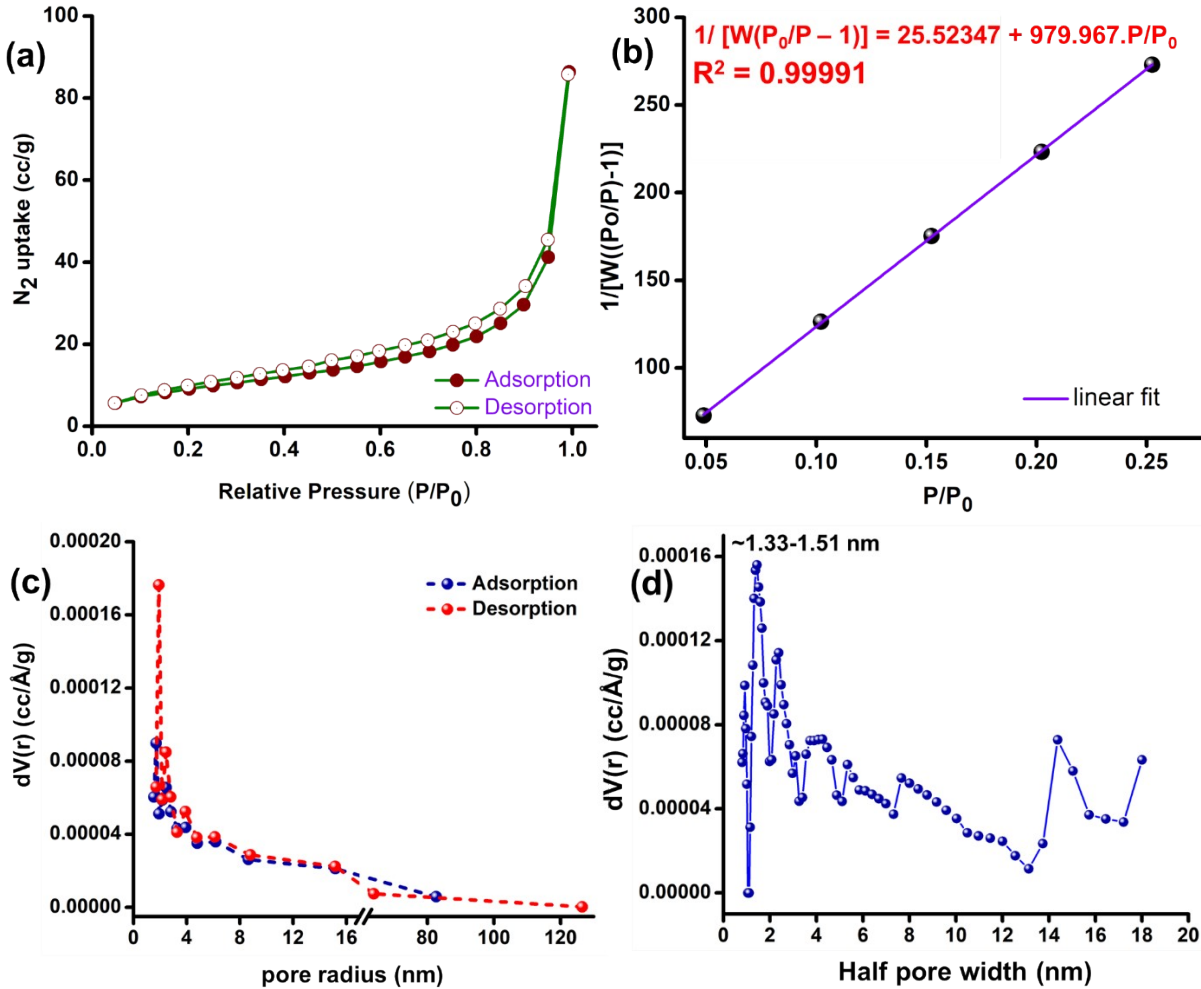


Fig. S14. (a) N_2 adsorption-desorption isotherm of **1**; (b) Linear fitting of the BET equation for calculation of surface area; (c) Pore Size distribution of **1**, calculated from BJH Method; (d) NLDFT pore width analysis.

Table S4. Outcome from N_2 adsorption-desorption analysis for **1**

BJH pore radius $D_V(r)$:	17.15 Å (absorption) 19.11 Å (desorption)
Half pore width (NLDFT method):	14.48 Å
Total pore volume:	0.026 cc/g

(where, BET: Brunauer–Emmett–Teller, BJH: Barrett–Joyner–Halenda Method, NLDFT: Non-local density functional theory)

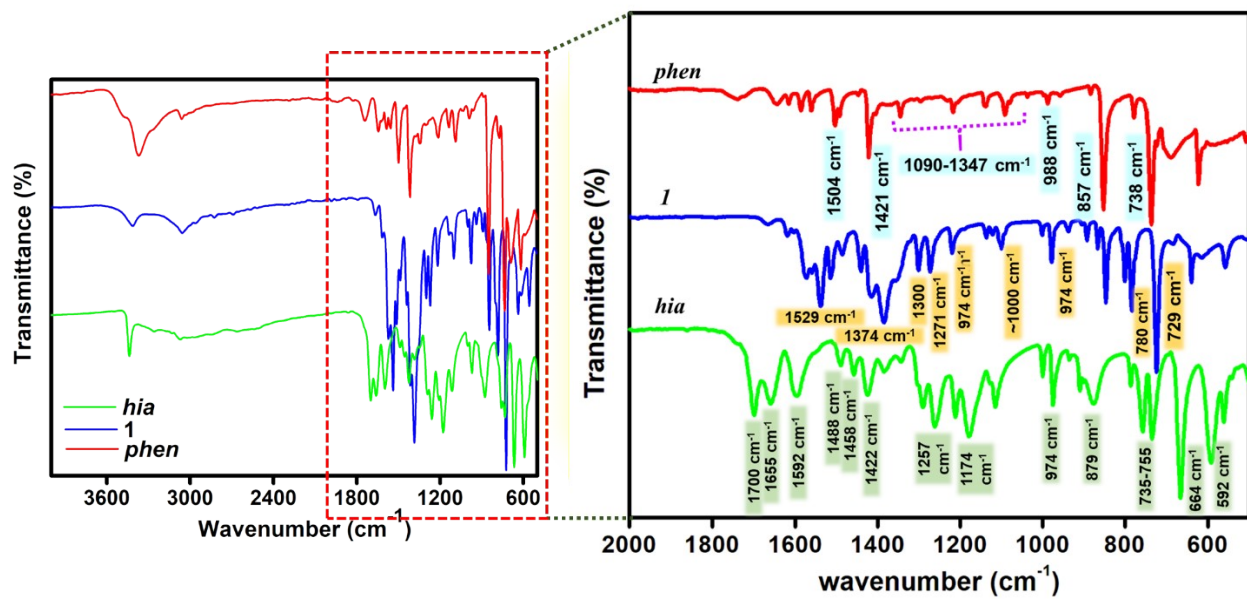


Fig S15. FT-IR spectra of **1**, *phen* and *hia*

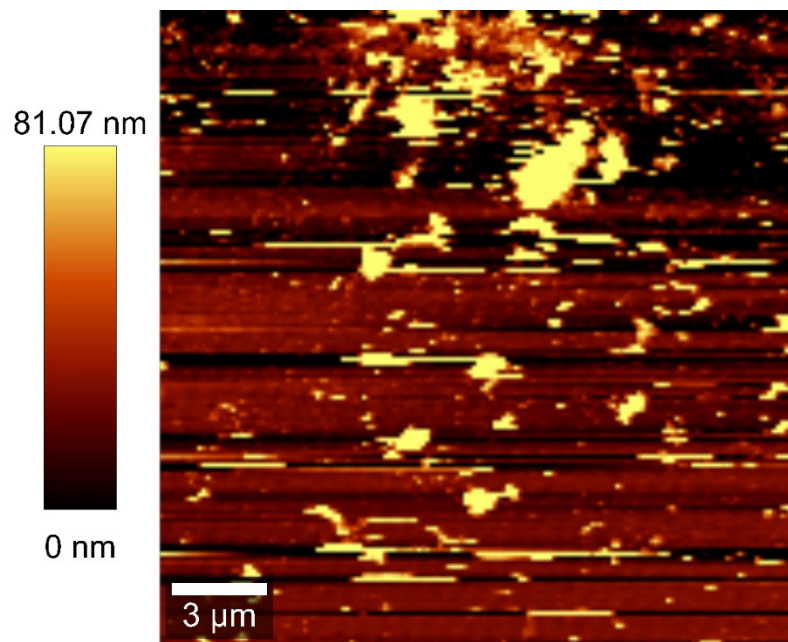


Fig. S16. 2D AFM surface image of **1**-acetonitrile dispersion

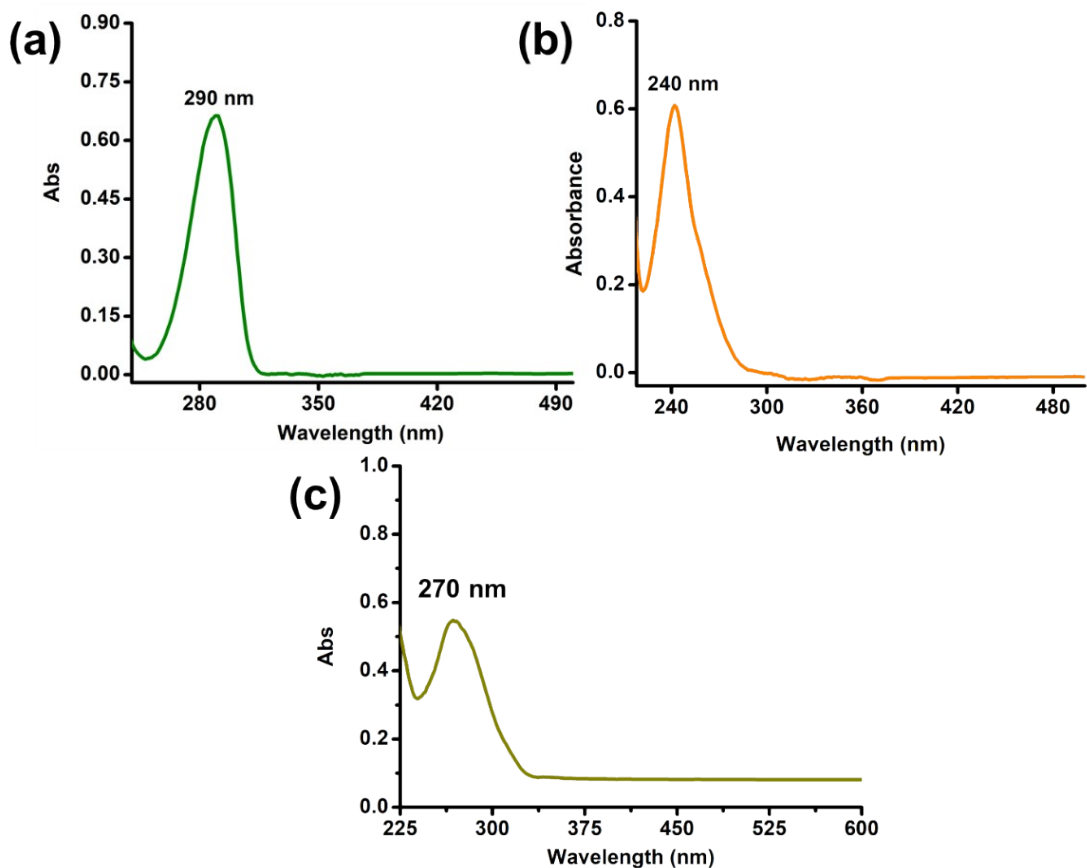


Fig S17. UV-vis spectra of (a) *hia*, (b) phen and (c) **1**.

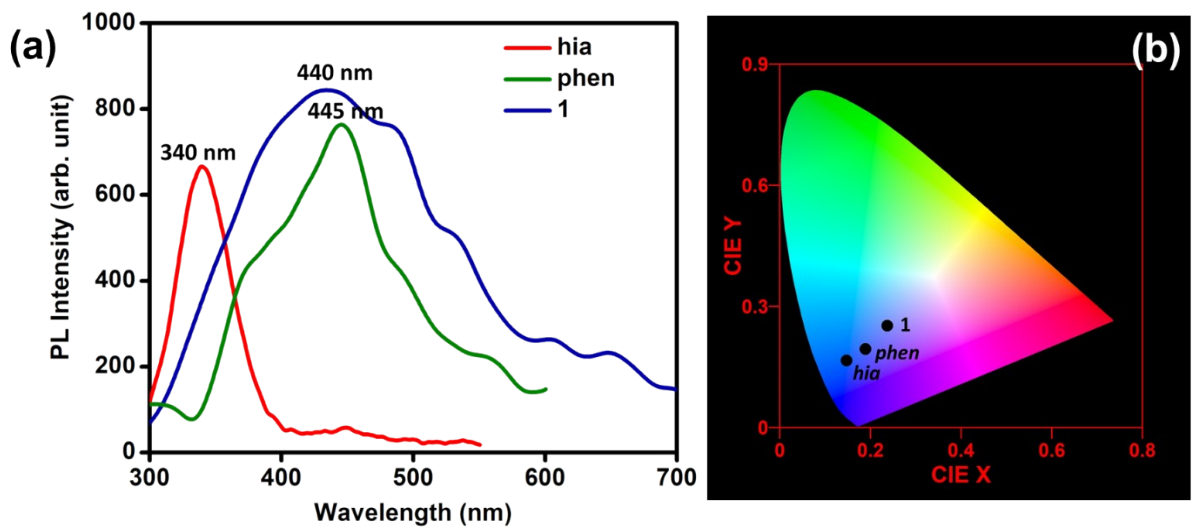


Fig S18. (a) PL spectra and (b) CIE co ordinates of *phen*, *hia* and **1** (dispersed)

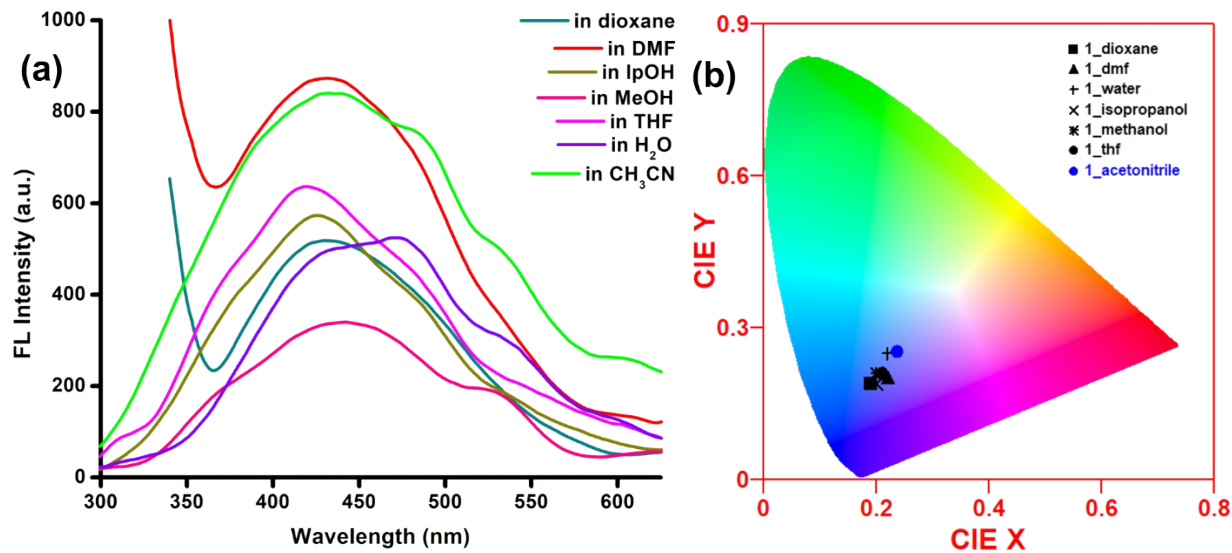


Fig. S19. Emission profile of 1, dispersed in different solvents of varying polarity and their corresponding CIE coordinates, exhibiting blue luminiscence.

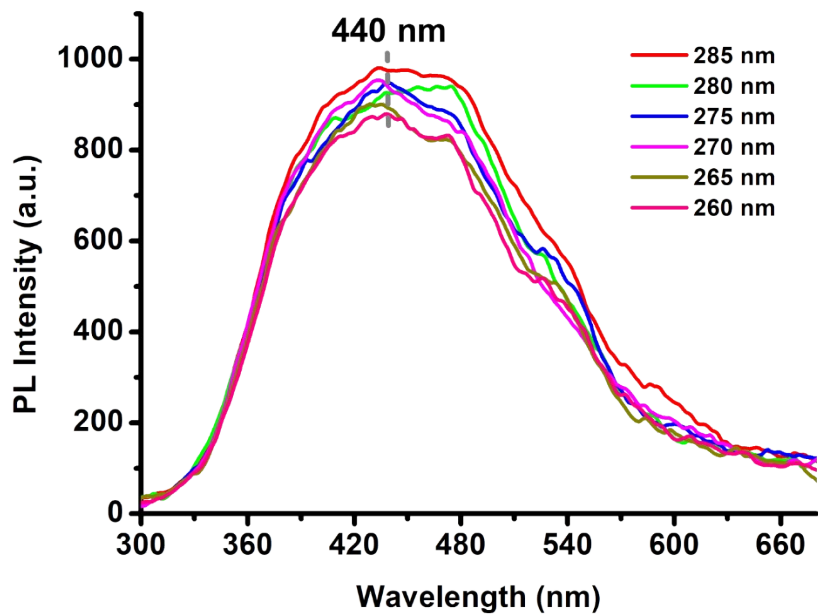


Fig. S20. Excitation dependent (λ_{Ex} : 260 – 285 nm) emission spectra of 1

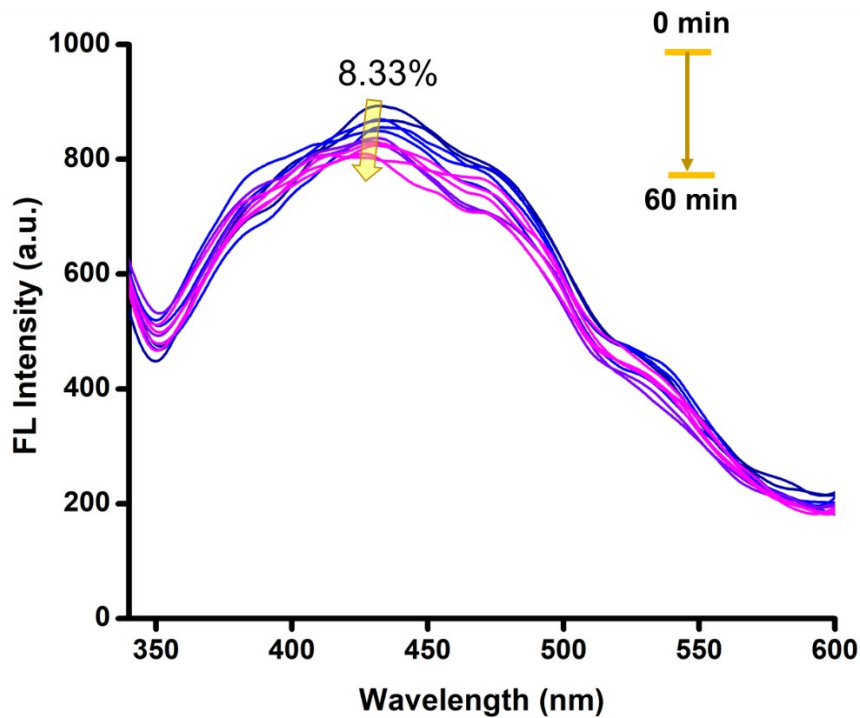


Fig. S21. Photostability of the MOF-sensor (**1**) in a time periods of 0-60 minutes.

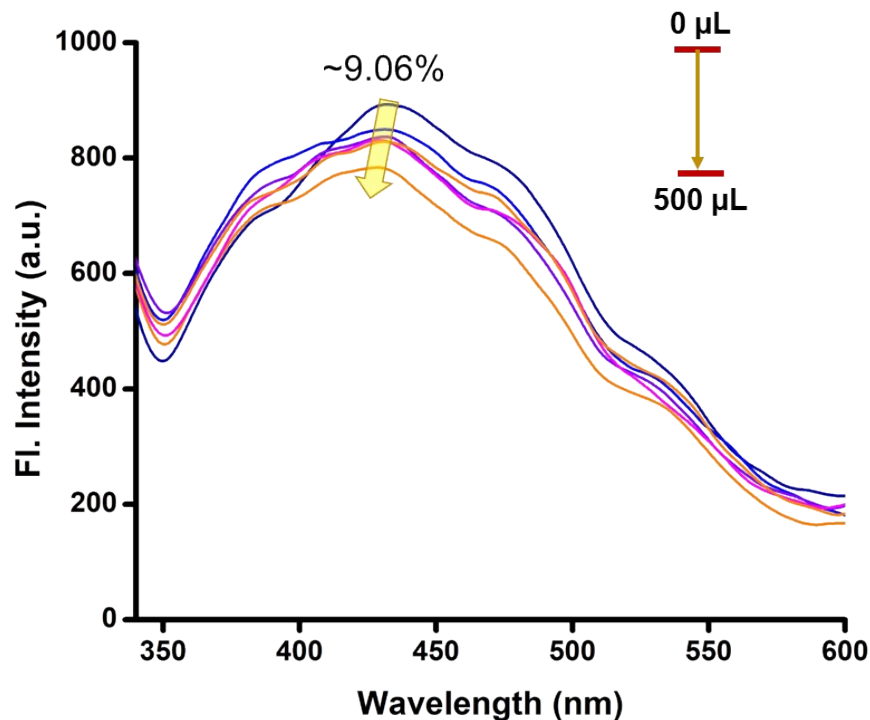


Fig. S22. Quenching effect from addition of water (~500 μL) to the sensor dispersion

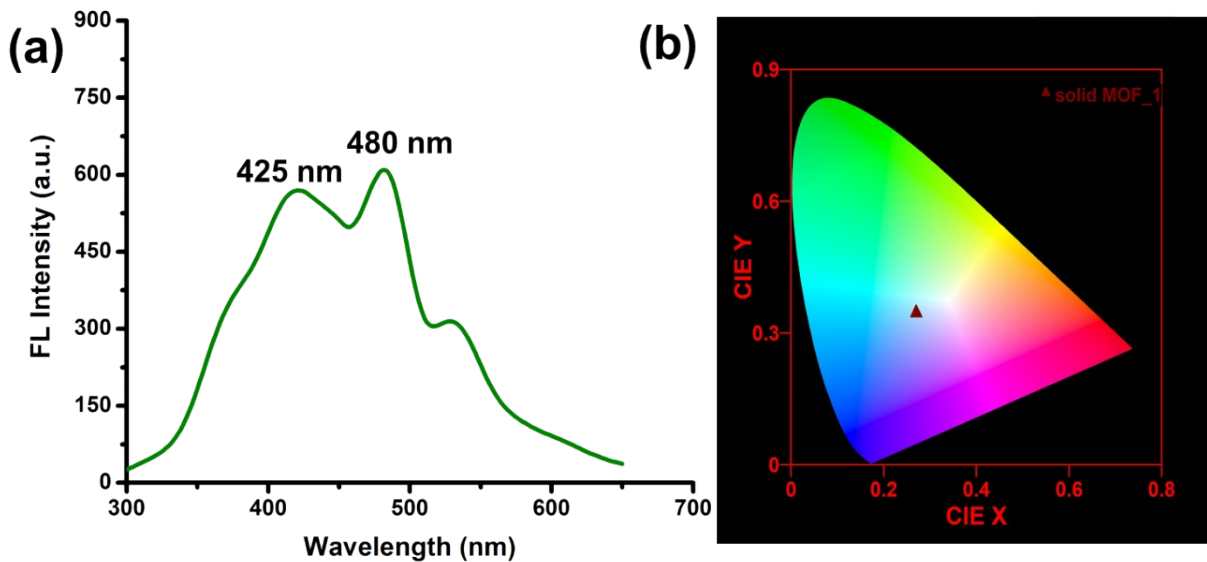


Fig. S23. Solid-state emissive nature of **1** (a) and CIE plot (b).

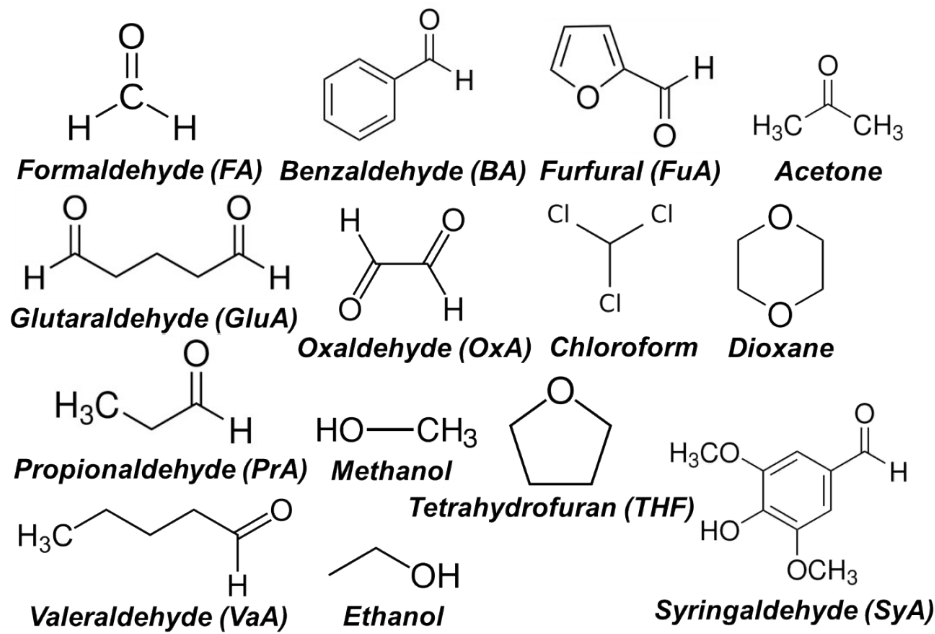
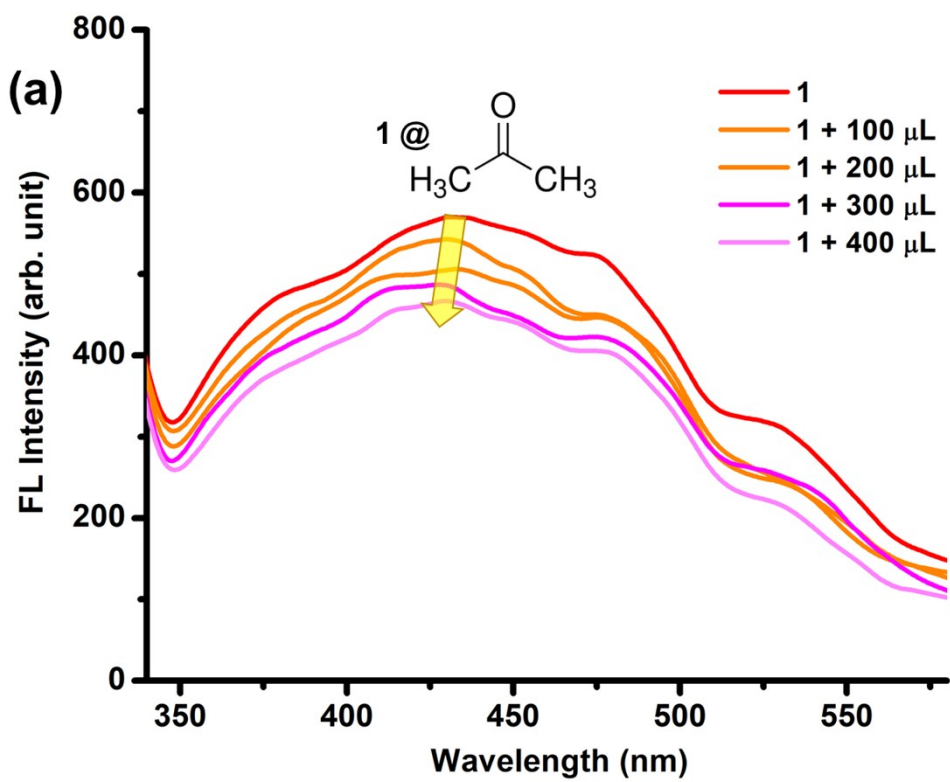
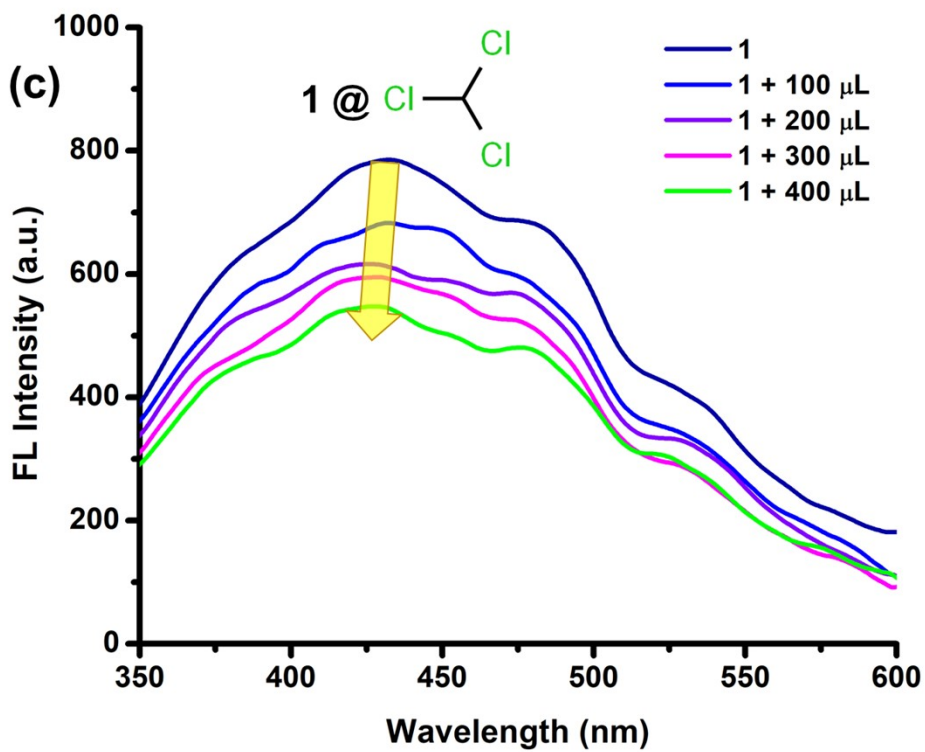
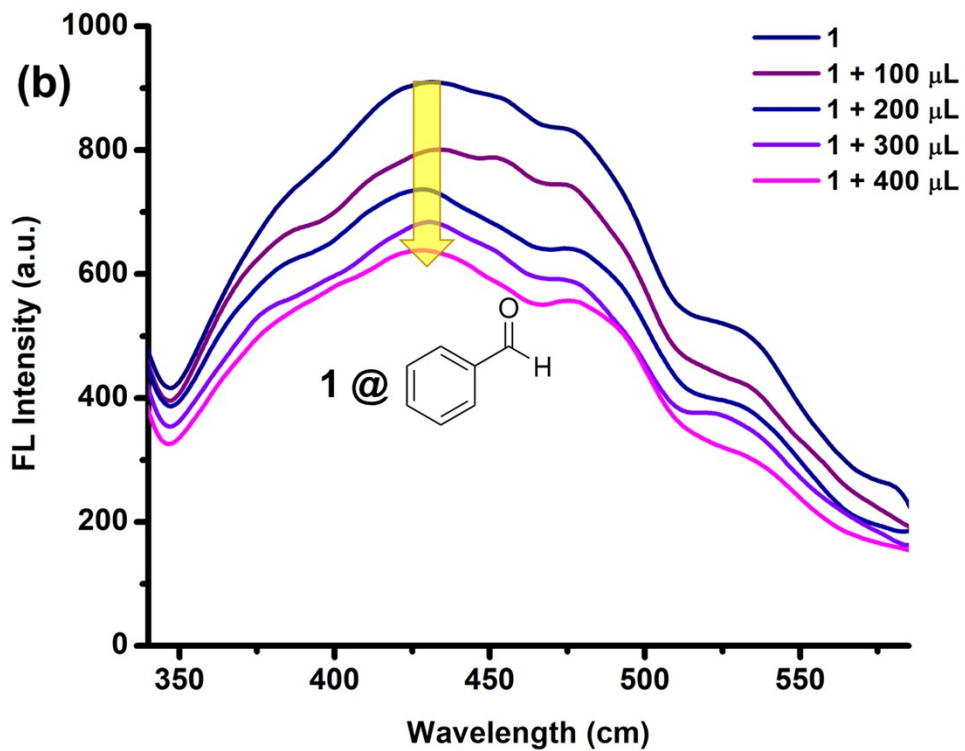


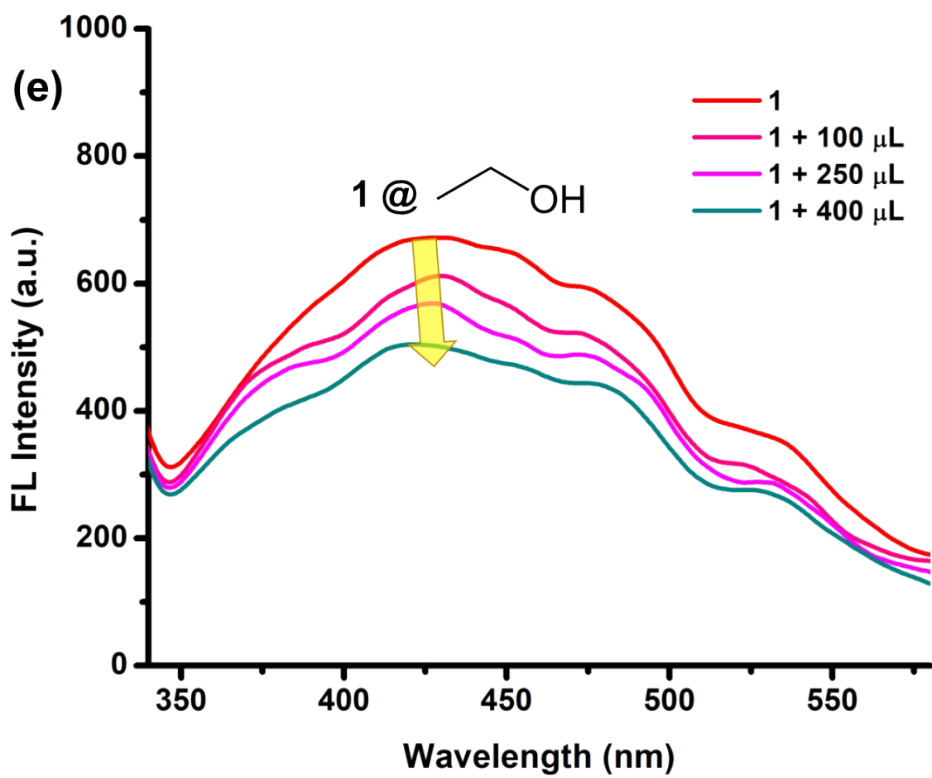
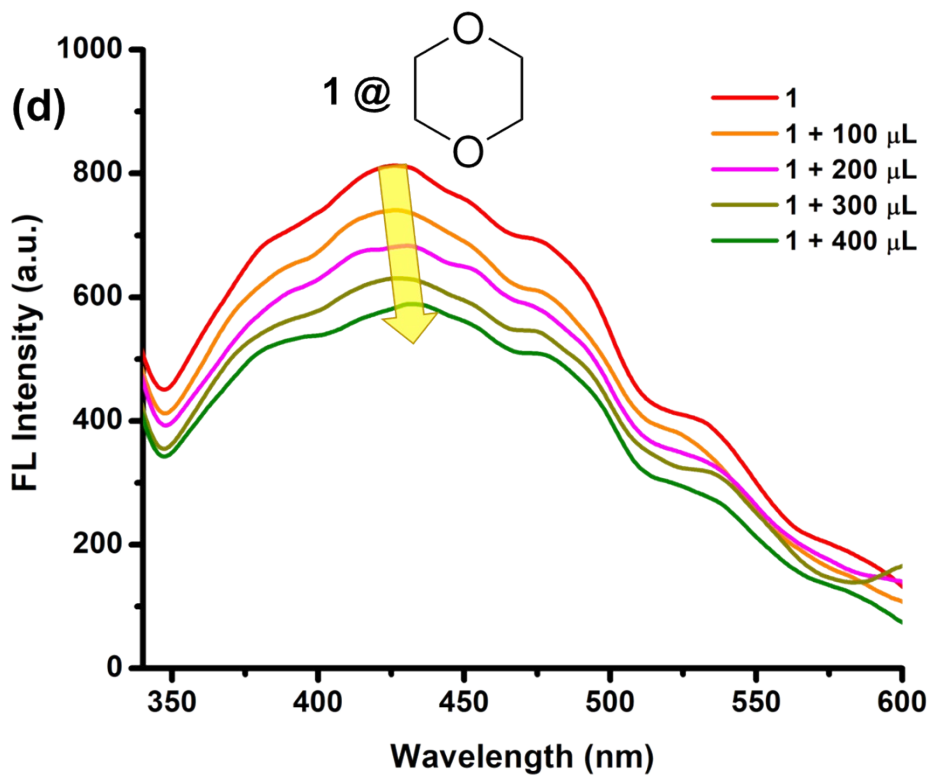
Fig. S24. Chemical structures of the targeted aldehyde and related solvents (analytes)

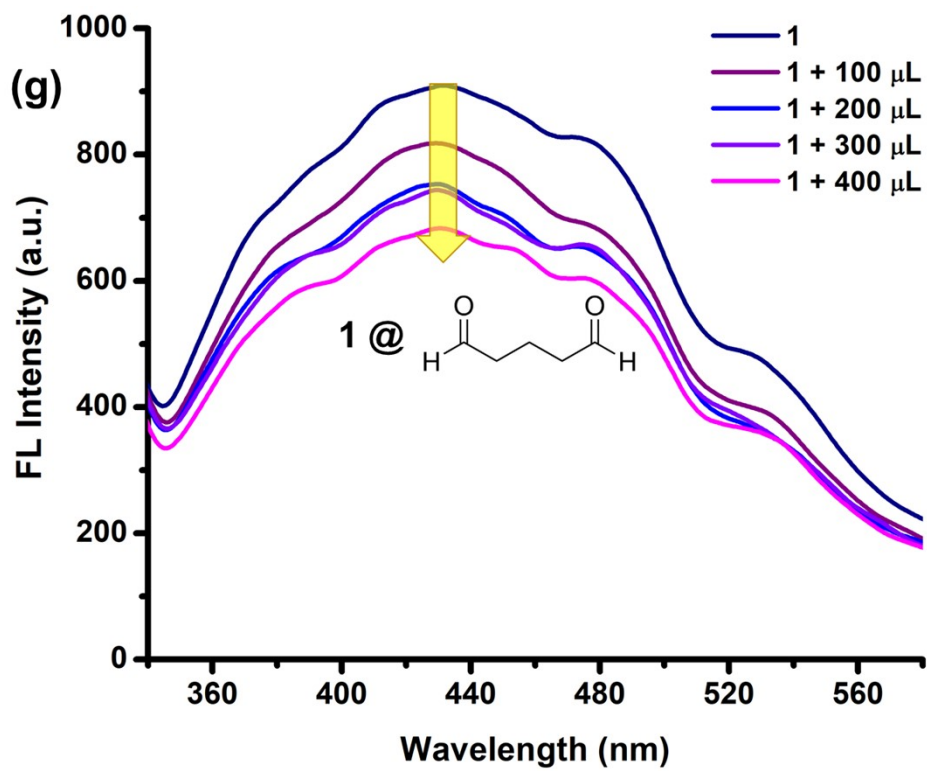
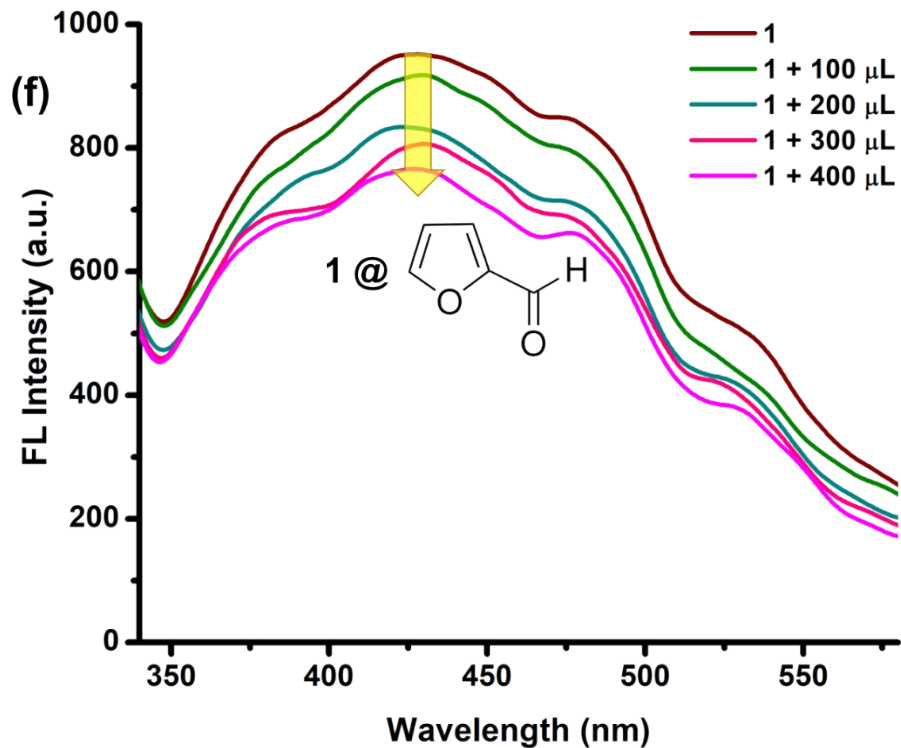


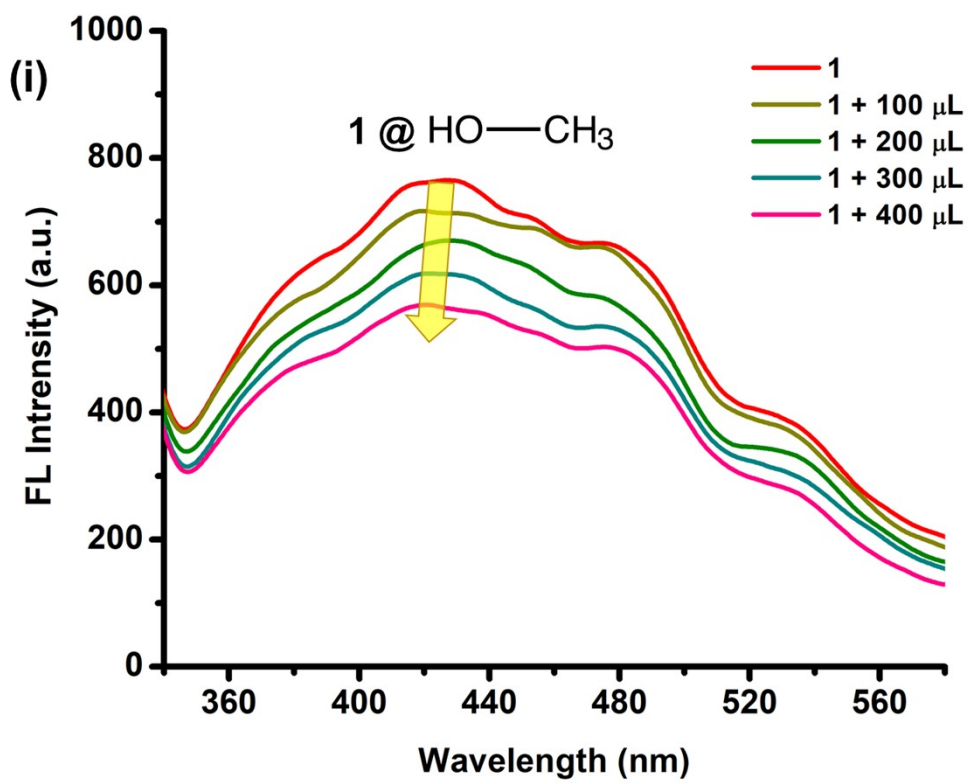
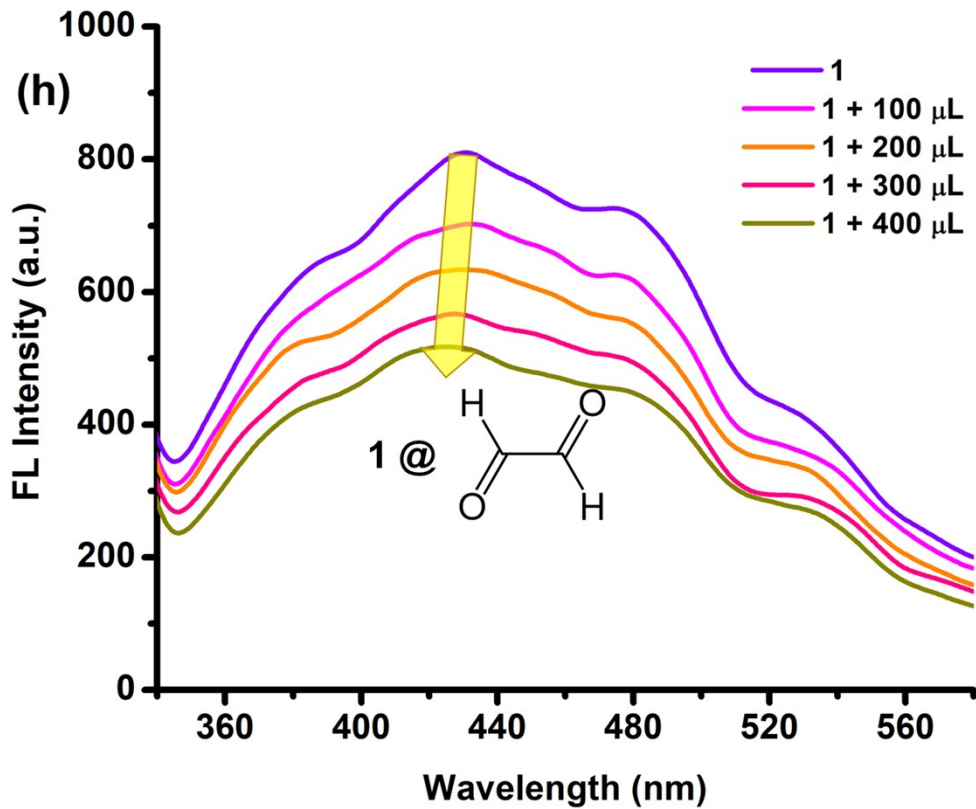
Fig S25. Physical image of the MOF-sensor (**1**) and sensor + analytes (aldehyde series) (1:1, v/v) under UV-irradiation.

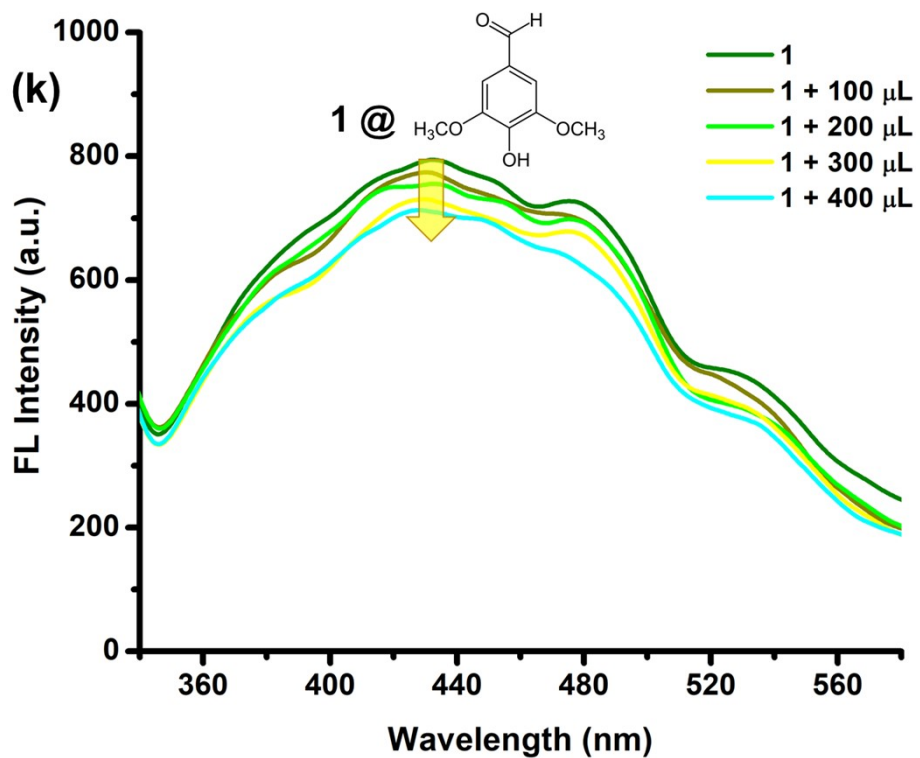
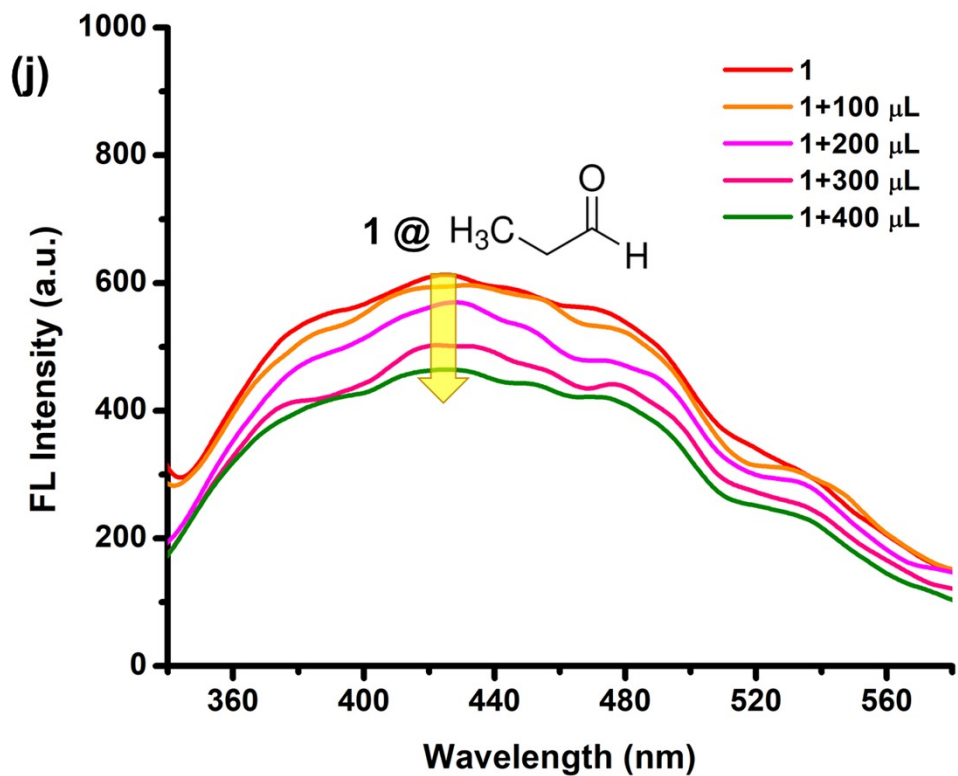












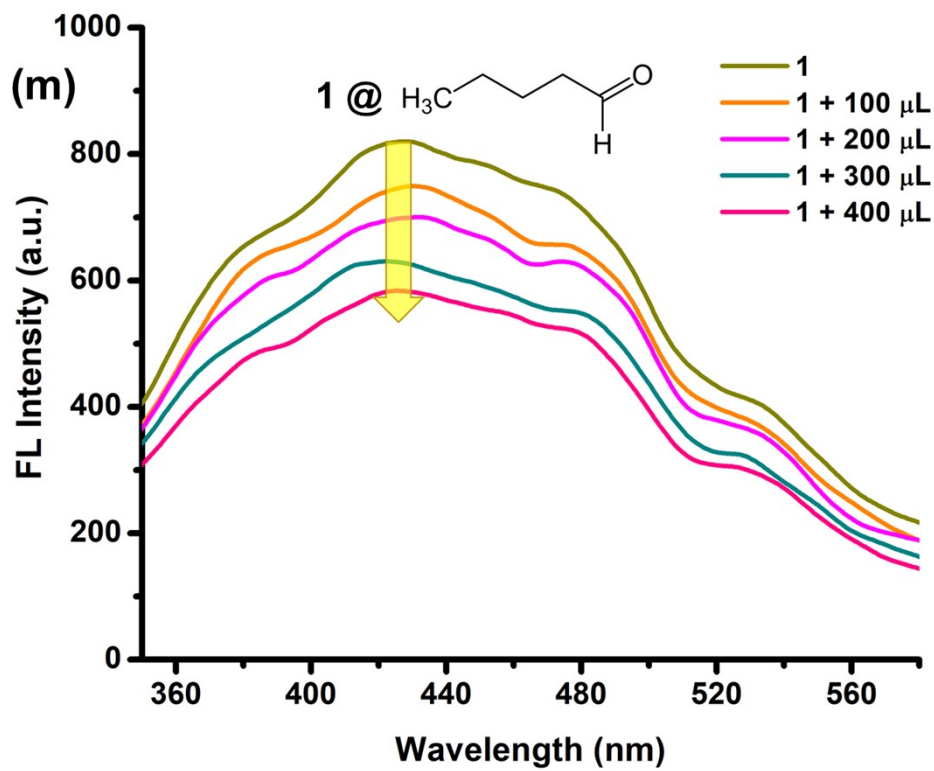
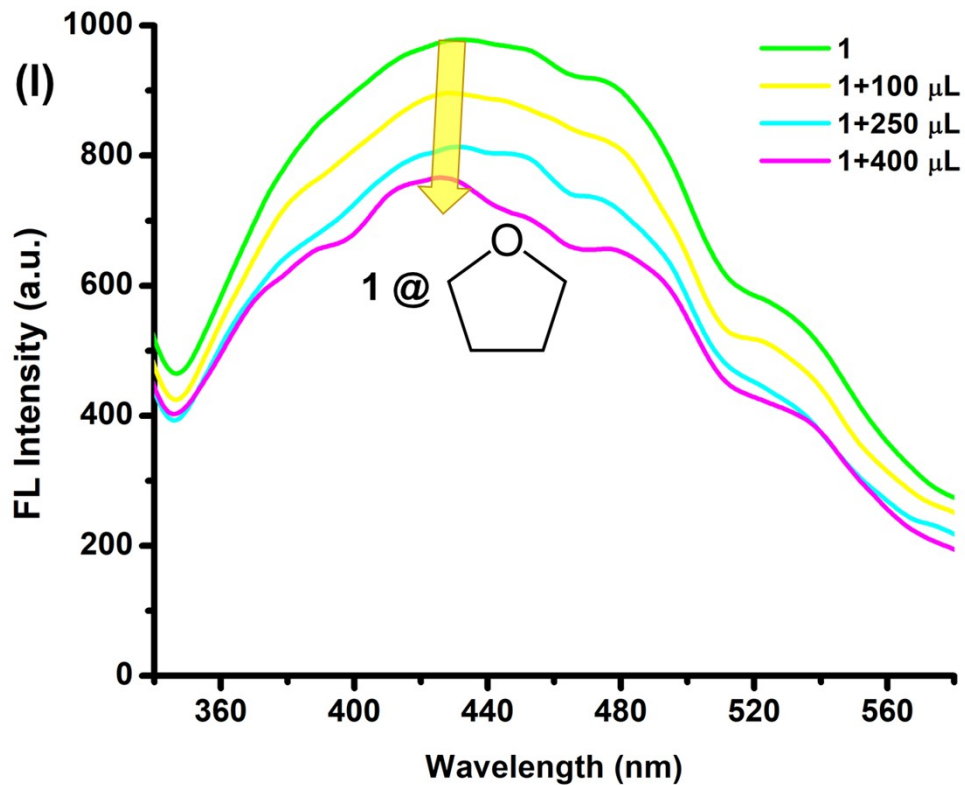


Fig S26. Emission spectra of **1** upon incremental addition of (a) acetone; (b) benzaldehyde; (c) chloroform; (d) dioxane; (e) ethanol; (f) furfural; (g) glutaraldehyde; (h) oxaldehyde; (i) methanol; (j) propionaldehyde; (k) syringaldehyde; (l) tetrahydrofuran; (m) valeraldehyde (1 mM) in water.

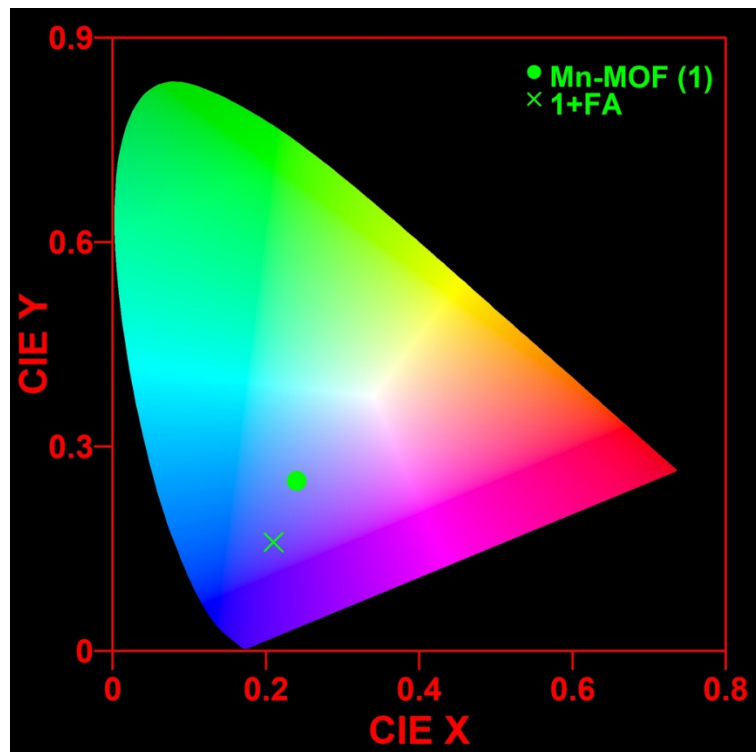


Fig S27. CIE coordinates of **1**-dispersion and **1** + HCHO, depicting a certain change.

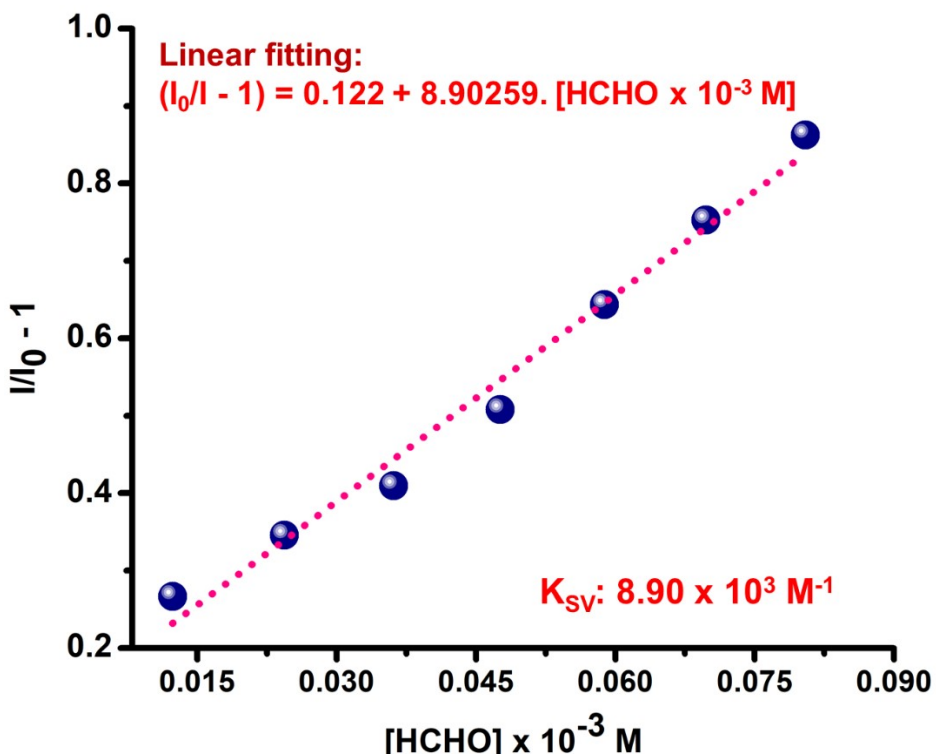


Fig S28. Linear range of the stern-volmer plot: calculation of quenching constant (K_{SV})

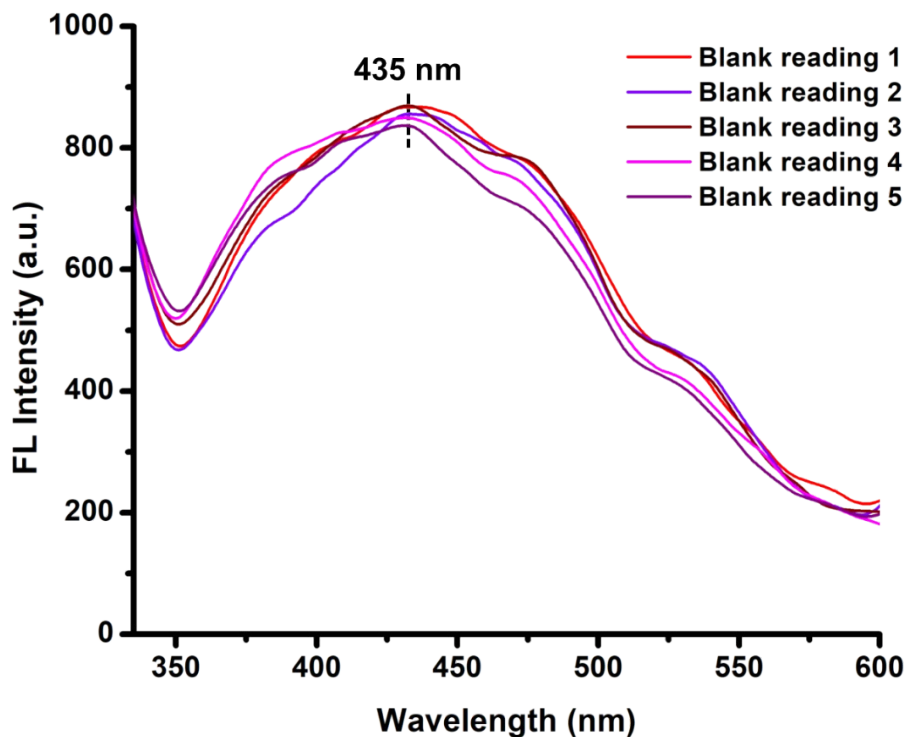


Fig S29. Blank titration: recording of the PL profile of **1** in consecutive five times (with uniform interval of ~ 1 min) and calculation of standard deviation (σ)

Table S5. Calculation of standard deviation (σ):

Blank Reading	Fl. Intensity
1	868.700
2	862.31
3	855.92
4	848.25
5	836.74
Standard Deviation (σ)	12.4405

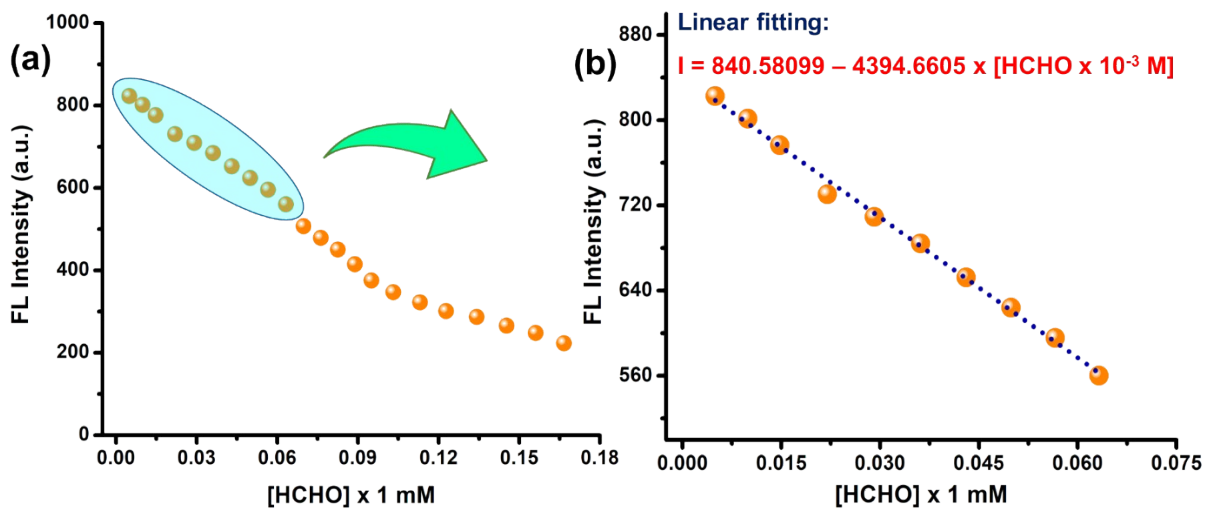


Fig S30. Plot of observed PL intensity vs equivalent concentration of FA: calculation of slope (k), to be used in $3\sigma/k$ equation

Calculation of limit of detection (LOD):

Therefore, Slope (k) = 4394.6605

Standard Deviation (σ) = 12.4405

LOD ($3\sigma/k$) = $8.49 \times 10^{-6} \text{ M} = 8.49 \mu\text{M}$ (0.25 ppm)

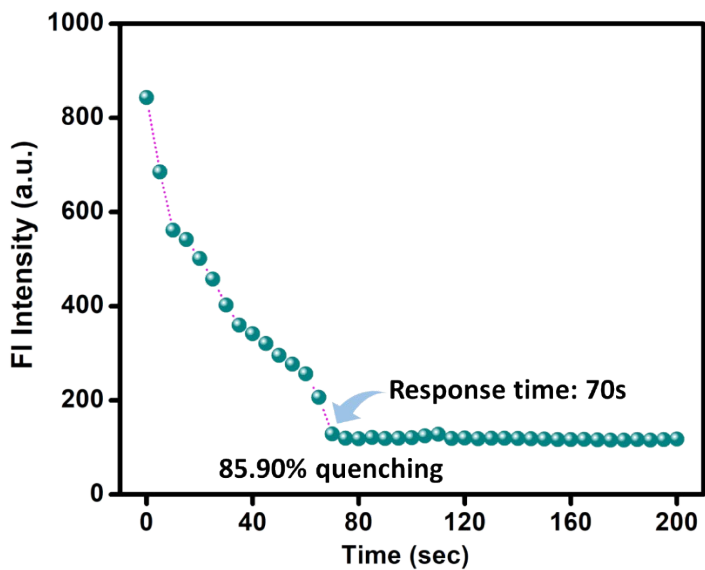


Fig S31. Fast responsive analyte (FRA) test: calculation of response time for **1** towards FA detection

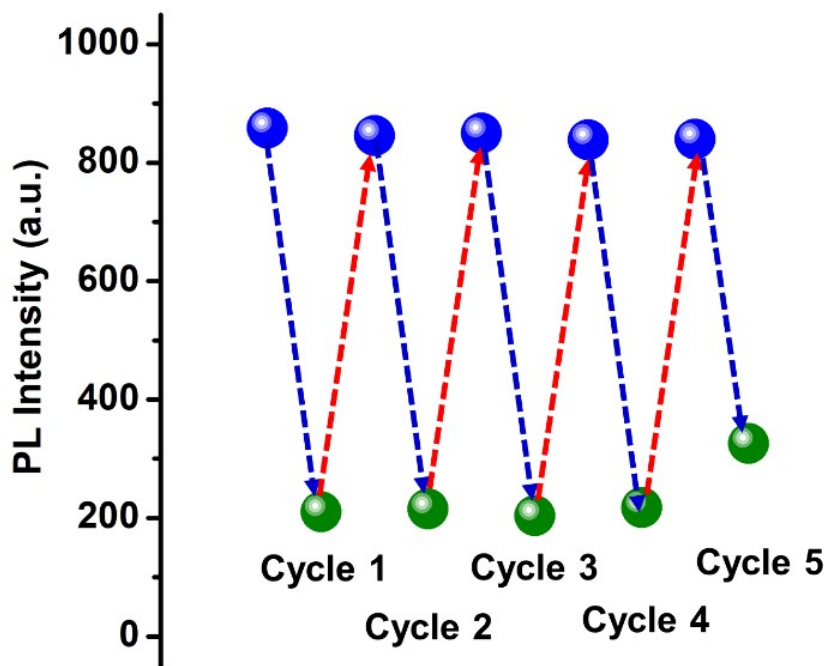


Fig S32. Four times recyclable FA sensing behaviour in **1**

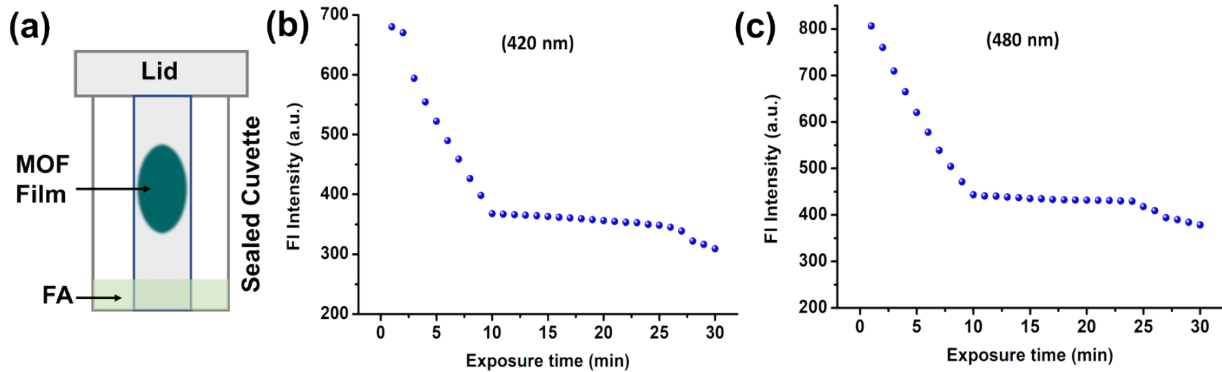


Fig S33. (a) Schematic representation of the vapor phase FA sensing set-up, (b, c) PL intensity *vs.* elapsed time plot (monitored at 420 nm and 480 nm).

Table S6. Truth Table for obtaining the logic functions (response of **1** towards FA)

Input				Output		
IN1 (SENSOR)	IN2 HCHO (10 ppm)	IN3 HCHO (15 ppm)	IN4 HCHO (25 ppm)	OUT1 (630 a.u)	OUT2 (511 a.u)	OUT3 (330 a.u)
0	0	0	0	0	0	0
1	0	0	0	0	0	0
0	1	0	0	0	0	0
0	0	1	0	0	0	0
0	0	0	1	0	0	0
1	1	0	0	1	0	0
1	0	1	0	0	1	0
1	0	0	1	0	0	1

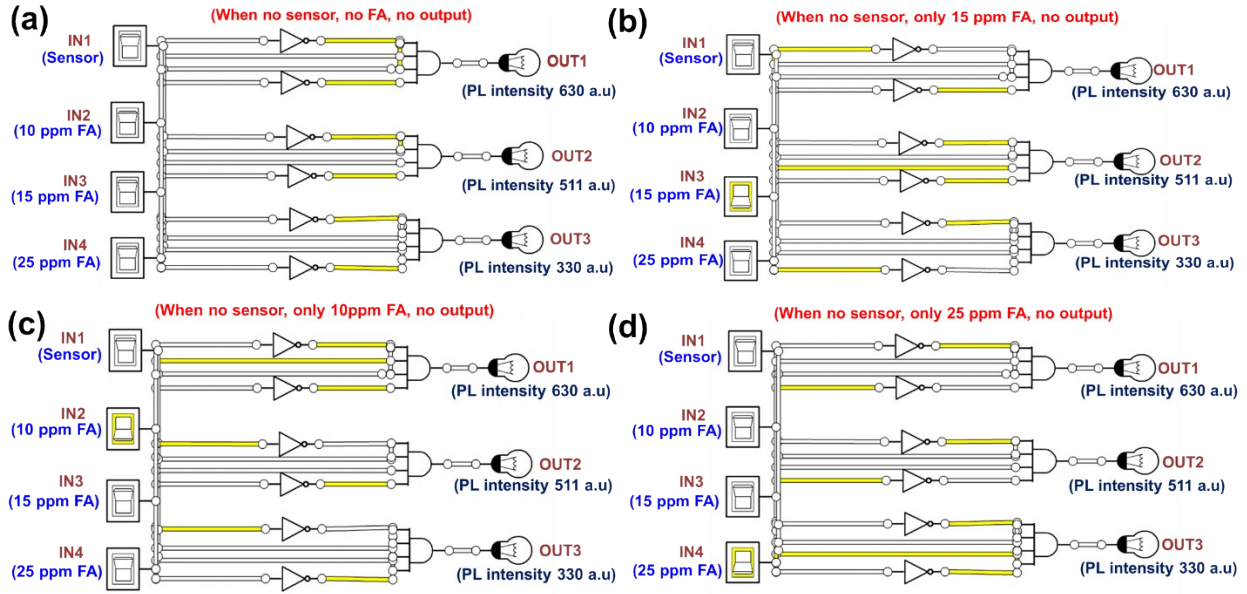
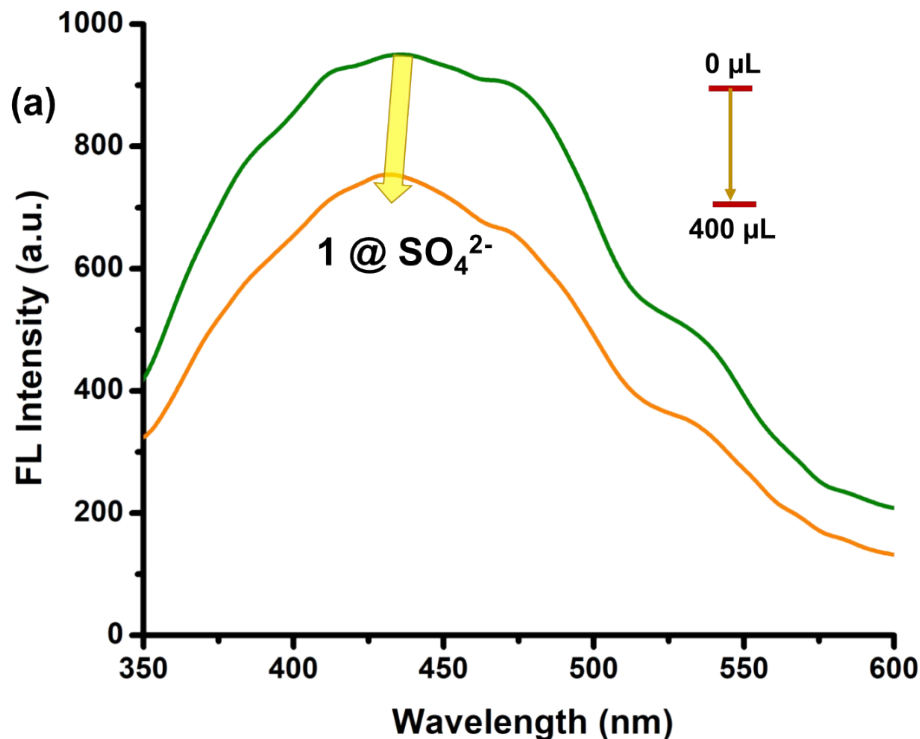
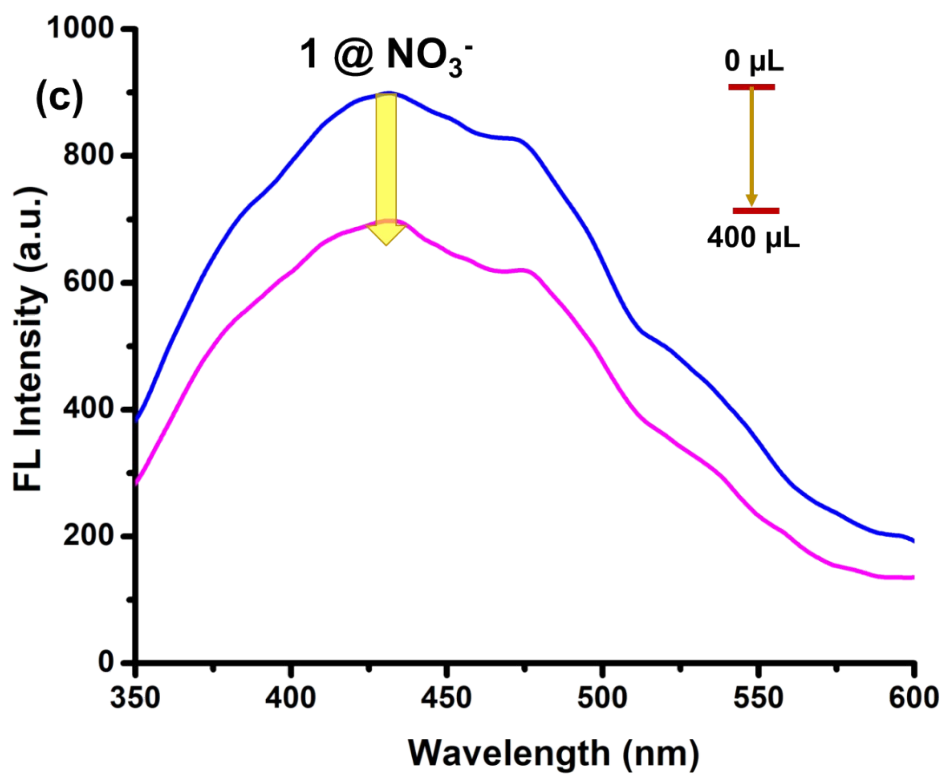
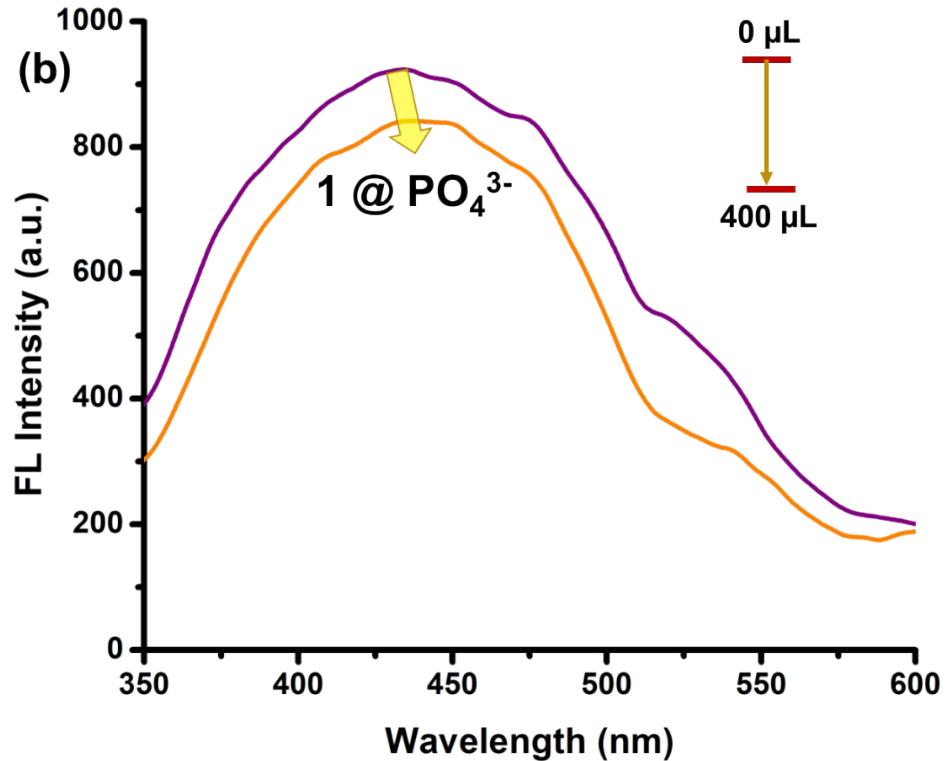
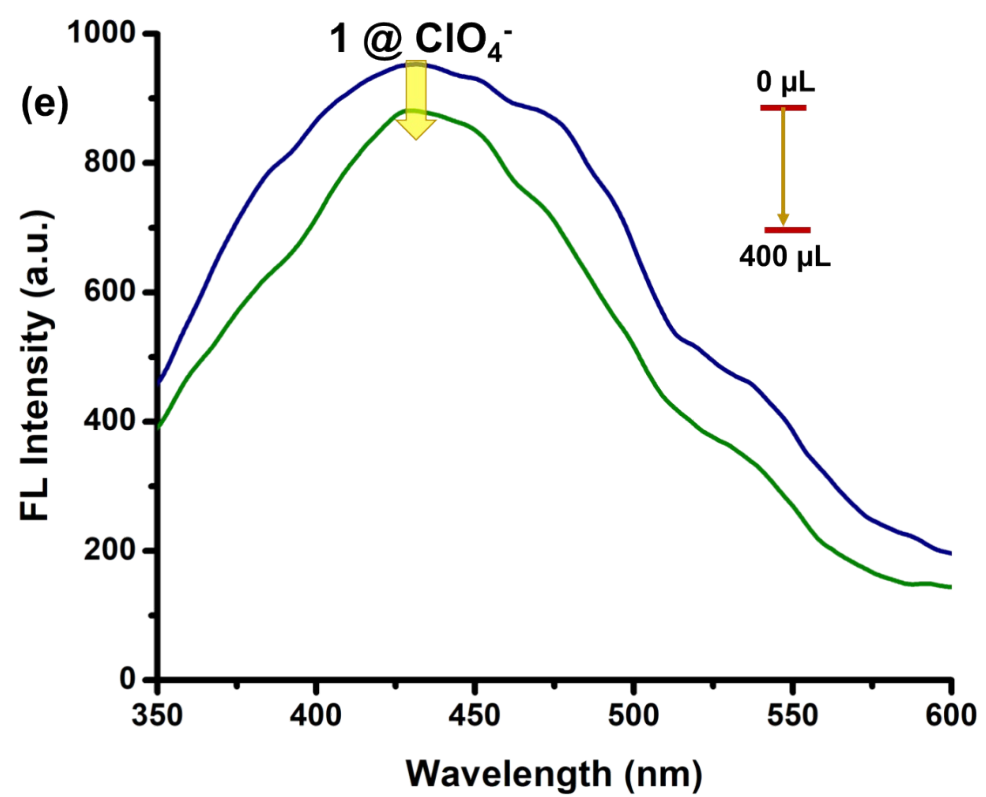
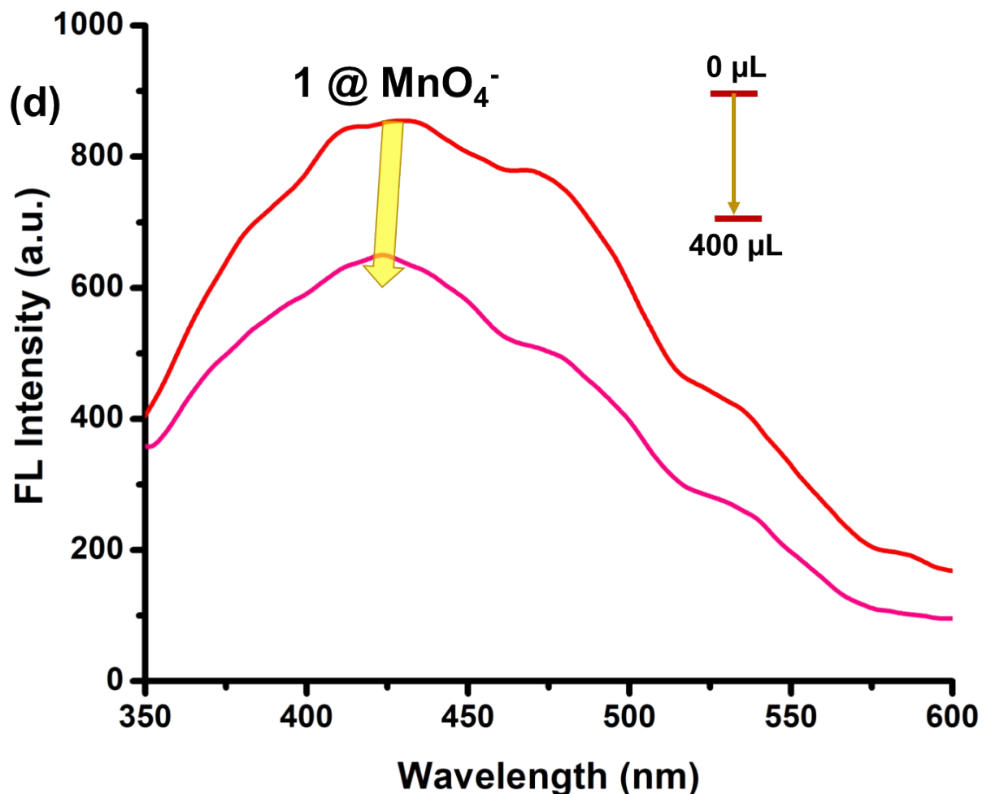
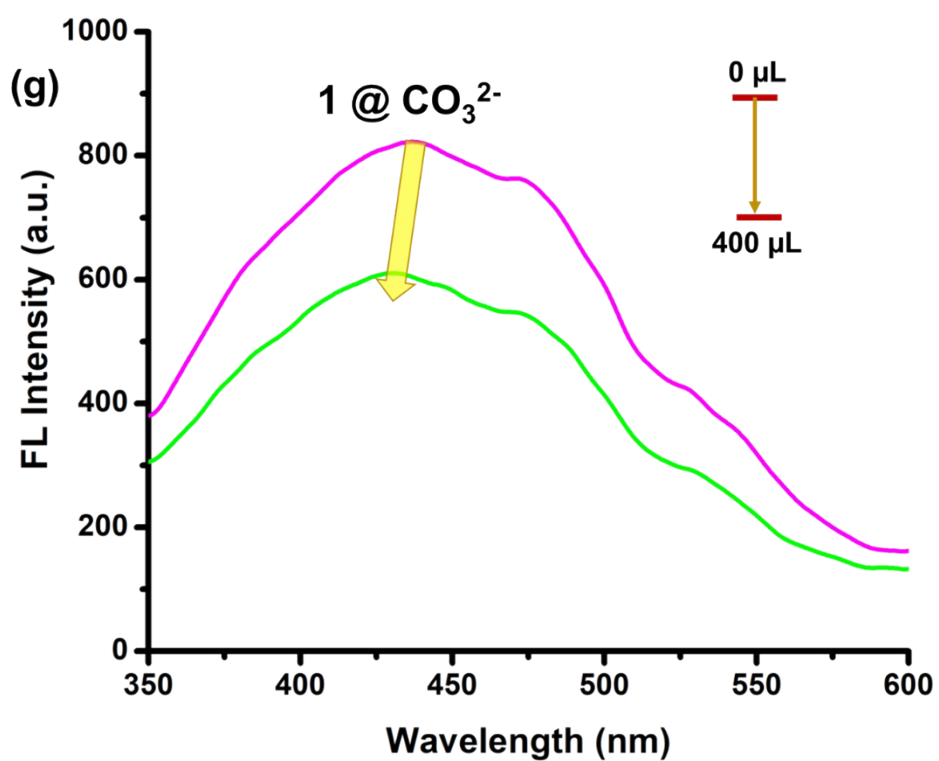
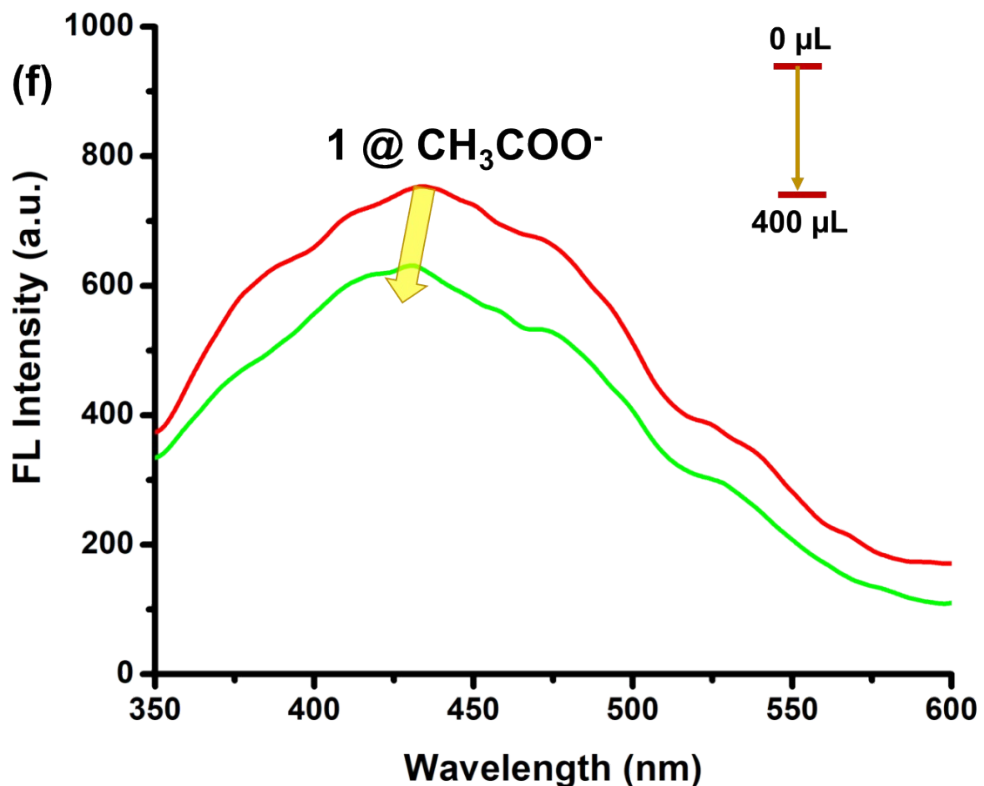


Fig S34. Fabrication of logic gate with outputs (OUT1, OUT2, OUT3) upon varying inputs (AND-NOT logic functions) for Sensor (1) with 10, 15 and 25 ppm of analyte (FA), where (a) IN1: IN2: IN3: IN4 :: 0000, (b) IN1: IN2: IN3: IN4 :: 0100, (c) IN1: IN2: IN3: IN4 :: 0010, (d) IN1: IN2: IN3: IN4 :: 0001. (see truth table *vide* Table S6, the other possibilities of IN1: IN2: IN3: IN4 :: 1000, 1100, 1010 and 1001 are given in Fig 5, main manuscript).









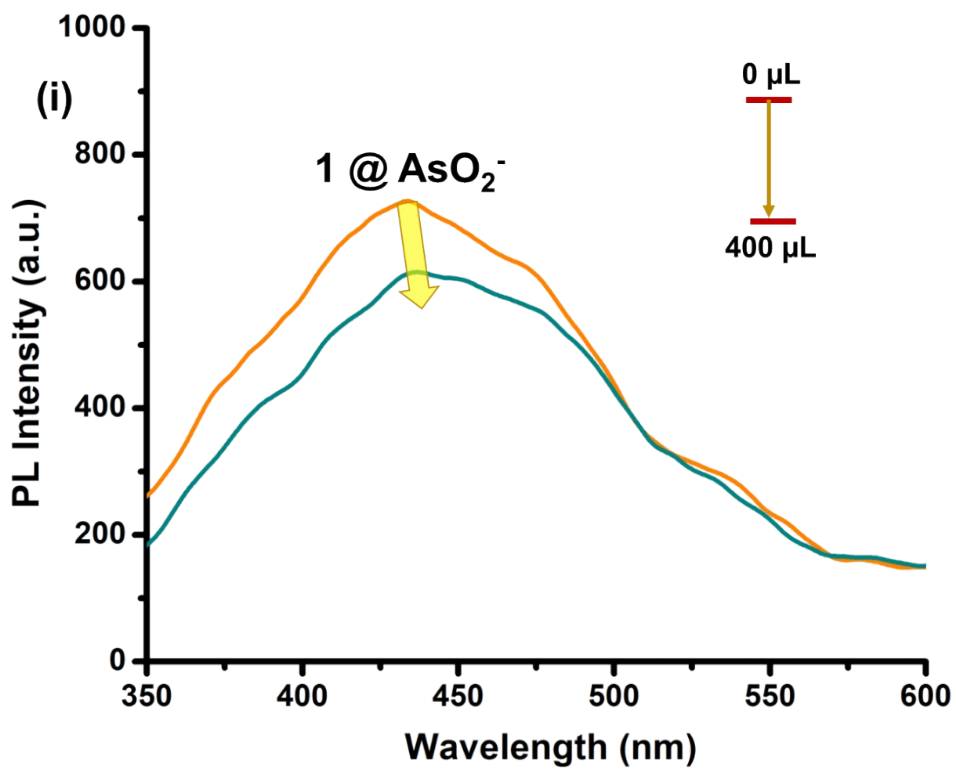
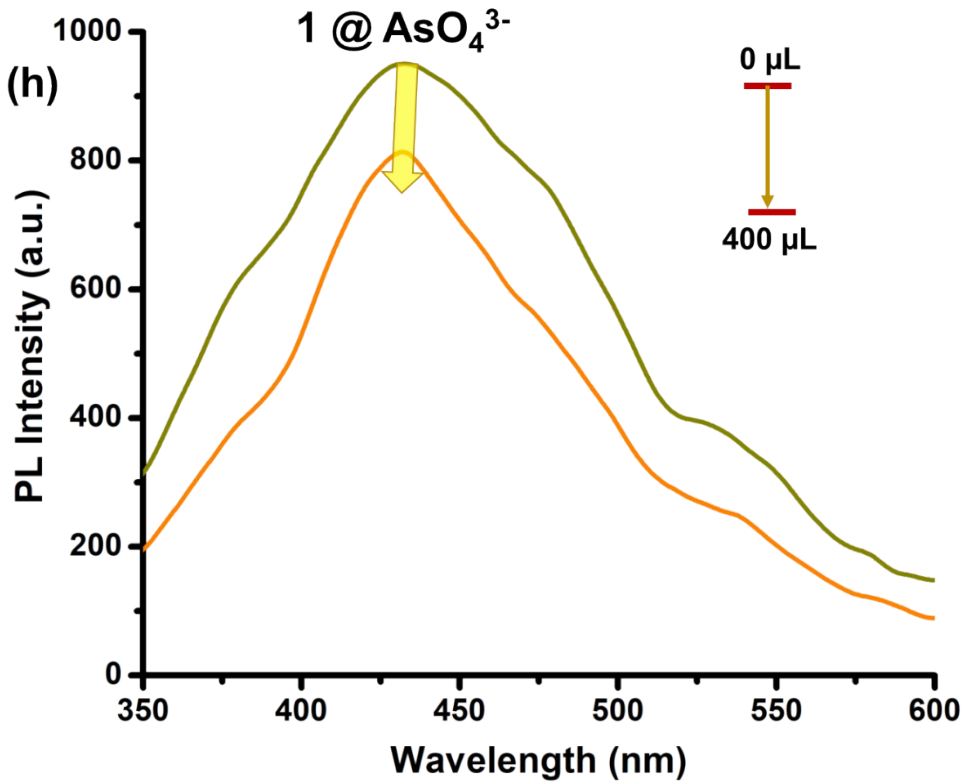


Fig S35. Diminution of the emission spectra of **1** upon incremental addition of (a) sulphate, (b) phosphate, (c) nitrate, (d) manganate, (e) perchlorate, (f) acetate, (g) carbonate, (h) arsenate, (i) arsenite (10^{-4} M) in water.

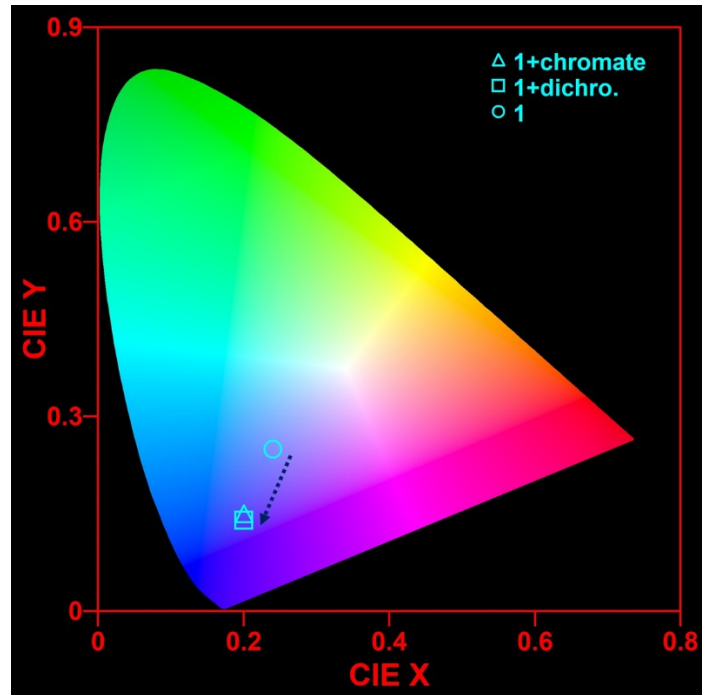


Fig S36. CIE coordinates of **1**-acetonitrile dispersion, **1** + $\text{Cr}_2\text{O}_7^{2-}$ and **1** + CrO_4^{2-} , confirming the fluorescence quenching phenomenon.

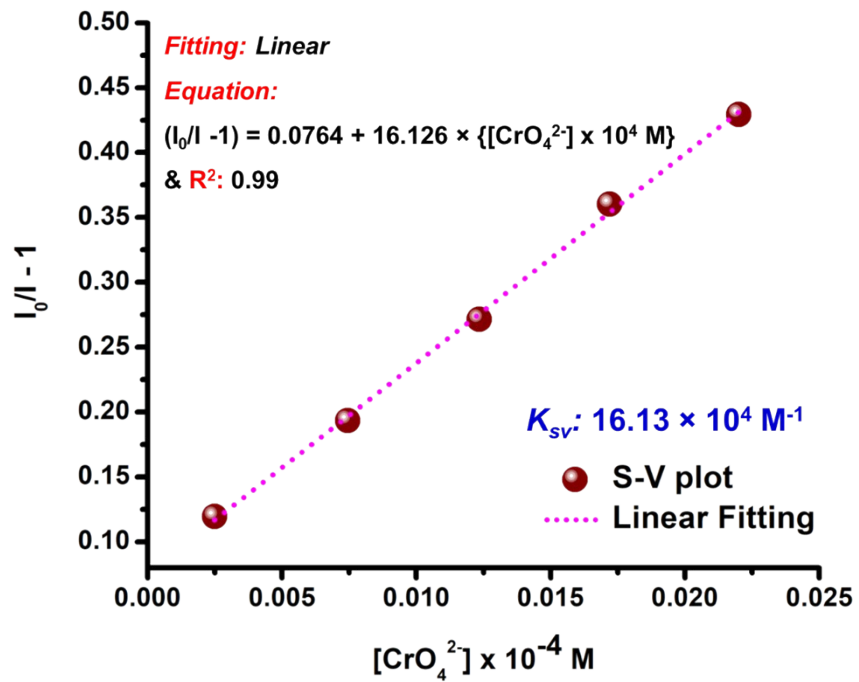


Fig S37. Linear range of the stern-volmer equation for calculation of quenching constant (K_{SV}) (for CrO_4^{2-})

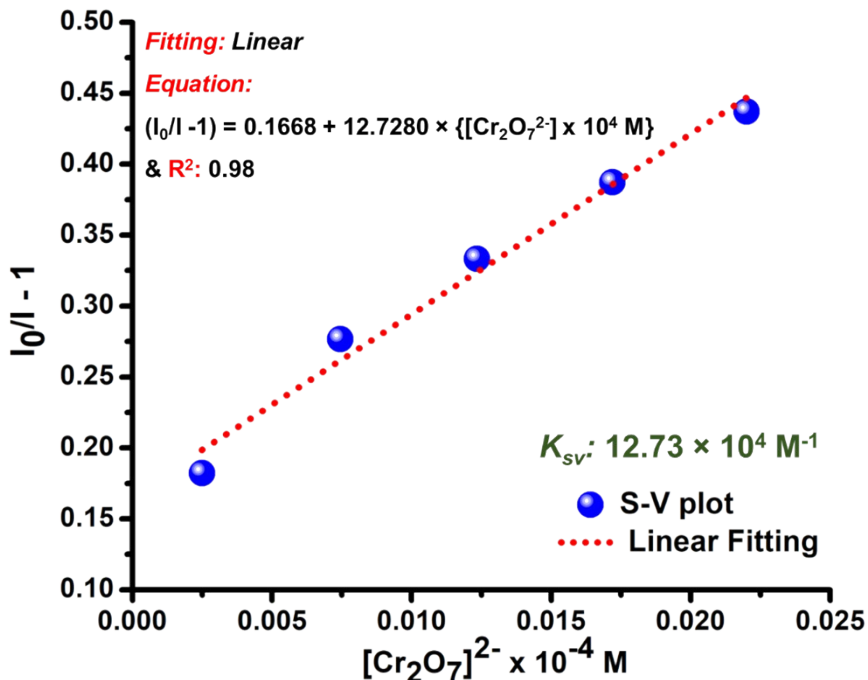


Fig S38. Linear range of the stern-volmer equation for calculation of quenching constant (K_{SV}) (for $Cr_2O_7^{2-}$)

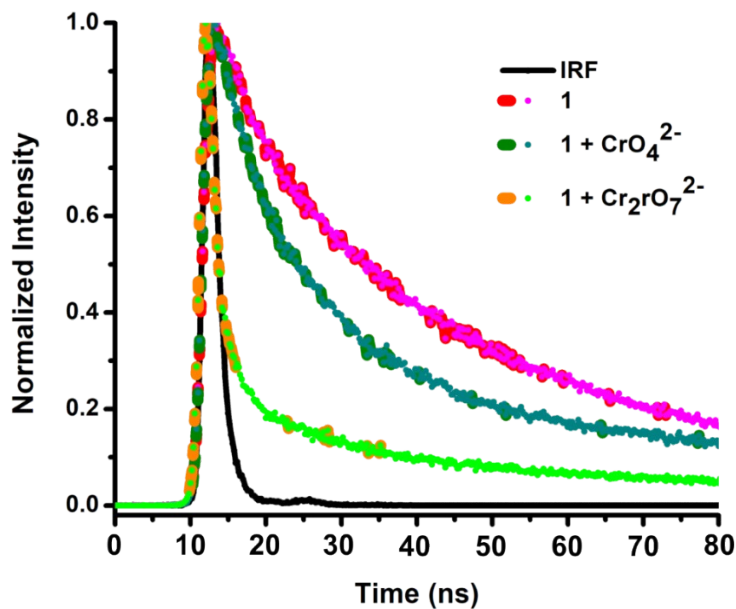


Fig S39. Lifetime decay profile of **1**, **1+CrO₄²⁻** and **1+Cr₂O₇²⁻**

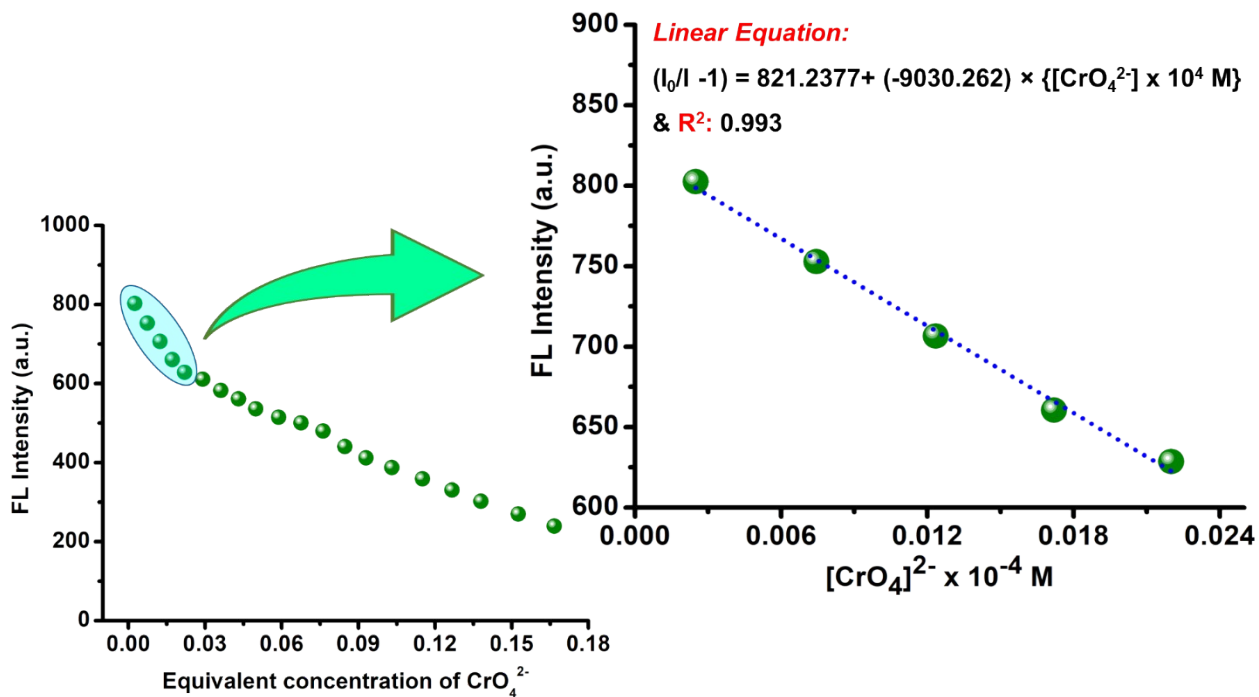


Fig S40. Plot of PL intensity *vs.* equivalent concentration of CrO₄²⁻ calculation of slope (*k*) from the linear range (lower concentration part) of the plot for evaluation of LOD.

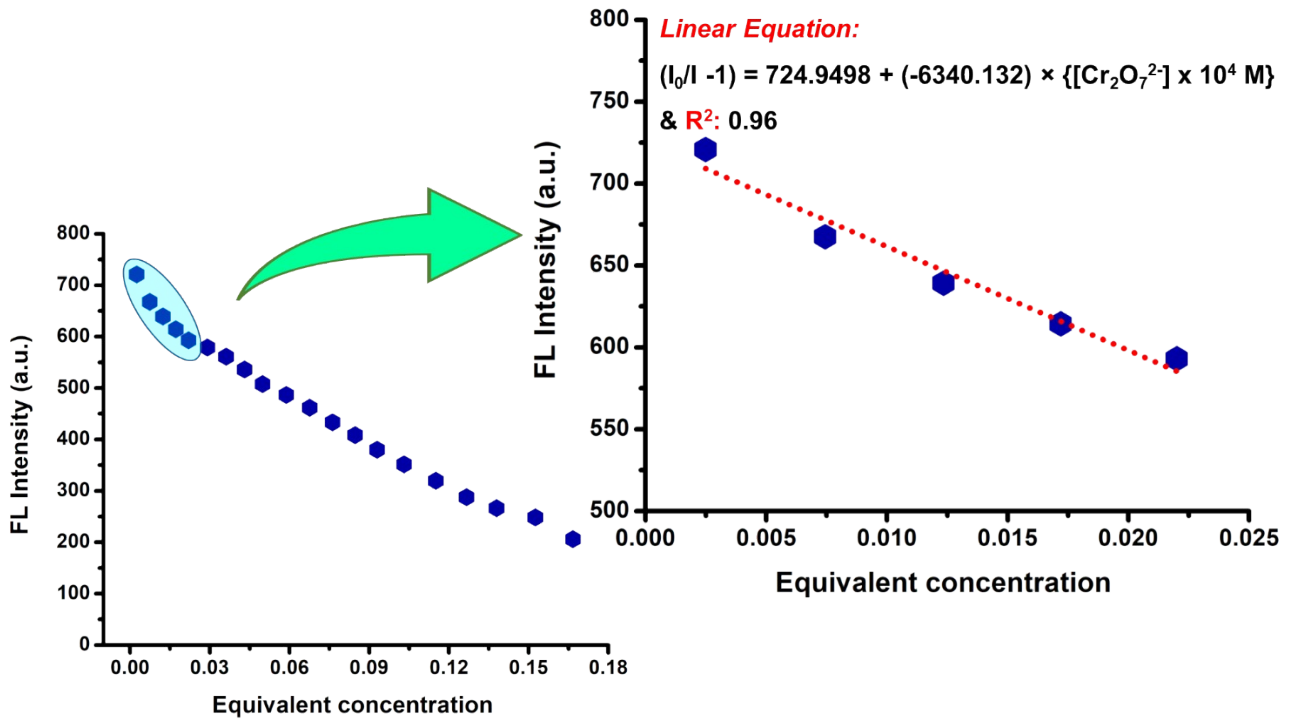


Fig S41. Plot of FL intensity vs. equivalent concentration of $\text{Cr}_2\text{O}_7^{2-}$: calculation of slope (k) from the linear range (lower concentration part) of the plot for evaluation of LOD.

Calculation of limit of detection (LoD):

1. For Chromate:

$$\text{Slope (k)} = 9030.262$$

$$\text{Standard Deviation (\sigma)} = 12.4405$$

Therefore, **LOD** (following equation: $3\sigma/k = 4.13 \times 10^{-7} \text{ M} = 0.41 \mu\text{M}$ (0.079 ppm/ 79 ppb)

2. For Dichromate:

$$\text{Slope (k)} = 6340.132$$

$$\text{Standard Deviation (\sigma)} = 12.4405 \text{ (Figure SX.)}$$

Therefore, **LOD** (following equation: $3\sigma/k = 5.89 \times 10^{-7} \text{ M} = 0.59 \mu\text{M}$ (0.17 ppm)

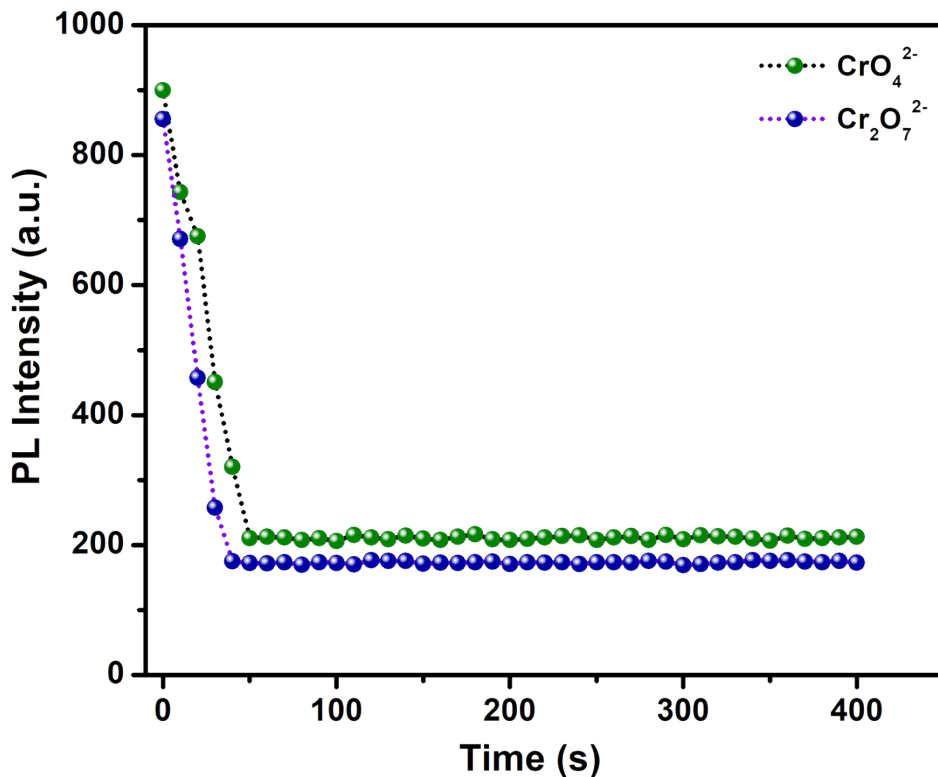


Fig S42. Response Time for CrO_4^{2-} and $\text{Cr}_2\text{O}_7^{2-}$ sensing events

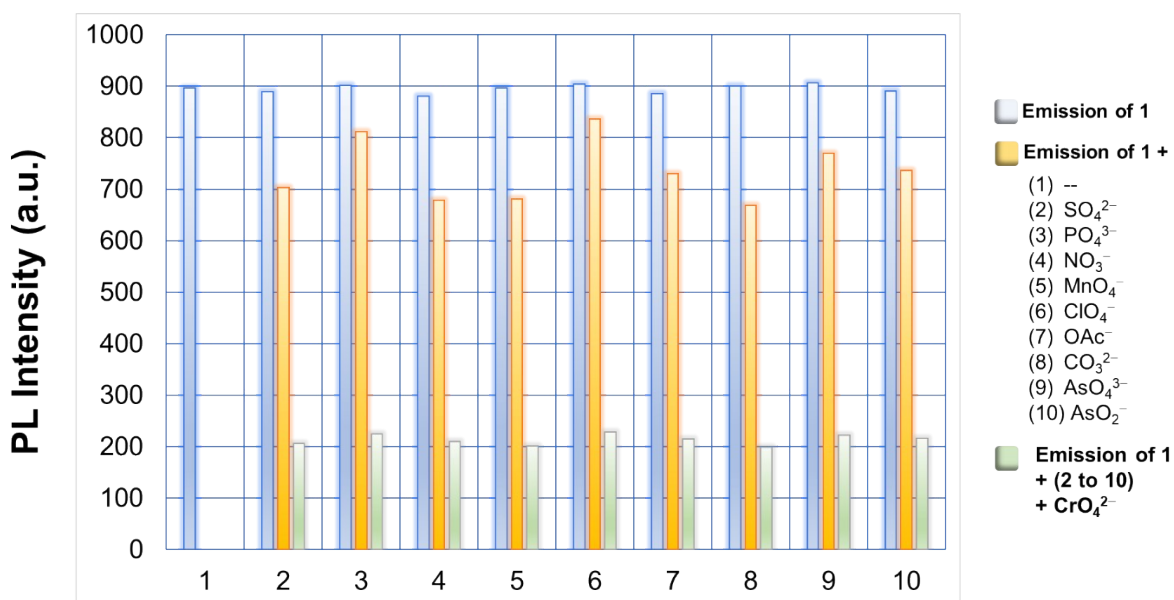


Fig S43. Cross-interference study for CrO_4^{2-} : PL intensities of **1**, **1** + other competing analytes (oxyanions), **1** + competing oxyanions + CrO_4^{2-}

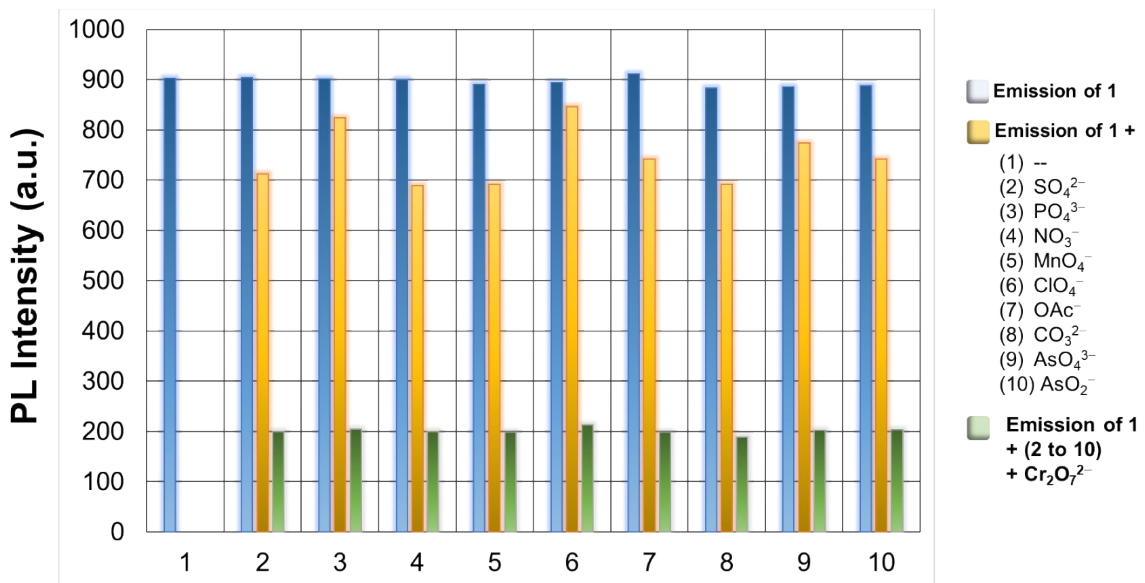


Fig S44. Cross-interference study for Cr₂O₇²⁻: PL intensities of **1**, **1** + other competing analytes (oxyanions), **1** + competing oxyanions + Cr₂O₇²⁻

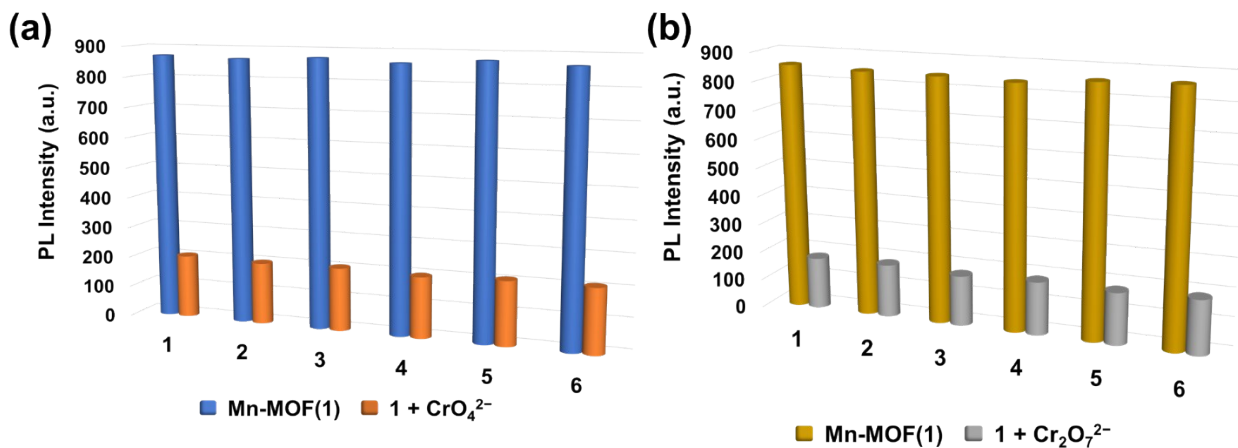


Fig S45. Rejuvenation of the PL profile of **1**·analyte adduct after centrifugation and drying: showing six times recyclable luminescence behaviour, for (a) CrO₄²⁻ and (b) Cr₂O₇²⁻

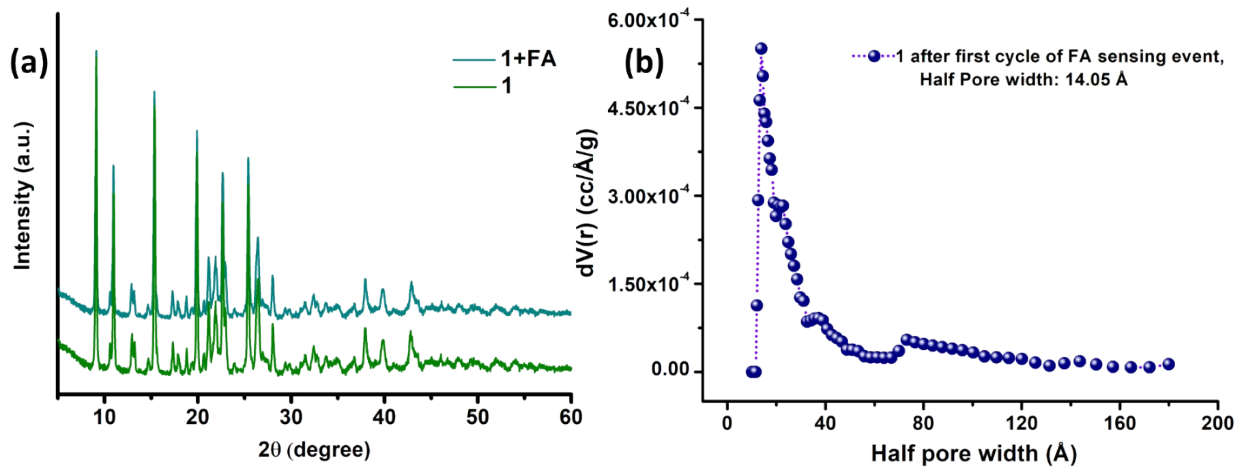


Fig S46. (a) superimposing of PXRD pattern of **1** before and after the first cycle of FA sensing event; (b) NLDFT pore size analysis of dried **1** after FA sensing event, from N_2 ads-des study

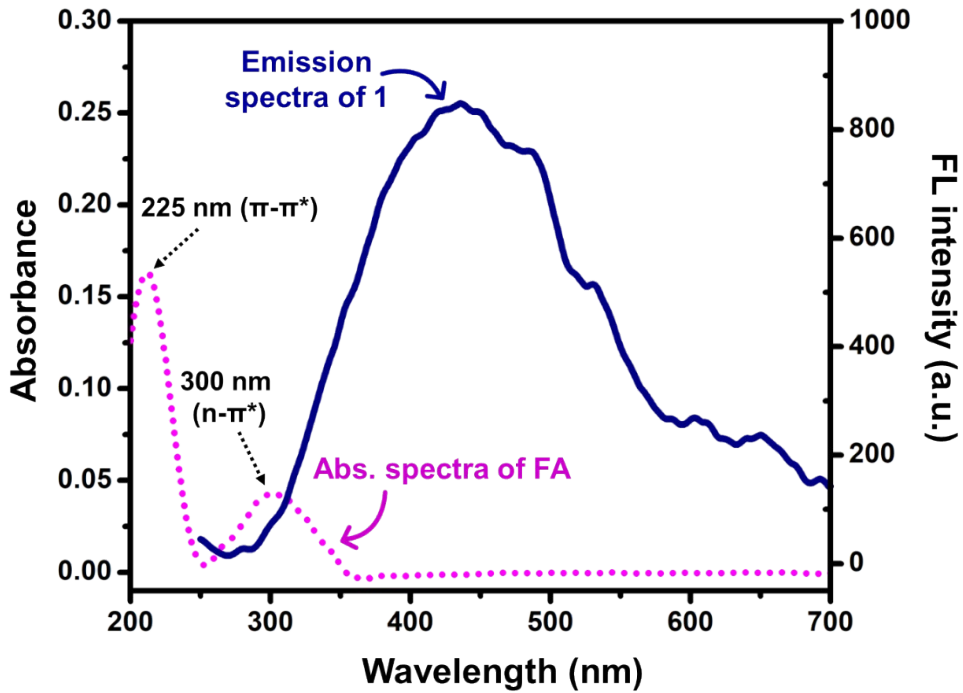


Fig S47. Overlapping of the absorption spectra of FA and emission spectra of **1**

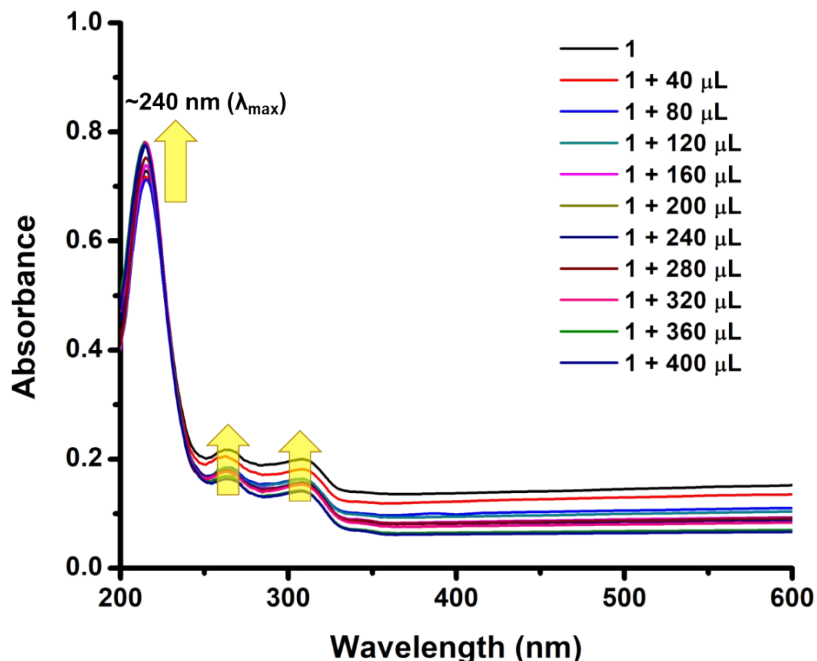


Fig S48. UV-Vis spectra of **1** during gradual addition of 1 mM FA

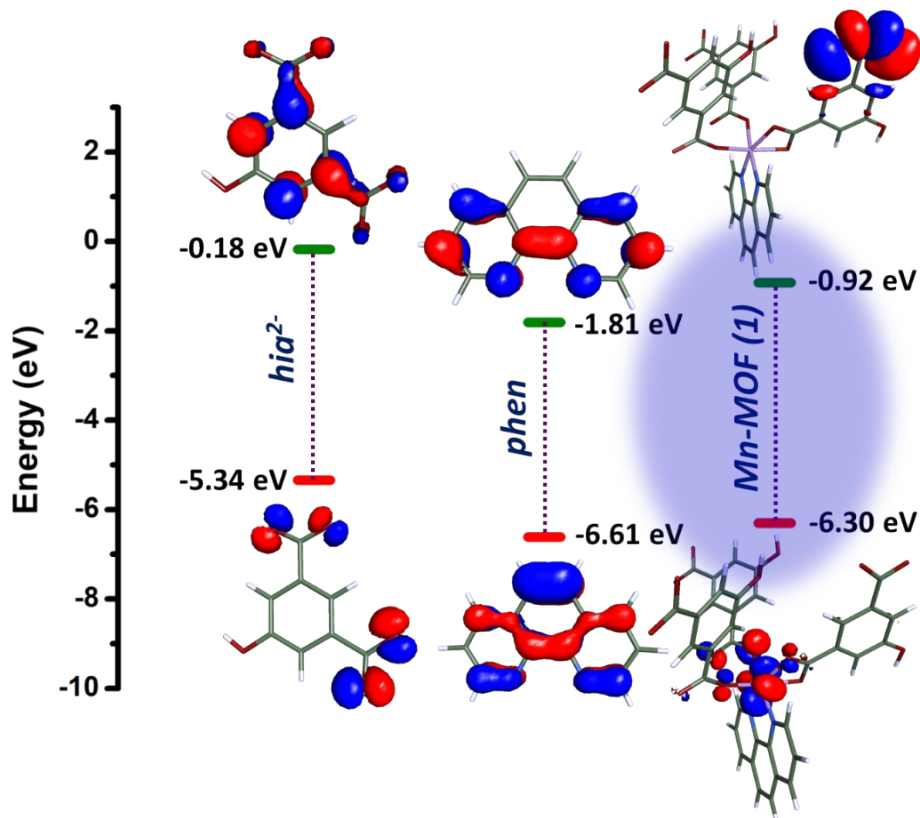


Fig S49. HOMO, LUMO energy levels and depiction of orbital lobes for struts (hia^{2-} and *phen*) and Mn-MOF (**1**)

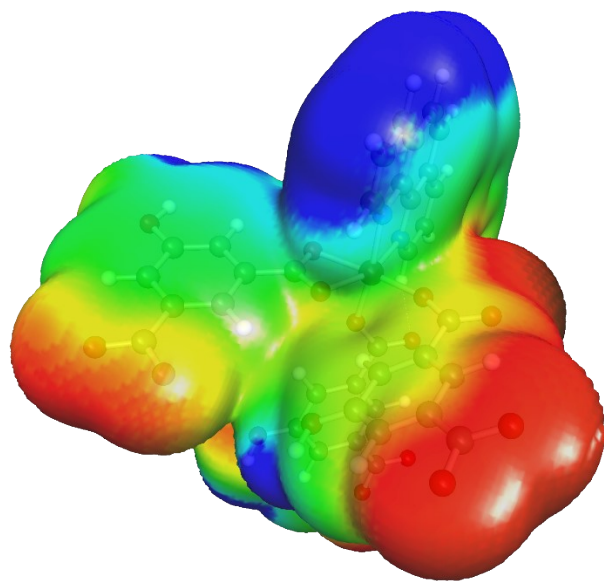
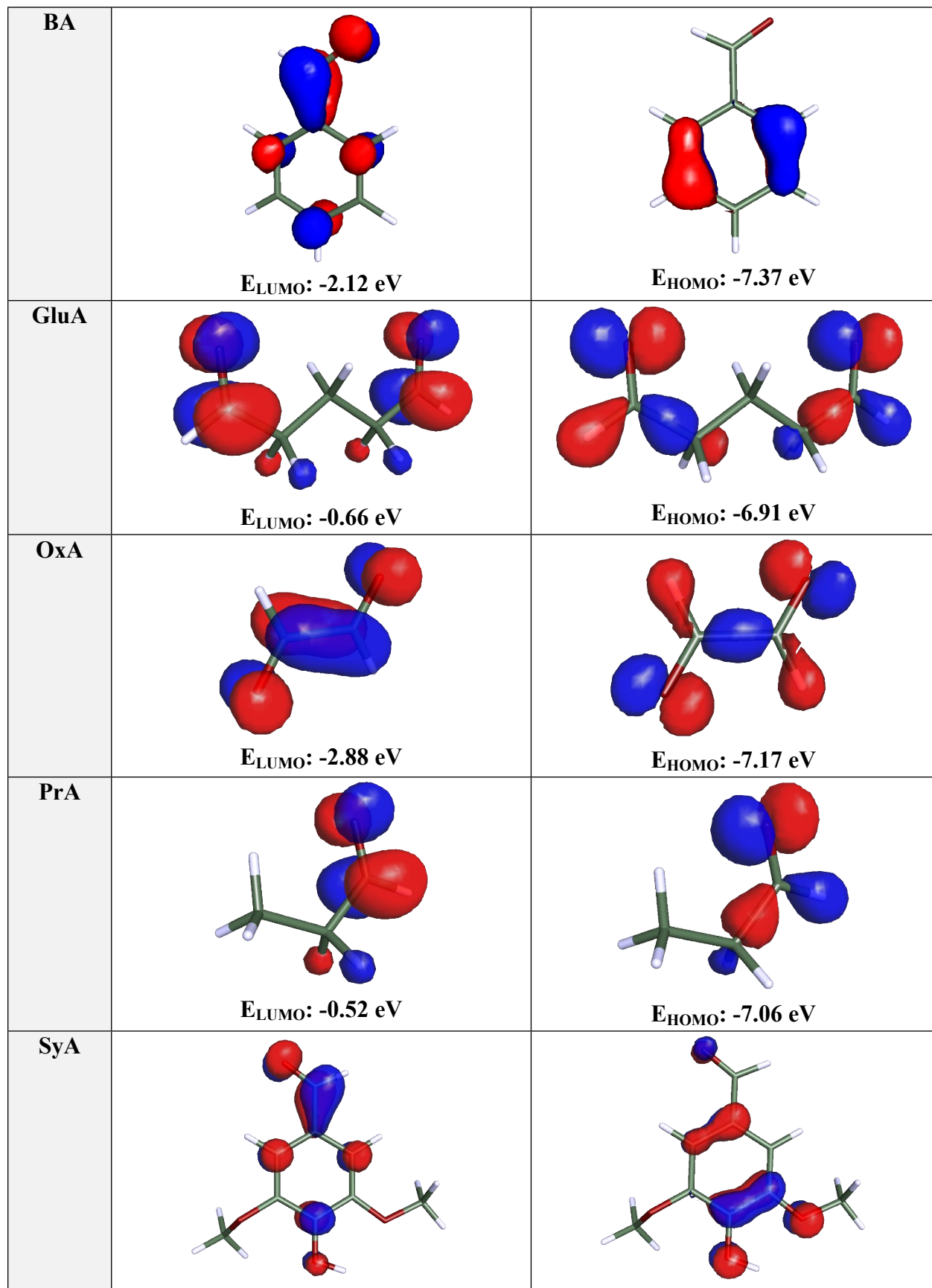
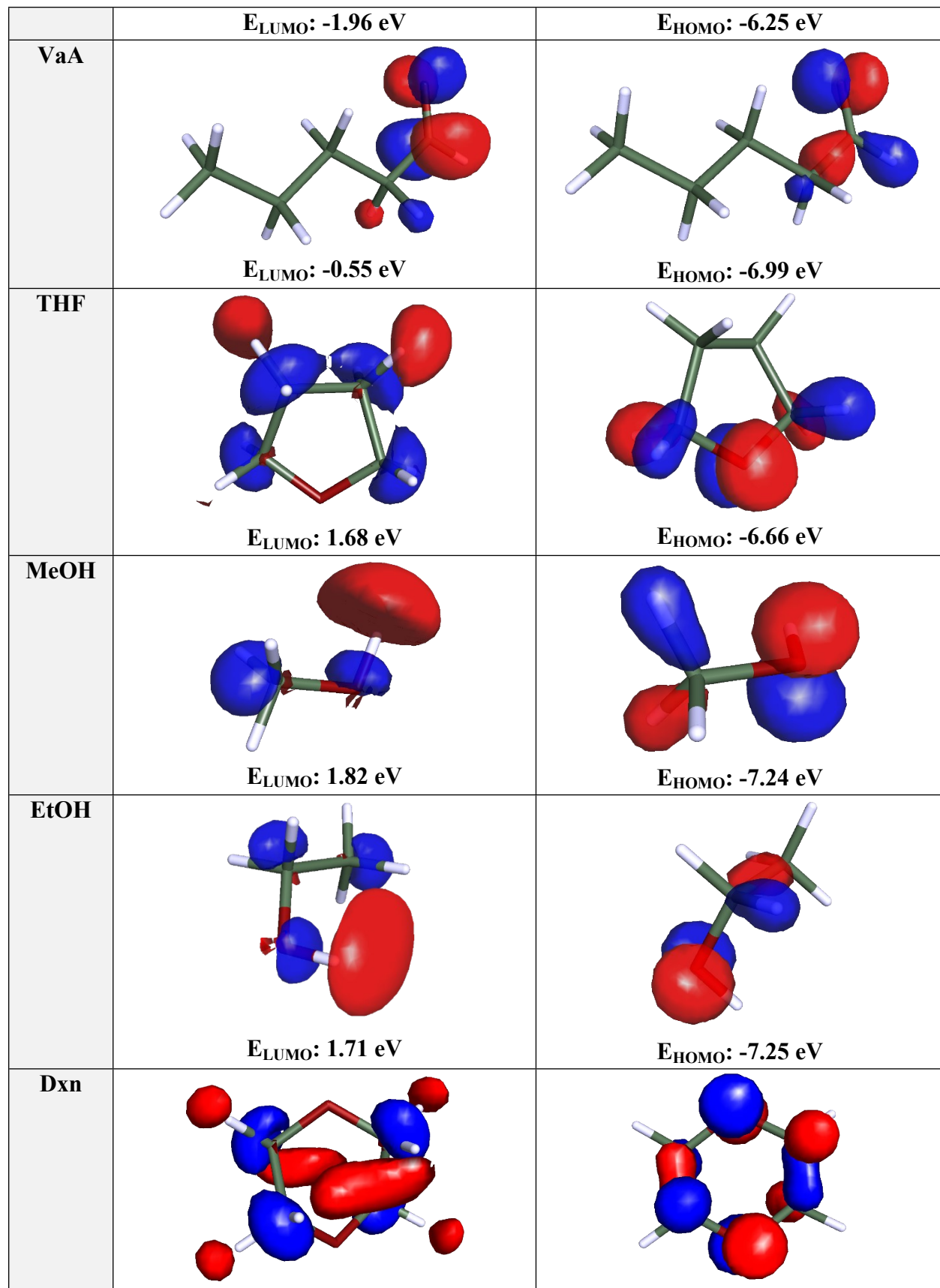


Fig S50. Electrostatic potential (ESP) surface of **1**

Table S7. HOMO, LUMO energy levels and orbital lobes for aldehydes and common organosolvents considered as analytes:

Analyte	LUMO (eV)	HOMO (eV)
FA	 $E_{\text{LUMO}}: -1.03 \text{ eV}$	 $E_{\text{HOMO}}: -7.24 \text{ eV}$
FuA	 $E_{\text{LUMO}}: -2.08 \text{ eV}$	 $E_{\text{HOMO}}: -6.99 \text{ eV}$





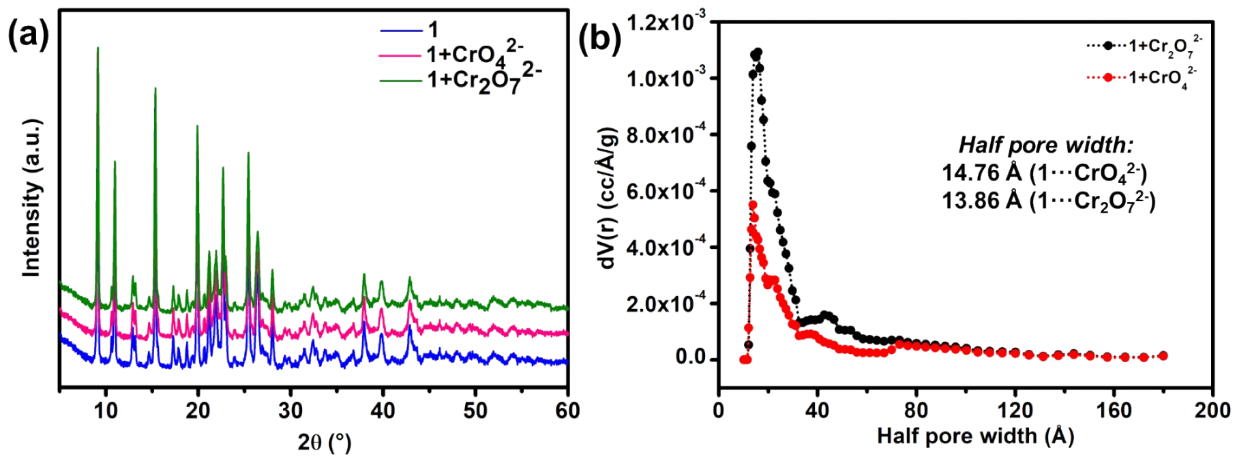
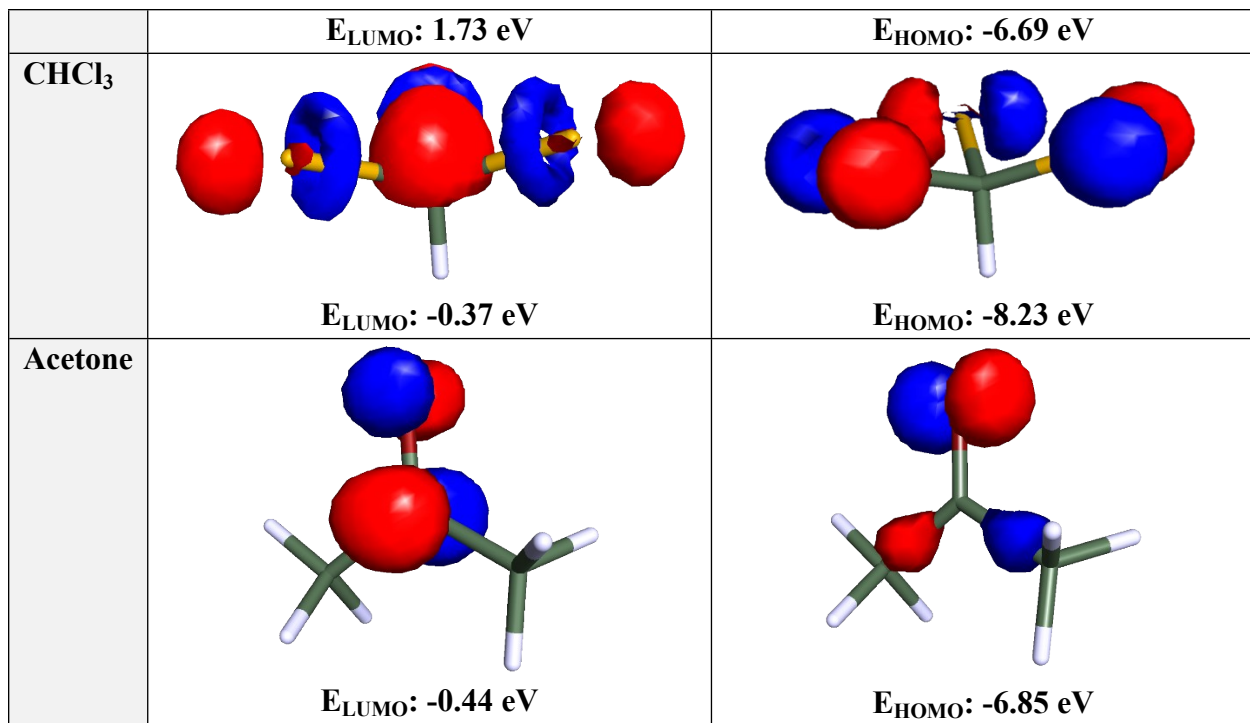


Fig S51. PXRD pattern and NLDFT Half pore width calculation of **1**, **1**••• CrO_4^{2-} and **1**••• $\text{Cr}_2\text{O}_7^{2-}$

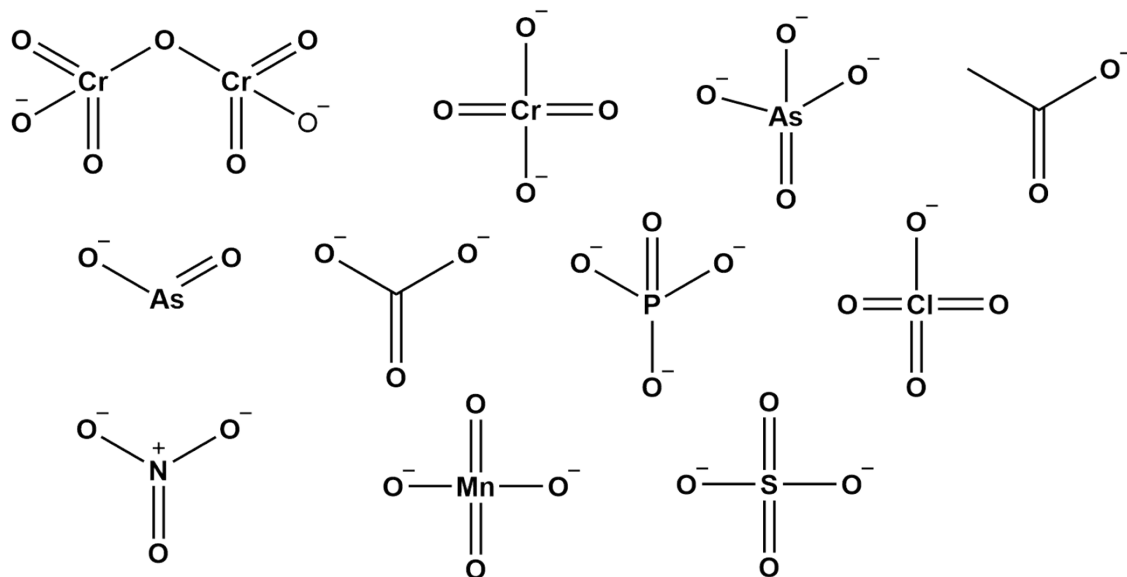
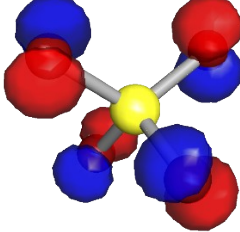
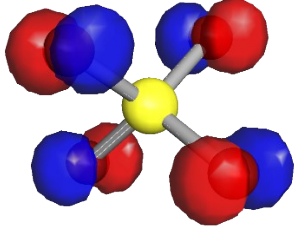
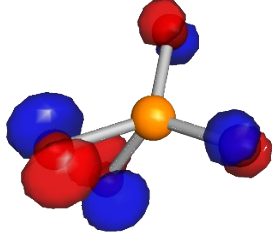
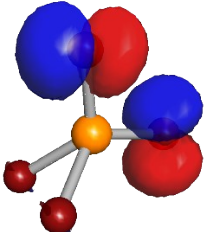
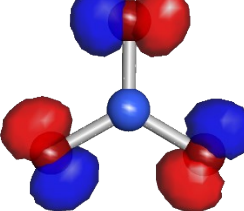
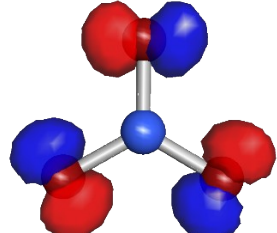


Fig S52. Chemical structure of oxyanions used for DFT calculations

Table S8. HOMO, LUMO energy levels and orbital lobes for oxo-anions:

Analyte	HOMO (eV)	LUMO (eV)
SO_4^{2-}	 -9.85 eV	 -8.44 eV
PO_4^{3-}	 -9.02 eV	 -6.42 eV
NO_3^-		

	-8.42 eV	-7.16 eV
MnO_4^-	 -9.27 eV	 -6.27 eV
ClO_4^-	 -8.50 eV	 -5.24 eV
CH_3COO^-	 -7.36 eV	 -5.99 eV
CrO_4^{2-}	 -9.87 eV	 -6.82 eV
CO_3^{2-}	 -9.05 eV	 -8.23 eV

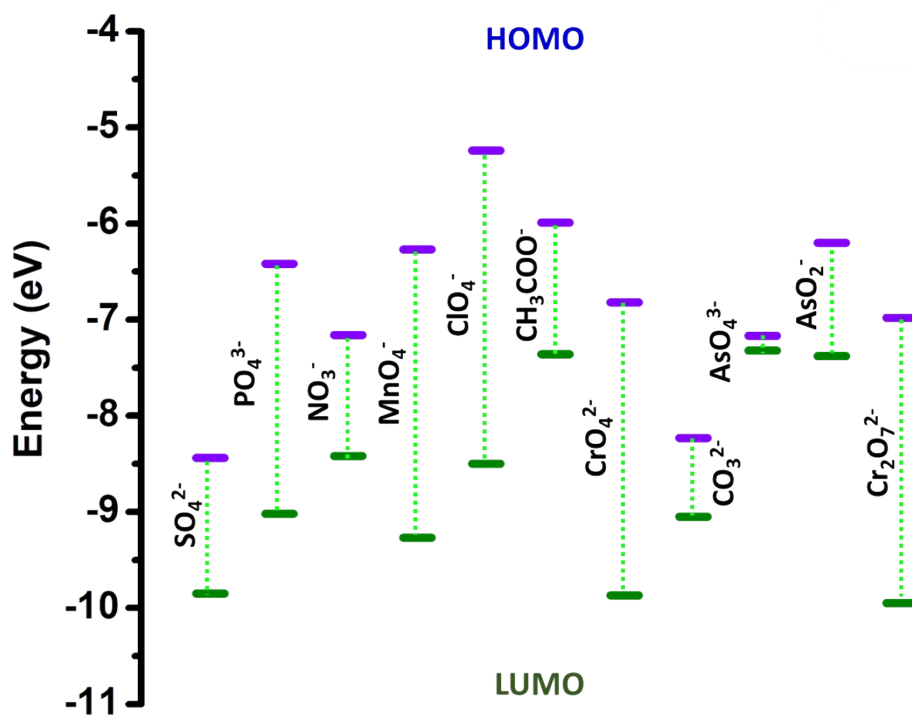
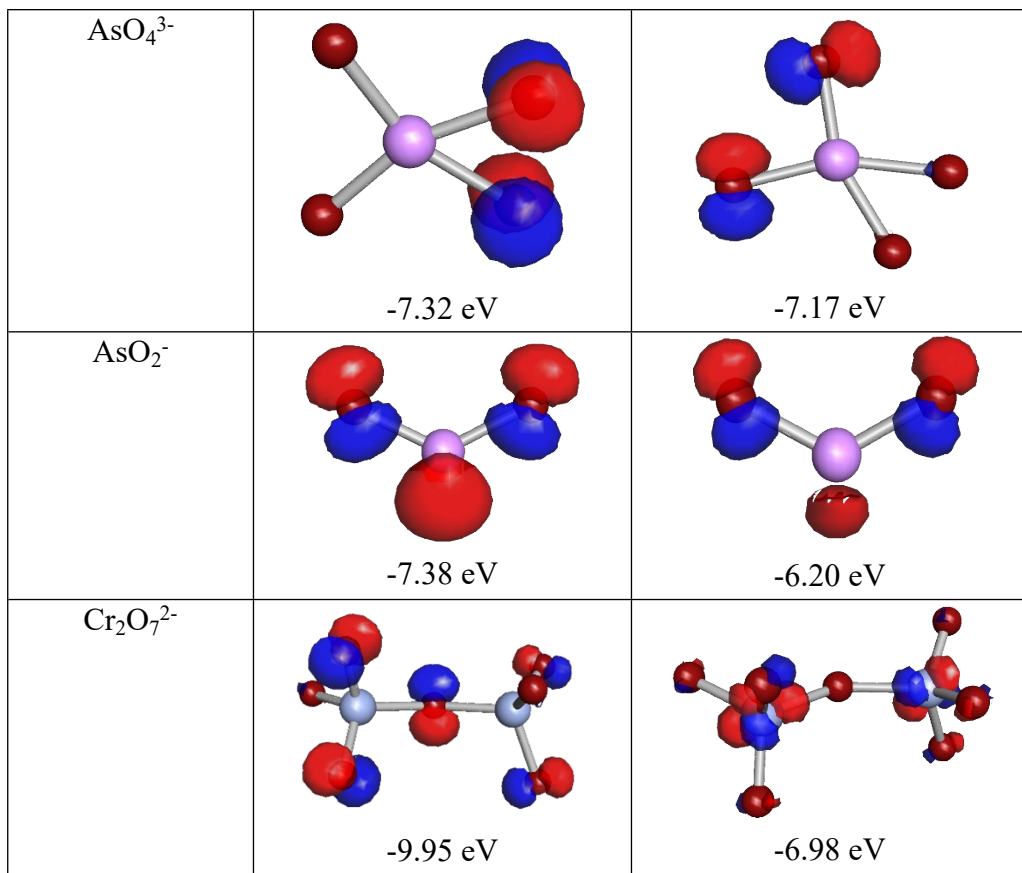


Fig S53. Graphical comparison of the HOMO and LUMO energy levels of oxoanions

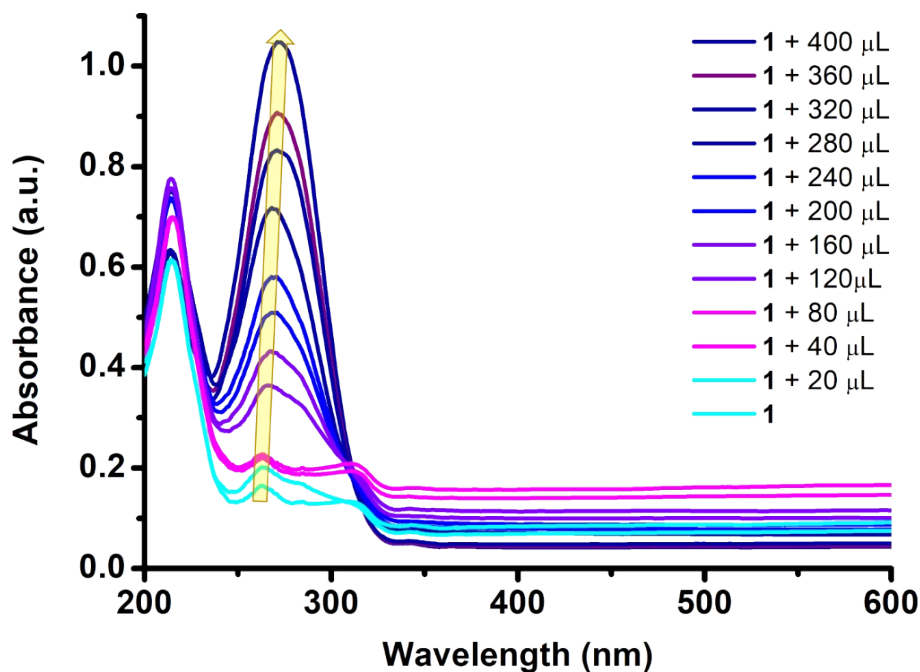


Fig S54. UV-Vis spectra of **1** during gradual addition of 10^{-4} M 400 μL CrO_4^{2-}

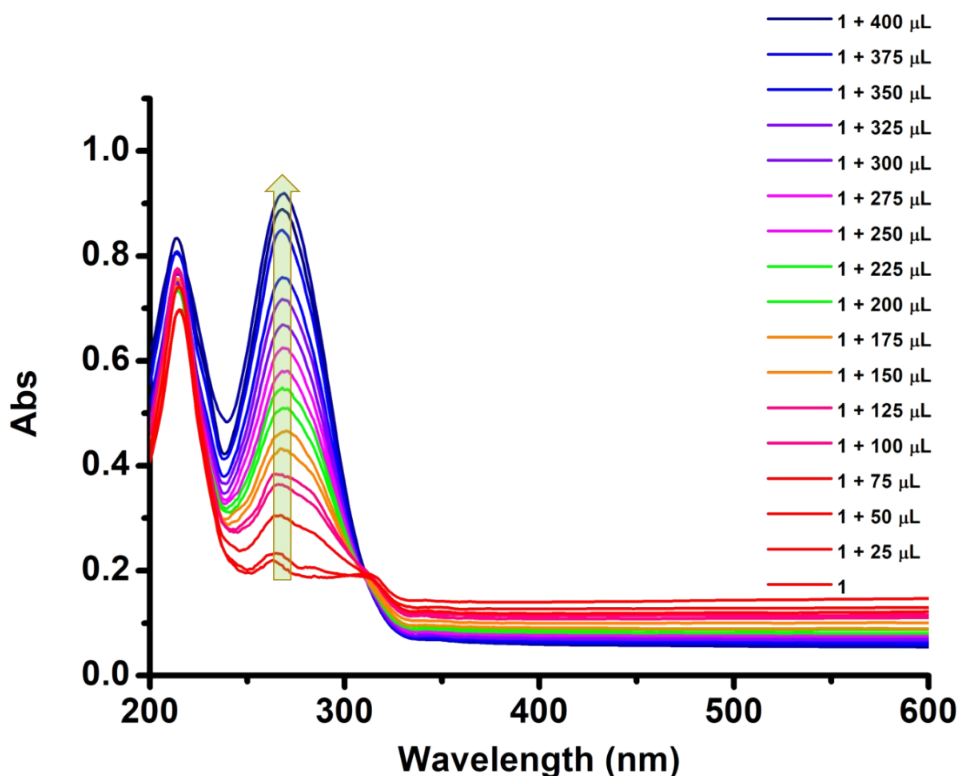


Fig S55. UV-Vis spectra of **1** during gradual addition of 10^{-4} M 400 μL $\text{Cr}_2\text{O}_7^{2-}$

Table S9. Contribution from the Inner Filter Effect (IFE) during PL titration of **1** CrO₄²⁻ (rounded to three decimal places)

Sl. No.	Analyte added (μL)	A_{ex}	A_{em}	I_{obs}	I_{corr}	$I_{\text{corr}}/I_{\text{obs}}$ (correction factor, CF)	QE_{obs} (%)	QE_{corr} (%)
1.	0	0.151	0.094	898.39	1191.145	1.326	0	0
2.	20	0.173	0.085	752.80	1013.164	1.346	16.206	14.942
3.	40	0.205	0.07	706.64	969.83	1.372	21.344	18.580
4.	80	0.188	0.065	628.52	841.425	1.339	30.039	22.936
5.	120	0.362	0.061	561.05	912.786	1.627	37.549	23.369
6.	160	0.423	0.058	514.89	895.300	1.738	42.687	24.837
7.	200	0.481	0.055	479.38	888.356	1.853	46.640	25.420
8.	240	0.595	0.052	411.91	867.963	2.107	54.150	27.132
9.	280	0.700	0.050	358.65	850.370	2.371	60.079	28.609
10.	320	0.843	0.048	301.83	842.020	2.790	66.403	29.310
11.	360	0.933	0.046	269.87	833.230	3.088	69.961	30.048
12.	400	1.016	0.042	238.96	808.309	3.383	73.401	32.128

Table S10. Contribution from the Inner Filter Effect (IFE) during PL titration of **1** Cr₂O₇²⁻

Sl. No.	Analyte added (μL)	A_{ex}	A_{em}	I_{obs}	I_{corr}	$I_{\text{corr}}/I_{\text{obs}}$ (correction factor, CF)	QE_{obs} (%)	QE_{corr} (%)
1.	0	0.216	0.141	853.32	1287.099	1.508	0	0
2.	25	0.236	0.128	714.83	1086.933	1.521	16.230	15.552
3.	50	0.303	0.119	661.57	1075.414	1.626	22.471	16.447
4.	75	0.361	0.114	633.16	1093.990	1.728	25.800	15.003
5.	100	0.386	0.109	611.85	1081.795	1.768	28.298	15.951
6.	125	0.427	0.099	576.35	1056.054	1.832	32.458	17.951
7.	150	0.465	0.091	544.38	1032.529	1.897	36.204	19.779
8.	175	0.510	0.087	508.87	1011.829	1.988	40.366	21.387
9.	200	0.548	0.082	484.02	999.685	2.065	43.278	22.330
10.	225	0.581	0.079	459.16	981.667	2.138	46.191	23.7302
11.	250	0.622	0.076	430.76	962.134	2.234	49.520	25.248
12.	275	0.663	0.073	409.45	955.435	2.333	52.017	25.768
13.	300	0.714	0.069	381.04	938.579	2.463	55.346	27.078
14.	325	0.755	0.066	349.08	898.307	2.573	59.092	30.207
15.	350	0.847	0.063	295.82	843.388	2.851	65.333	34.474
16.	375	0.888	0.060	249.66	743.617	2.976	70.743	42.225

17.	400	0.917	0.057	217.70	668.126	3.069	74.488	48.091
-----	-----	-------	-------	--------	---------	-------	--------	--------

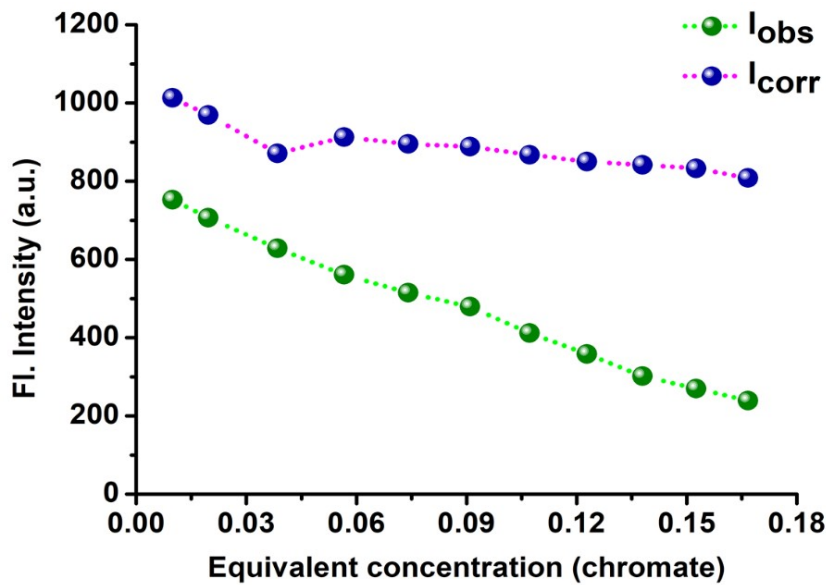


Fig S56. Calculation of IFE: observed and corrected fluorescence intensity (I_{obs} and I_{corr}) for **1** during CrO_4^{2-} titration

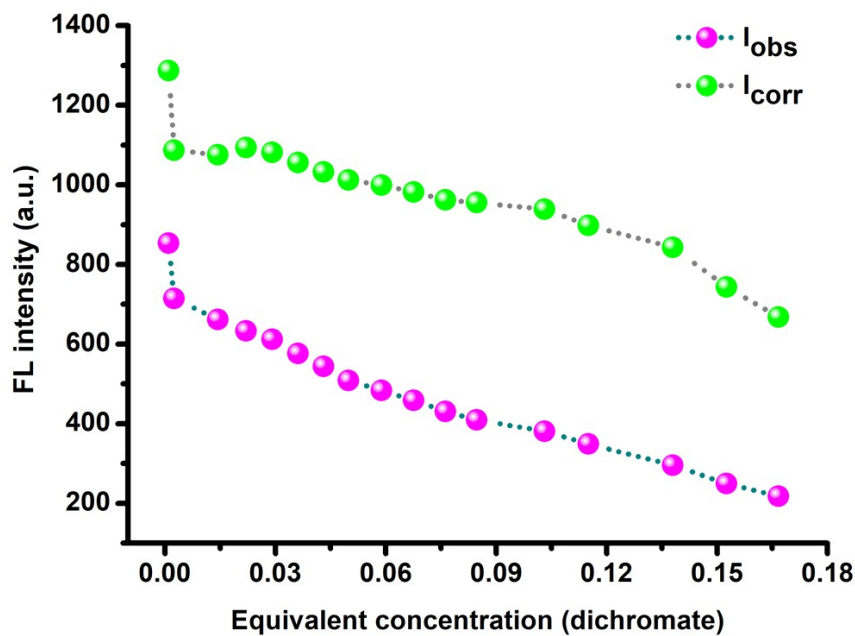


Fig S57. Calculation of IFE: observed and corrected fluorescence intensity (I_{obs} and I_{corr}) for **1** during $\text{Cr}_2\text{O}_7^{2-}$ titration

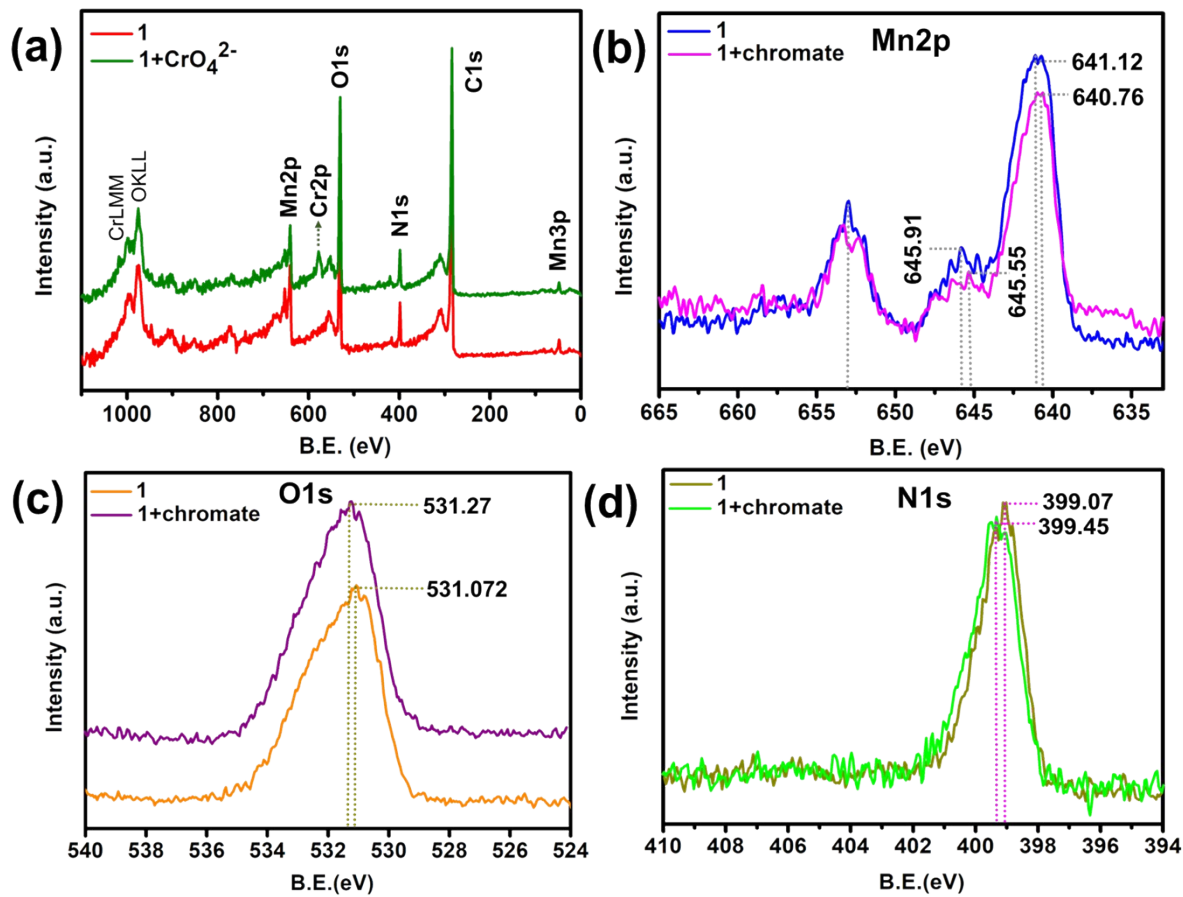


Fig S58. High resolution XPS of CrO_4^{2-} soaked **1**: (a) survey scan, (b) Mn2p, (c) O1s, (d) N1s.

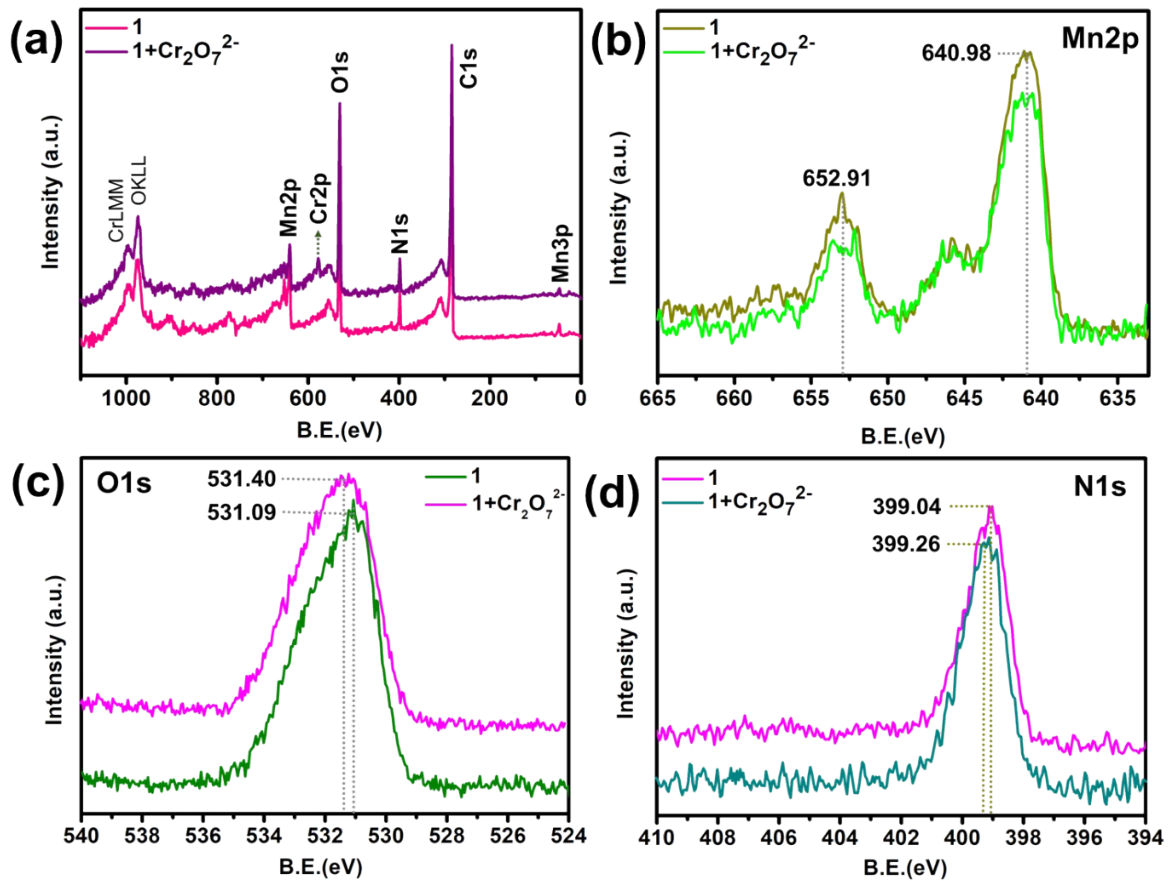
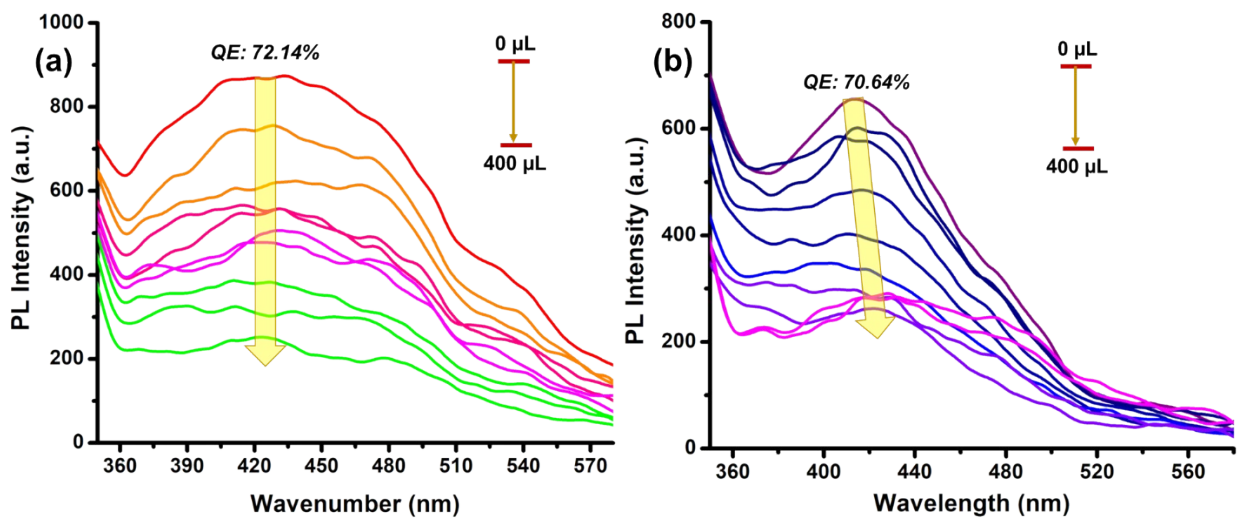


Fig S59. High resolution XPS of Cr₂O₇²⁻ soaked 1: (a) survey scan, (b) Mn2p, (c) O1s, (d) N1s.



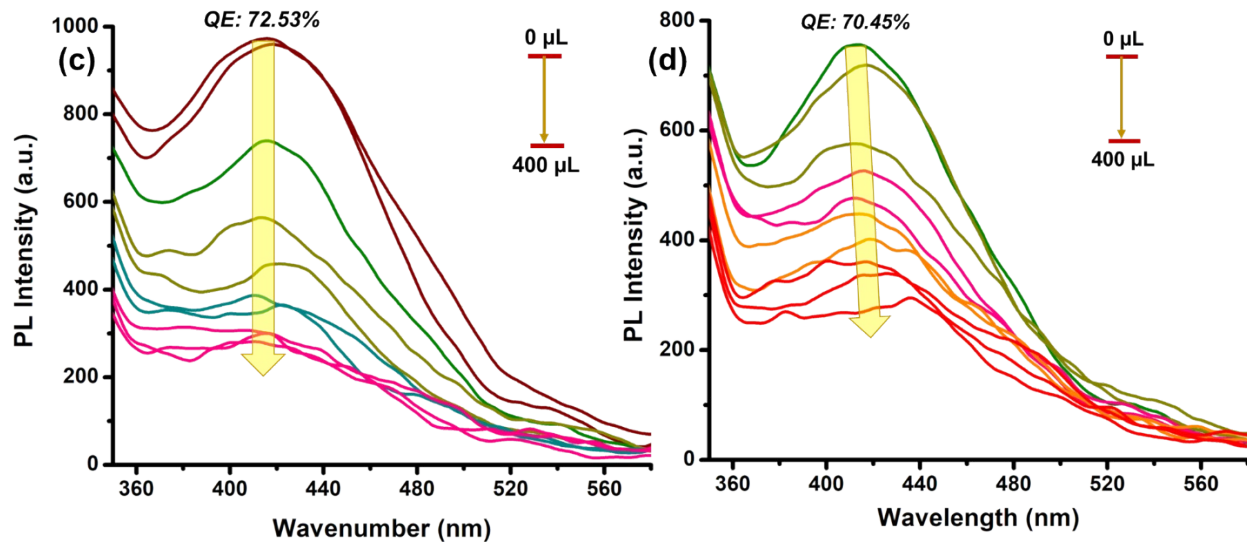


Fig S60. Fluorescence quenching of **1** during gradual addition of FA spiked 1mM solutions: (a) fish extract, (b) meat extract, (c) tap water and (d) sewage water.

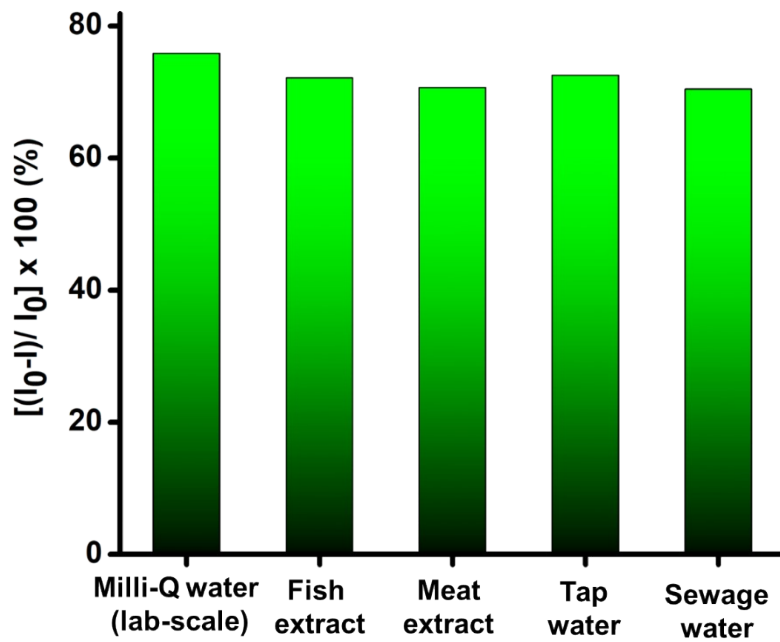


Fig S61. Bar diagram depicting the comparative quenching efficiency (QE, in %) observed for lab scale experiment (with milli-Q water), fish extract, meat extract, sewage water and tap water.

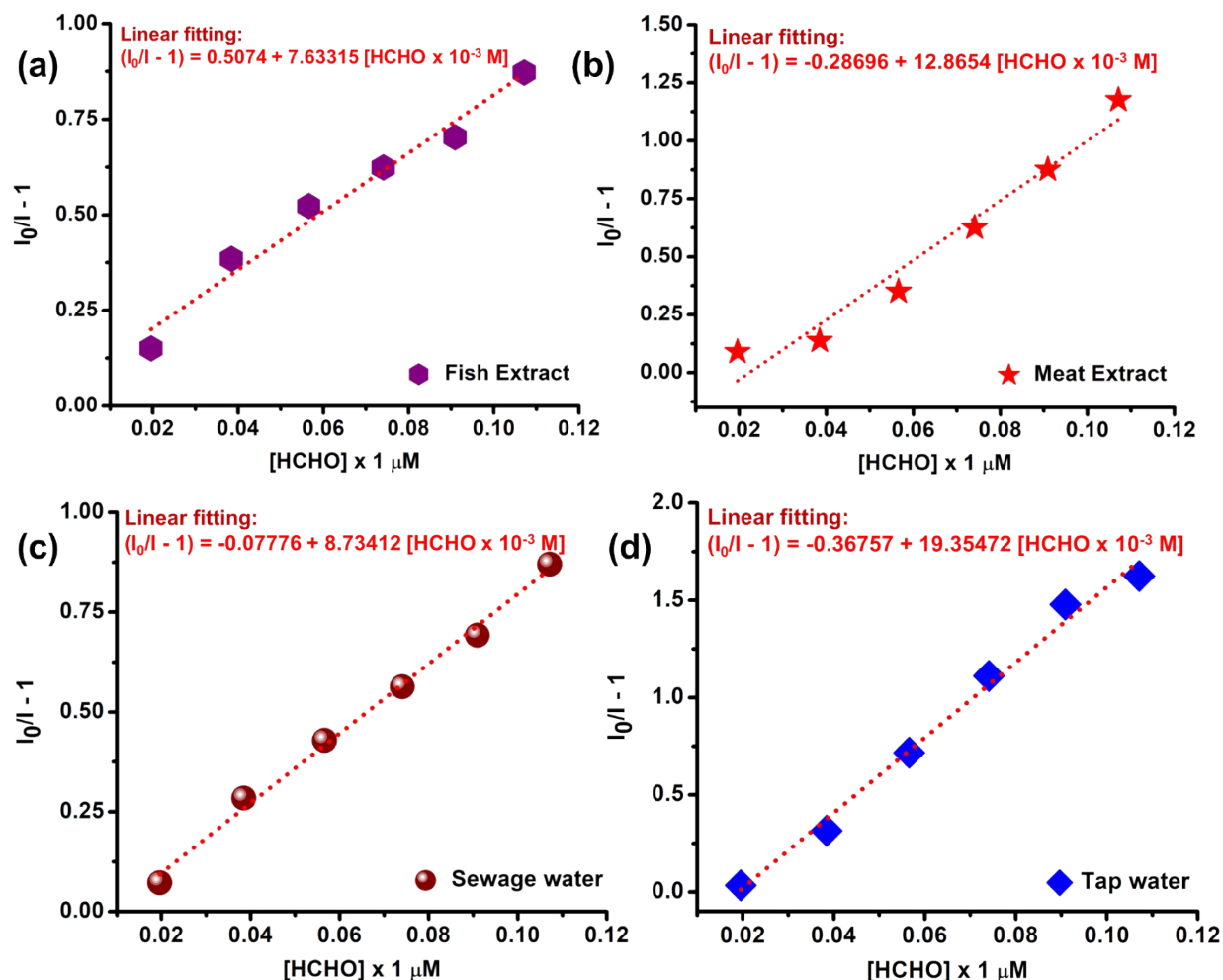
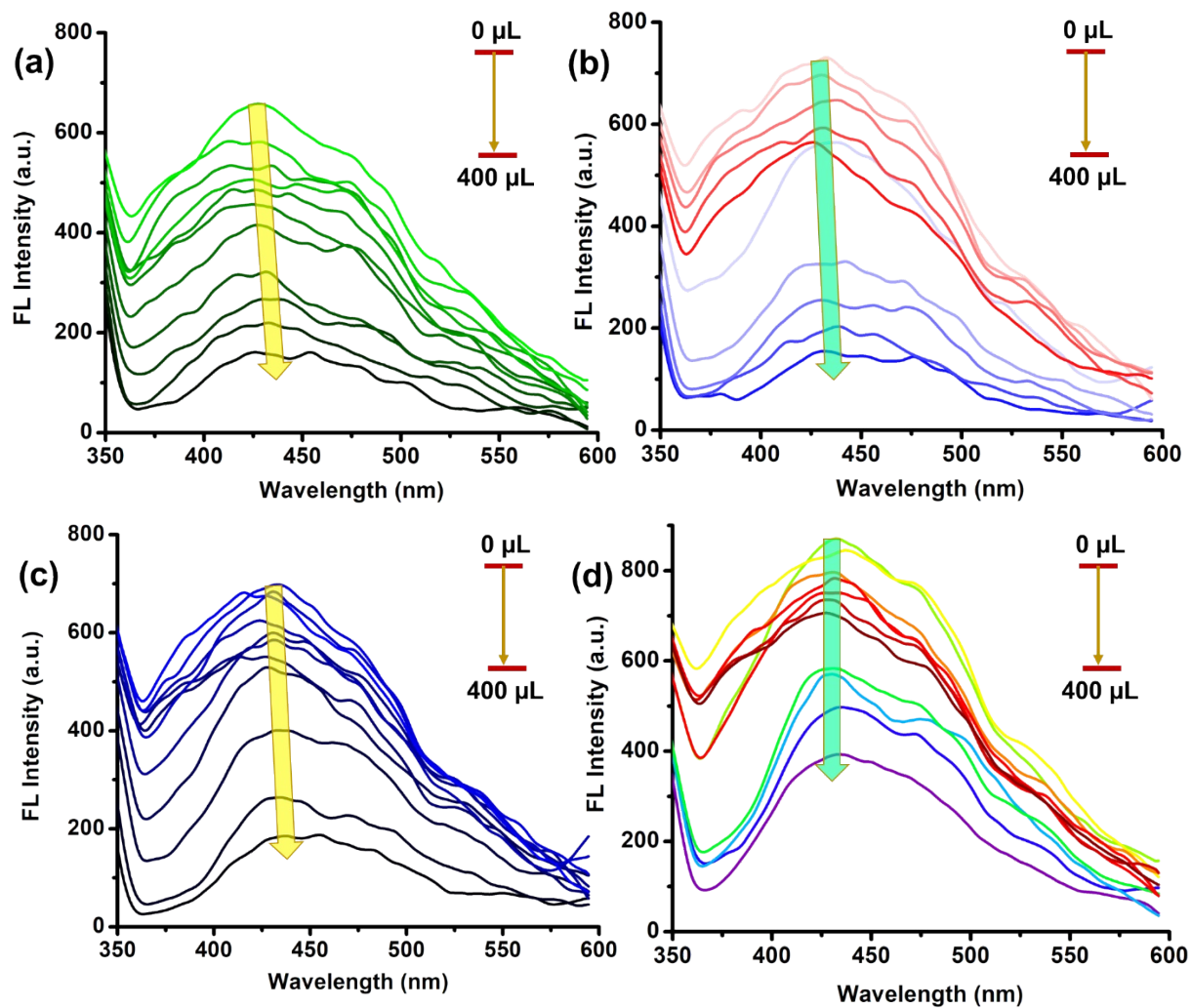


Fig S62. Linear range of the S-V plot obtained for fluorescence titration of **1** with fish, meat extracts and sewage, tap water specimens: calculation of K_{SV} .

Table S11. Preparation of $\text{CrO}_4^{2-}/\text{Cr}_2\text{O}_7^{2-}$ spiked complex environmental matrices

Sample Code	Description
CMW	Coal mine wastewater (CMW) was collected from Dhandadihi pit-lake water, which is accumulated from surrounding abandoned coal-mines ($\sim 23.63555^\circ\text{N}$, $\sim 87.16505^\circ\text{E}$). Dhandadihi is a small village, located approximately 22 kms away from CSIR-CMERI in Andal Block, Durgapur subdivision, West Bengal, India. The collected water was filtered first by a filter paper to eliminate any sediments. Next, 10^{-4} M spiked $\text{CrO}_4^{2-}/\text{Cr}_2\text{O}_7^{2-}$ solution was prepared using this water sample. The sample was chosen keeping in mind

	presence of several hazardous elements in mine wastewater including heavy metals (HMs). ^{4,5,6}
SW	The sewage water (SW) was collected from the Wastewater Reclamation Plant inlet, filtered using a filter paper and was used to prepare simulated 10^{-4} (M) Cr(VI) aq. Solutions.
TW	Spiked 10^{-4} M aq. Cr(VI) solutions were prepared with the running tap water in our wet-chemical laboratory.



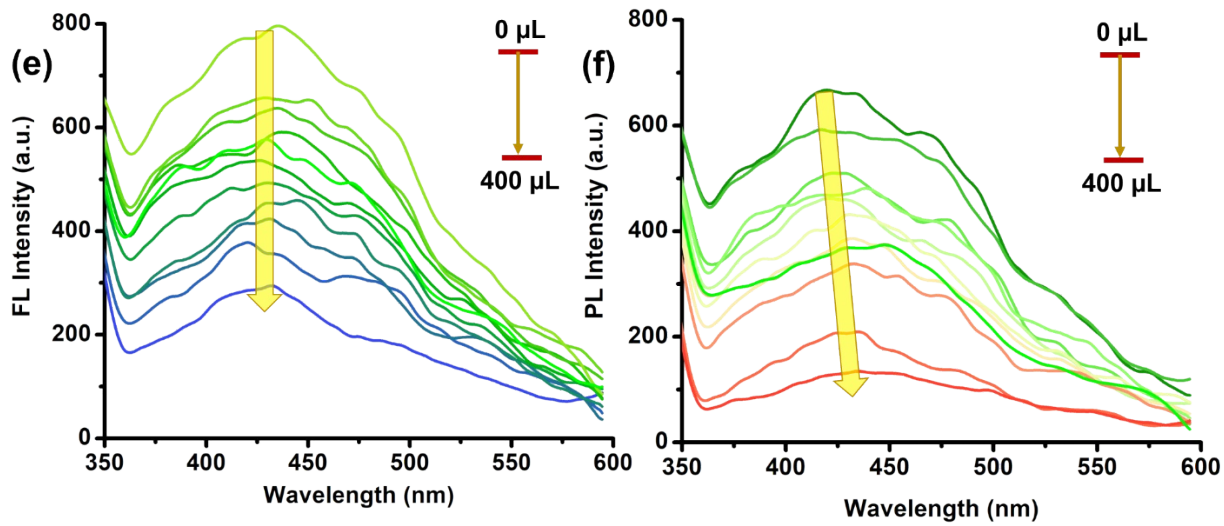
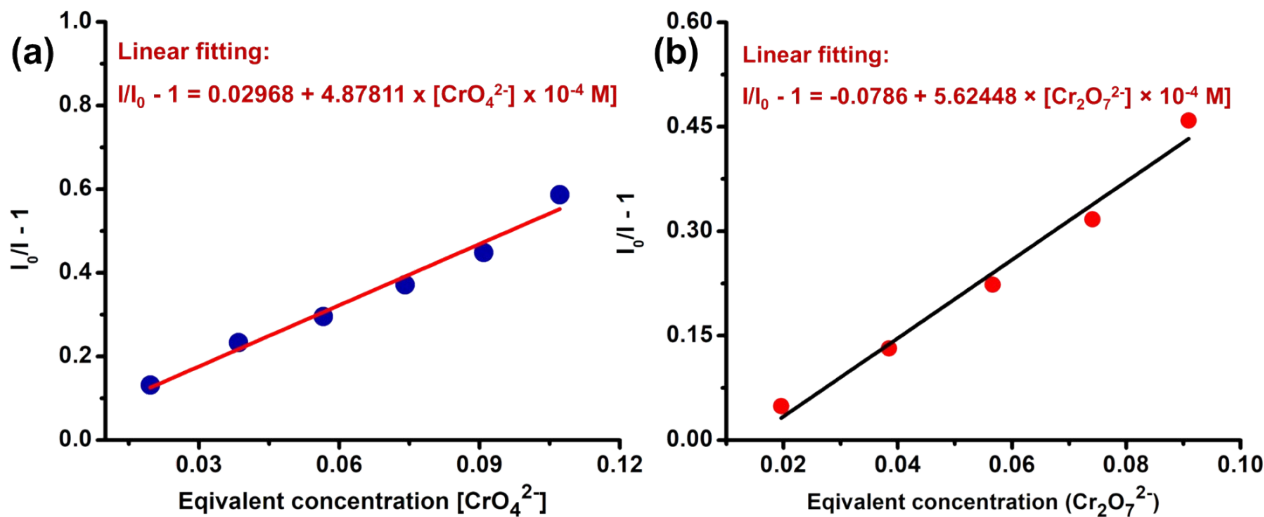


Fig S63. Quenching response observed during gradual addition of 400 μL , 10^{-4} M Cr(VI)-oxoanion spiked complicated environmental matrices: coal-mine wastewater (CMW) - (a) CrO_4^{2-} and (b) $\text{Cr}_2\text{O}_7^{2-}$; sewage water (SW) - (c) CrO_4^{2-} and (d) $\text{Cr}_2\text{O}_7^{2-}$; tap water (TW) - (e) CrO_4^{2-} and (f) $\text{Cr}_2\text{O}_7^{2-}$.



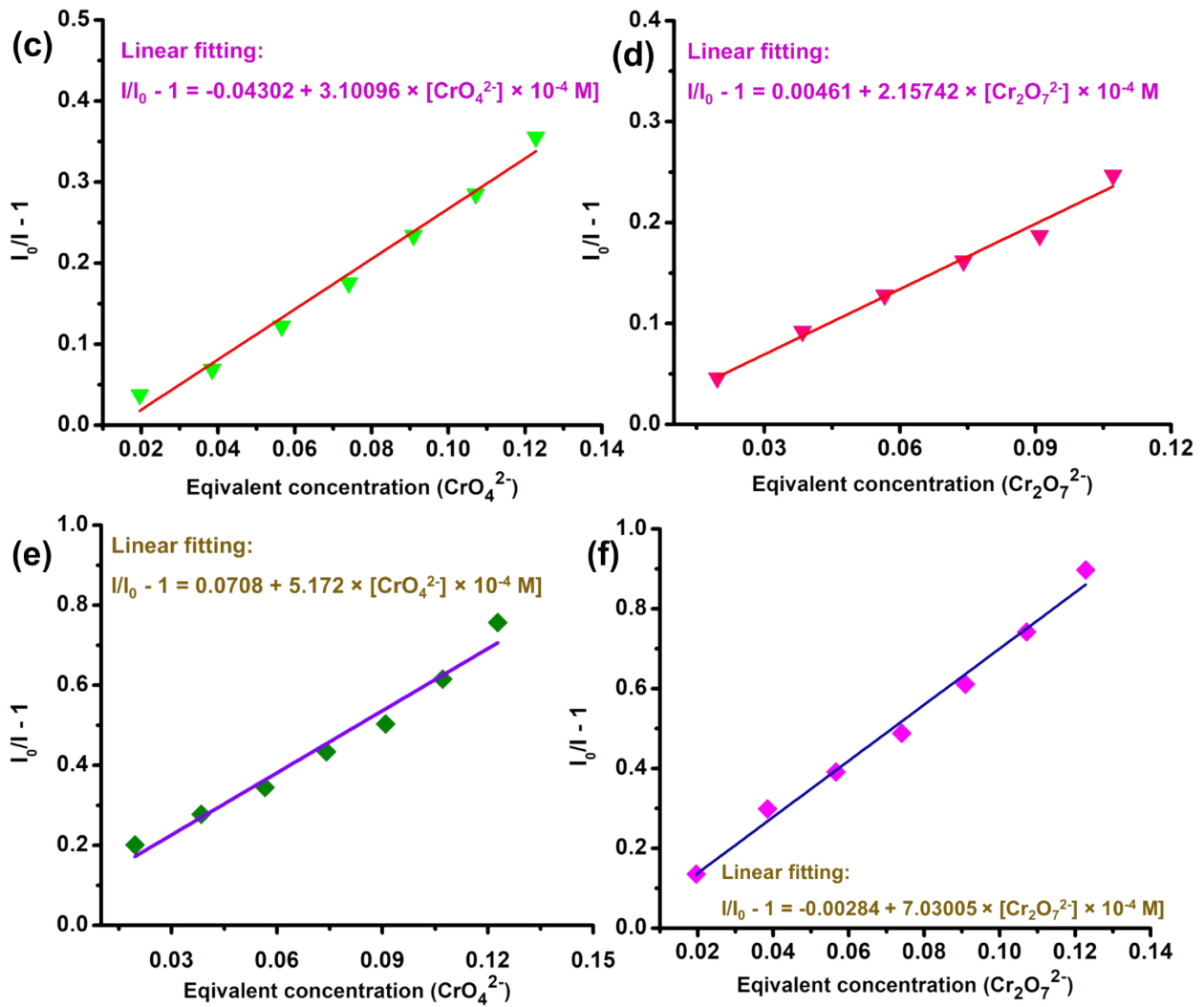


Fig S64. Linear region of the S-V Plots for detection of CrO_4^{2-} and $\text{Cr}_2\text{O}_7^{2-}$ from coal-mine wastewater (a, b), sewage water (c, d) and tap water (e, f) samples.

Table S12. Comparative Table for FA sensing performance of **1** with other FA-sensors

Sl. No.	Material	Detection medium	LOD	Linear Range	Response Time	Ref.
1.	Zr-Uio-66-NH ₂	Trizma Base Buffer	4.0 ppm	10-100 ppm	120 s	7
2.	Al-MIL-53-NHNH ₂	HEPES buffer	0.25 ppm	--	60 s	8
3.	FAP-1	PBS buffer	0.15 ppm	--	7200 s	9
4.	Eu/Zr-Uio-66-NH ₂	Ethyl acetate	0.20 ppm	--	--	10
5.	Screen-printed	phosphate	60 $\mu\text{M L}^{-1}$	60-460 $\mu\text{M L}^{-1}$	--	11

	carbon electrodes (SPC _{Pt} Es)	buffer + KCl electrolyte				
6.	Pd-modified TiO ₂ electrode	AgCl electrolyte	0.015 mM	0 - 17.7 mM	--	12
7.	AgPd/Ch-IL nanoparticles	phosphate buffer	0.022 mM	0.060 - 20 mM	5 s	13
8.	Thin-film planar electrodes and immobilised alcohol oxidase	--	0.05 mM	0.05 - 500 mM	60 s	14
9.	Gold clusters	0.1 M NaOH electrolyte	930 μM	1-10 mM	--	15
10.	QCM	--	3 ppm	3-140 ppm	16 min	16
11.	MIL-101(Cr)		1.79 ppm	2-700 ppm	14-69 s	17
12.	Eu ³⁺ @Bio-MOF-1	Water, food	5.50 ppm	0-14 ppm	2 min	18
13.	2-amino-6-(piperazin-1-yl)-1H-benzo[de]isoquinoline-1,3(2H)-dione	Water, air	8.33 μM	0-1.6 mM	4 min	19
14.	2-(1-aminobut-3-en-1-yl)-N,N-dimethylquinolin-6-amine	Water	0.5 mM	0-200 mM	5 min	20
15.	Naphthalene-based Fluorescent Probe	Water	0.57 mM	0-1.0 mM	--	21
9.	Na-FA	PBS buffer	0.2 ppm	--	1800 s	22
10.	1	Water	8.49 μM (0.25 ppm)	0.014 – 0.063 mM	70 s	This work

Table S13. Brief comparison of Cr(VI)-sensing performance of **1** with recently reported MOF-based sensors

Sl. No.	Material	Detection medium	LOD (M)	K _{sv} (M ⁻¹)	Ref
1.	[Ni ₂ (μ ₂ -OH)(azdc)(tpim)](NO ₃).6DMA.6MeOH	Water	0.30×10 ⁻⁶ (CrO ₄ ²⁻); 0.95×10 ⁻⁶ (Cr ₂ O ₇ ²⁻)	7.90×10 ³ (CrO ₄ ²⁻); 1.31×10 ⁴ (Cr ₂ O ₇ ²⁻)	23
2.	{[Zn(btz)] _n }	Water	1×10 ⁻⁵ (CrO ₄ ²⁻); 2×10 ⁻⁶ (Cr ₂ O ₇ ²⁻)	3.19 × 10 ³ (CrO ₄ ²⁻); 4.23 × 10 ³ (Cr ₂ O ₇ ²⁻)	24
3.	{[Zn ₂ (ttz)H ₂ O] _n }	Water	2×10 ⁻⁵ (CrO ₄ ²⁻ ; Cr ₂ O ₇ ²⁻)	2.35 × 10 ³ (CrO ₄ ²⁻); 2.19 × 10 ³ (Cr ₂ O ₇ ²⁻)	24
4.	{[Zn(IPA)(L)]}n	Water	18.33×10 ⁻⁶ (CrO ₄ ²⁻); 12.02×10 ⁻⁶ (Cr ₂ O ₇ ²⁻)	1×10 ³ (CrO ₄ ²⁻); 1.37×10 ³ (Cr ₂ O ₇ ²⁻)	25
5.	{[Cd(IPA)(L)]}n	Water	2.52×10 ⁻⁶ (CrO ₄ ²⁻); 2.26×10 ⁻⁶ (Cr ₂ O ₇ ²⁻)	1.3×10 ³ (CrO ₄ ²⁻); 2.91×10 ³ (Cr ₂ O ₇ ²⁻)	25
6.	[Cd ₃ (cpota) ₂ (phen) ₃] _n ·5nH ₂ O	Water	0.418×10 ⁻⁶ (CrO ₄ ²⁻); 0.37×10 ⁻⁶ (Cr ₂ O ₇ ²⁻)	6.9×10 ³ (CrO ₄ ²⁻); 1.21×10 ⁴ (Cr ₂ O ₇ ²⁻)	26
7.	[Cd(bipy)][HL] _n	Water	QE: 99.7%	2.7×10 ⁵ (Cr ₂ O ₇ ²⁻)	27
8.	[Zn ₂ (L) ₂ (TPA)]·2H ₂ O	Water	2.10×10 ⁻⁶ (CrO ₄ ²⁻); 3.80×10 ⁻⁶ (Cr ₂ O ₇ ²⁻)	1.3×10 ⁴ (CrO ₄ ²⁻); 6.05×10 ³ (Cr ₂ O ₇ ²⁻)	28
9.	NU-1000	Water	1.8×10 ⁻⁶ (Cr ₂ O ₇ ²⁻)	1.337×10 ⁴ (Cr ₂ O ₇ ²⁻)	29
10.	{[Cd(L)(SDBA)(H ₂ O)]·0.5H ₂ O} _n	Water	3.76×10 ⁻⁵ (Cr ₂ O ₇ ²⁻)	6.40×10 ³ (Cr ₂ O ₇ ²⁻)	30
11.	{[Cd(L)(BPDC)]·2H ₂ O} _n	Water	3.76×10 ⁻⁵ (Cr ₂ O ₇ ²⁻)	6.40×10 ³ (Cr ₂ O ₇ ²⁻)	30
12.	{[Eu(L)(H ₂ O)]·7H ₂ O} _n	Water	0.53×10 ⁻⁶ (CrO ₄ ²⁻); 0.32×10 ⁻⁶ (Cr ₂ O ₇ ²⁻)	3.53×10 ⁴ (CrO ₄ ²⁻); 5.89×10 ⁴ (Cr ₂ O ₇ ²⁻)	31
13.	{[Tb(L)(H ₂ O)]·7H ₂ O} _n	Water	0.75×10 ⁻⁶ (CrO ₄ ²⁻); 0.57×10 ⁻⁶ (Cr ₂ O ₇ ²⁻)	2.48×10 ⁴ (CrO ₄ ²⁻); 3.26×10 ⁴ (Cr ₂ O ₇ ²⁻)	31
14.	{[Zn ₂ (TRZ) ₂ (DBTDC-O ₂)].DMAc} _n	Water	2.55×10 ⁻⁶ (Cr ₂ O ₇ ²⁻)	1.24×10 ⁴ (Cr ₂ O ₇ ²⁻)	32
15.	[Eu ₂ (tpbpc) ₄ .CO ₃ .H ₂ O].DMF. solvent	Water	0.33×10 ⁻⁶ (CrO ₄ ²⁻); 1.07×10 ⁻⁶ (Cr ₂ O ₇ ²⁻)	4.85×10 ³ (CrO ₄ ²⁻); 1.04×10 ³ (Cr ₂ O ₇ ²⁻)	33
16.	[Zn ₂ (tpeb)(bpdc) ₂]	Water	1.07×10 ⁻⁶ (CrO ₄ ²⁻); 1.04×10 ⁻⁶ (Cr ₂ O ₇ ²⁻)	1.085×10 ⁴ (CrO ₄ ²⁻); 1.122×10 ⁴ (Cr ₂ O ₇ ²⁻)	34

17.	$\text{Zr}_6\text{O}_4(\text{OH})_7(\text{H}_2\text{O})_3(\text{BTBA})_3$	Water	1.50×10^{-6} ($\text{Cr}_2\text{O}_7^{2-}$)	1.57×10^4 ($\text{Cr}_2\text{O}_7^{2-}$)	35
18.	Zn-MOF based on 1,5-bis(5-tetrazolo)-3-oxapentane (H_2btz) ligand	Water	3×10^{-6} ($\text{CrO}_4^{2-}/\text{Cr}_2\text{O}_7^{2-}$)	0.1998×10^4 (CrO_4^{2-}); 0.1789×10^4 ($\text{Cr}_2\text{O}_7^{2-}$)	36
19.	$[\text{Cd}(\text{L})(4,4\text{-bpy})]\cdot\text{DMF}\cdot\text{H}_2\text{O}]_n$ (1), $\{\text{[Cd}_2(\text{L})_2(\text{bpe})_2]\cdot3\text{DMF}\cdot2.5\text{H}_2\text{O}\}_n$ (2), $\{\text{[Cd}(\text{L})(\text{bibp})]\cdot2\text{DMF}\}_n$ (3)	DMF	7.10×10^{-6} (compound 1) 1.65×10^{-6} (2) 5.30×10^{-6} (3) [all for $\text{Cr}_2\text{O}_7^{2-}$]	2.83×10^3 (1) 3.70×10^3 (2) 6.15×10^3 (3)	37
20.	FDA-based Eu (1), and Tb (2) MOF	Water	114×10^{-6} (1) and 74.2×10^{-6} (2) for $\text{Cr}_2\text{O}_7^{2-}$; and 112×10^{-4} (1) and 127×10^{-6} (2) for CrO_4^{2-}	1.25×10^4 (1) and 1.46×10^4 (2) (for $\text{Cr}_2\text{O}_7^{2-}$); 3.56×10^3 (1) and 4.35×10^3 (2) (for CrO_4^{2-});	38
21.	$\{\text{[Cd}_2\text{L}_2(\text{H}_2\text{O})_4]\cdot\text{H}_2\text{O}\}_n$ (1) and $\{\text{[Zn}_2\text{L}_2(\text{H}_2\text{O})_4]\cdot\text{H}_2\text{O}\}_n$ (2)	Water	4.8×10^{-6} (CrO_4^{2-}), 3.53×10^{-6} (CrO_4^{2-}),	1.25×10^4 and 1.21×10^4 for CrO_4^{2-} and CrO_4^{2-} .	39
22.	$[\text{Ag}(\text{CIP}^-)]$	Water	0.45×10^{-6} (CrO_4^{2-}); 0.14×10^{-6} ($\text{Cr}_2\text{O}_7^{2-}$)	2×10^4 (CrO_4^{2-}); 6.3×10^4 ($\text{Cr}_2\text{O}_7^{2-}$)	40
23.	$\text{Cd}_3(\text{bpe})_2(\text{ceba})_2(\text{fa})_2(\text{H}_2\text{O})_2]_n$ (1), $[\text{Cd}_3(\text{rctt-tpcb})$ $(\text{ceba})_2(\text{fa})_2(\text{H}_2\text{O})_2]_n$ (1a)	DMF + water	--	0.95×10^4 (CrO_4^{2-}); 0.63×10^4 ($\text{Cr}_2\text{O}_7^{2-}$)	41
24.	$\{\text{[Ln}_2(\text{L})_2(\text{H}_2\text{O})_2]\cdot5\text{H}_2\text{O}\cdot6\text{DMA C}\}_n$, [Lns: Eu (1) and Tb (2)]	Water	89.40×10^{-6} ($\text{Cr}_2\text{O}_7^{2-}$)	0.1052×10^4 ($\text{Cr}_2\text{O}_7^{2-}$)	42
25.	$\{\text{[Eu}(\text{dpc})(2\text{H}_2\text{O})].(\text{Hbibp})_{0.5}\}_n$ ($\text{H}_4\text{dpc} = 2\text{-}(3',4'\text{-dicarboxylphenoxy})\text{isophthalic acid}$, bibp = 4,4'-bis(imidazolyl)biphenyl)	DMF	10.1×10^{-6} ($\text{Cr}_2\text{O}_7^{2-}$)	3.97×10^3 ($\text{Cr}_2\text{O}_7^{2-}$)	43
26.	$[\text{Eu}(\text{L})(\text{H}_2\text{O})(\text{DMA})]$	Water	7.30×10^{-6} (CrO_4^{2-}) 6.29×10^{-6} ($\text{Cr}_2\text{O}_7^{2-}$)	5.339×10^4 (CrO_4^{2-}); 5.722×10^4 ($\text{Cr}_2\text{O}_7^{2-}$)	44

27.	[M(5-hip)(H ₂ O) ₃] _n [M: Cd ²⁺ (1), Zn ²⁺ (2)]	Water	0.8 × 10 ⁻⁶ (1) 1.0 × 10 ⁻⁶ (2) (Cr ₂ O ₇ ²⁻)	1.15 × 10 ⁴ (1) 1.80 × 10 ⁴ (2) (Cr ₂ O ₇ ²⁻)	45
28.	iMOF-4C	Water	3 × 10 ⁻⁶ (CrO ₄ ²⁻) 4.1 × 10 ⁻⁶ (Cr ₂ O ₇ ²⁻)	13.1 × 10 ⁴ (CrO ₄ ²⁻); 48.5 × 10 ⁴ (Cr ₂ O ₇ ²⁻)	46
29.	[Zn(DPA)(HNTB)]·H ₂ O	water	148 × 10 ⁻⁶ (CrO ₄ ²⁻) 258 × 10 ⁻⁶ (Cr ₂ O ₇ ²⁻)	0.403 × 10 ⁴ (CrO ₄ ²⁻); 0.405 × 10 ⁴ (Cr ₂ O ₇ ²⁻)	47
30.	{[Zn(BBDF) (ATP)]·2DMF·3H ₂ O} _n	water	0.17×10 ⁻⁶ (Cr ₂ O ₇ ²⁻) 0.21× 10 ⁻⁶ (CrO ₄ ²⁻)	2.64 × 10 ⁴ (Cr ₂ O ₇ ²⁻) 2.52× 10 ⁴ (Cr ₂ O ₇ ²⁻)	48
31.	Mn-MOF (1)	Water	0.41 × 10⁻⁶(CrO₄²⁻); 0.59 × 10⁻⁶ (Cr₂O₇²⁻)	16.13 × 10⁴(CrO₄²⁻); 12.73 × 10⁴ (Cr₂O₇²⁻)	This Work

[Abbreviations: H₂btz: 1,5-bis(5-tetrazolo)-3-oxapentane; H₃ttz: 1,2,3-tris-[2-(5-tetrazolo)-ethoxy]propane; IPA: isophthalic acid; L (Entry 3,4): 3-pyridylcarboxaldehyde nicotinoylhydrazone; H₃L (entry 6) = 2'-carboxybiphenyl-4-ylmethylphosphonic acid; bipy = 2,2'-bipyridine; Htpbpc = 4'-[4,2';6',4'']-terpyridin-4'-yl-biphenyl-4-carboxylic acid); H₂BPDC = 4,4'-biphenyldicarboxylic acid, H₂SDBA= 4,4'-sulfonyldibenzoic acid; L (Entry 9, 10)= 4,4'-(2,5-bis-(methylthio)-1,4-phenylene)dipyridine; tpim = 4,4',4''-(1H-imidazole-2,4,5-triyl)trypyridine; H₂azdc= azobenzene-4,4'-dicarboxylic acid; L (Entry 7) = 4-(tetrazol-5-yl)phenyl-4,2':6',4''-terpyridine, TPA = terephthalic acid; H₃cpota = 2-(4-carboxyphenoxy)terephthalic acid; phen = 1,10-phenanthroline; H₃L (Entry 11, 12) = 5-(3',5'-dicarboxylphenyl)picolinic acid; tpeb = 1,3,5-tri-4-pyridyl-1,2-ethenylbenzene; H₃BTBA: 4,4',4''-(1H-benzo[d]imidazole-2,4,7-triyl)tribenzoic acid; H₂DBTDC-O₂ = S,S-dioxodibenzothiophen-3,7-dicarboxylic acid and HTRZ = 1,2,4-triazole, H₂L (entry 21): 5-(1H-1,2,4-triazol-1-yl)isophthalic acid), H₂L (entry 19) = 4,4'-(benzene-1,3-diylbis(methanediylsulfanediyl)])dibenzoic acid, 4,4-bpy = 4,4-bipyridine, bpe = 1,2-bis(4-pyridyl)ethylene, bibp =4,4'-bis(benzoimidazo-1-ly)biphenyl), FDA: furan-2,5-dicarboxylic acid, HCIP = 4-(4-carboxylphenyl)- 2,6-di(4-imidazol-1-yl)phenyl)pyridine, fa = formate anions, bpe: trans-1,2-bis(4'-pyridyl)ethylene ligand (bpe) and H₂ceba: 4-(1-carboxy-ethoxy)-benzoic acid, rctt-tpcb = tetrakis(4-pyridyl)-cyclobutane; H₃L (entry 24) = 4,4'-(5-carboxy-1,3-phenylene)bis(azanediyl))bis(carbonyl))dibenzoic acid; DMAC = N,N'-dimethylacetamide; L (entry 26) = 2-(2-nitro-4-carboxylphenyl)terephthalic acid); 5-hip = 5-hydroxyisophthalic acid; DPA = 2,5-di(pyridin-4-yl)aniline, H₃NTB = 4,4',4''-nitrilotribenzoic acid]

References:

- 1 O. V. Dolomanov, L. J. Bourhis, R. J. Gildea, J. A. K. Howard and H. Puschmann, *J. Appl. Crystallogr.*, 2009, **42**, 339–341.
- 2 G. M. Sheldrick, *Acta Crystallogr. Sect. A Found. Adv.*, 2015, **71**, 3–8.
- 3 G. M. Sheldrick, *Acta Crystallogr. Sect. C Struct. Chem.*, 2015, **71**, 3–8.
- 4 M. A. Hossen, A. I. H. Chowdhury, M. R. A. Mullick and A. Hoque, *Environ. Nanotechnology, Monit. Manag.*, 2021, **16**, 100469.
- 5 L. A. Ivanova, O. V. Salishcheva, I. V. Timoshchuk, N. S. Golubeva and A. K. Gorelkina, *Coke Chem.*, 2023, **66**, 227–231.
- 6 F. Li, X. Li, L. Hou and A. Shao, *Sci. Rep.*, 2018, **8**, 14925.
- 7 K. Vellingiri, A. Deep, K.-H. Kim, D. W. Boukhvalov, P. Kumar and Q. Yao, *Sensors Actuators B Chem.*, 2017, **241**, 938–948.
- 8 S. Nandi, E. Sharma, V. Trivedi and S. Biswas, *Inorg. Chem.*, 2018, **57**, 15149–15157.
- 9 T. F. Brewer and C. J. Chang, *J. Am. Chem. Soc.*, 2015, **137**, 10886–10889.
- 10 C. Li, J. Huang, H. Zhu, L. Liu, Y. Feng, G. Hu and X. Yu, *Sensors Actuators B Chem.*, 2017, **253**, 275–282.
- 11 L. del Torno-de Román, M. A. Alonso-Lomillo, O. Domínguez-Renedo, C. Merino-Sánchez, M. P. Merino-Amayuelas and M. J. Arcos-Martínez, *Talanta*, 2011, **86**, 324–328.
- 12 Q. Yi, F. Niu and W. Yu, *Thin Solid Films*, 2011, **519**, 3155–3161.
- 13 Q. Wang, J. Zheng and H. Zhang, *J. Electroanal. Chem.*, 2012, **674**, 1–6.
- 14 S. V. Dzyadevych, V. N. Arkhypova, Y. I. Korpan, A. V. El'skaya, A. P. Soldatkin, N. Jaffrezic-Renault and C. Martelet, *Anal. Chim. Acta*, 2001, **445**, 47–55.
- 15 M. R. Baez-Gaxiola, C. Fernández-Sánchez and E. Mendoza, *Anal. Methods*, 2015, **7**, 538–542.
- 16 C. Zhang, X. Wang, J. Lin, B. Ding, J. Yu and N. Pan, *Sensors Actuators B Chem.*, 2011, **152**, 316–323.
- 17 E. Haghghi and S. Zeinali, *Microporous Mesoporous Mater.*, 2020, **300**, 110065.
- 18 Y. Zhang and B. Yan, *J. Mater. Chem. C*, 2019, **7**, 5652–5657.
- 19 B. Dong, X. Song, Y. Tang and W. Lin, *Sensors Actuators B Chem.*, 2016, **222**, 325–330.
- 20 Z. Li, Y. Xu, H. Zhu and Y. Qian, *Chem. Sci.*, 2017, **8**, 5616–5621.

- 21 J. Xu, Y. Zhang, L. Zeng, J. Liu, J. M. Kinsella and R. Sheng, *Talanta*, 2016, **160**, 645–652.
- 22 J.-B. Li, Q.-Q. Wang, L. Yuan, Y.-X. Wu, X.-X. Hu, X.-B. Zhang and W. Tan, *Analyst*, 2016, **141**, 3395–3402.
- 23 R. Goswami, N. Seal, S. R. Dash, A. Tyagi and S. Neogi, *ACS Appl. Mater. Interfaces*, 2019, **11**, 40134–40150.
- 24 C.-S. Cao, H.-C. Hu, H. Xu, W.-Z. Qiao and B. Zhao, *CrystEngComm*, 2016, **18**, 4445–4451.
- 25 B. Parmar, Y. Rachuri, K. K. Bisht, R. Laiya and E. Suresh, *Inorg. Chem.*, 2017, **56**, 2627–2638.
- 26 S. Li, L. Lu, M. Zhu, C. Yuan and S. Feng, *Sensors Actuators B Chem.*, 2018, **258**, 970–980.
- 27 W.-Q. Kan and S.-Z. Wen, *Dye. Pigment.*, 2017, **139**, 372–380.
- 28 X.-Y. Guo, Z.-P. Dong, F. Zhao, Z.-L. Liu and Y.-Q. Wang, *New J. Chem.*, 2019, **43**, 2353–2361.
- 29 Z.-J. Lin, H.-Q. Zheng, H.-Y. Zheng, L.-P. Lin, Q. Xin and R. Cao, *Inorg. Chem.*, 2017, **56**, 14178–14188.
- 30 S. Chen, Z. Shi, L. Qin, H. Jia and H. Zheng, *Cryst. Growth Des.*, 2017, **17**, 67–72.
- 31 J.-P. Dong, B. Li, Y.-J. Jin and L.-Y. Wang, *CrystEngComm*, 2021, **23**, 1677–1683.
- 32 H. He, Q.-Q. Zhu, C.-P. Li and M. Du, *Cryst. Growth Des.*, 2019, **19**, 694–703.
- 33 J. Liu, G. Ji, J. Xiao and Z. Liu, *Inorg. Chem.*, 2017, **56**, 4197–4205.
- 34 B. B. Rath and J. J. Vittal, *Inorg. Chem.*, 2020, **59**, 8818–8826.
- 35 T. He, Y.-Z. Zhang, X.-J. Kong, J. Yu, X.-L. Lv, Y. Wu, Z.-J. Guo and J.-R. Li, *ACS Appl. Mater. Interfaces*, 2018, **10**, 16650–16659.
- 36 C.-S. Cao, Y. Shi, H. Xu and B. Zhao, *Dalt. Trans.*, 2018, **47**, 4545–4553.
- 37 Z. Chen, X. Mi, J. Lu, S. Wang, Y. Li, J. Dou and D. Li, *Dalt. Trans.*, 2018, **47**, 6240–6249.
- 38 J.-Y. Zou, L. Li, S.-Y. You, Y.-W. Liu, H.-M. Cui, J.-Z. Cui and S.-W. Zhang, *Dalt. Trans.*, 2018, **47**, 15694–15702.
- 39 C.-X. Wang, Y.-P. Xia, Z.-Q. Yao, J. Xu, Z. Chang and X.-H. Bu, *Dalt. Trans.*, 2019, **48**, 387–394.

- 40 D.-D. Feng, Y.-D. Zhao, X.-Q. Wang, D.-D. Fang, J. Tang, L.-M. Fan and J. Yang, *Dalt. Trans.*, 2019, **48**, 10892–10900.
- 41 R.-R. Zhu, T. Wang, T. Yan, L. Jia, Z. Xue, J. Zhou, L. Du and Q.-H. Zhao, *Dalt. Trans.*, 2019, **48**, 12159–12167.
- 42 J.-J. Ma and W. Liu, *Dalt. Trans.*, 2019, **48**, 12287–12295.
- 43 Y. Du, H. Yang, R. Liu, C. Shao and L. Yang, *Dalt. Trans.*, 2020, **49**, 13003–13016.
- 44 J.-J. Zhao, P.-Y. Liu, L.-J. Song, L. Zhang, Z.-L. Liu and Y.-Q. Wang, *Dalt. Trans.*, 2021, **50**, 5236–5243.
- 45 X.-T. Liu, B.-C. Wang, B.-B. Hao, C.-X. Zhang and Q.-L. Wang, *Dalt. Trans.*, 2021, **50**, 8718–8726.
- 46 S. Dutta, S. Let, M. M. Shirolkar, A. V. Desai, P. Samanta, S. Fajal, Y. D. More and S. K. Ghosh, *Dalt. Trans.*, 2021, **50**, 10133–10141.
- 47 S.-M. Zhao, Z.-F. Qiu, Z.-H. Xu, Z.-Q. Huang, Y. Zhao and W.-Y. Sun, *Dalt. Trans.*, 2022, **51**, 3572–3580.
- 48 C. Li, X. Sun, X. Meng, D. Wang and C. Zheng, *Dalt. Trans.*, 2023, **52**, 7611–7619.